Modelling of hydrodynamic and erosion processes at vegetated lake shores

Development of a process-based tool for the design of the protection of a lake shore with reed-like vegetation

K. van Batenburg

Modelling of hydrodynamic and erosion processes at vegetated lake shores

Development of a process-based tool for the design of the protection of a lake shore with reed-like vegetation

by

Student name:	Kimberley van Batenburg	4380916
Project duration:	September 2, 2019 – July 15, 2020	
Supervisors:	Prof.dr.ir. W.S.J. Uijttewaal	TU Delft
	Prof. dr. P.M.J. Herman	TU Delft
	Ir. A. Gijón Mancheño	TU Delft
	Ir. T. Wilms	Witteveen + Bos

TUDelft
Delft University of Technology

Witteveen + Bos

Preface

With this thesis I conclude my Master of Science program in Hydraulic Engineering at the TU-Delft. The research was conducted in collaboration with engineering consultancy Witteveen + Bos in the period from September 2019 until July 2020.

First of all, I like to thank the members of my thesis committee for there guidance and support during the past year. I would like to thank Wim Uijttewaal for being the chair of my committee, the introduction towards this subject and giving his view in order to improve the work. Peter Herman for showing me the more ecological aspects and keeping me critical and looking from different perspectives. Tom Wilms for introducing me to Witteveen + Bos as well as giving his support and advice during my research. Especially, I want to thank Alejandra Gijón Mancheño for the many hours and conversations concerning almost all the aspects presented in this thesis and for the great support during this last year.

For the finalizing of this thesis I like to thank my friends Suzanne Assen, Lianne Bruijns, Jasper Coppen and Noortje van Wanrooij for reading my thesis in advance and improving the clarity, spelling and grammar of the report. I also like to thank my family and friends, not only for their support during this last year, but also for the amazing time I had in Delft these past 6 years.

K. van Batenburg
Delft, July 2020

Summary

In recent years, the interest in integrating shore protection with the local ecosystems has increased. In comparison with the traditional reinforced embankments, integrated shores form a gradual transition from land to water where shore vegetation can establish itself. These nature friendly shores have a positive impact upon the water quality, flora and fauna and the amenities of the shore. Some of the benefits of vegetation are its capability of reducing the hydrodynamic loads on the shore and its ability to increase the soil strength against erosion. Both effects have been investigated in detail in previous research and have been implemented for coastal protection designs in sandy coastal settings. But a designing tool for cohesive shorelines in lake environments is still missing. In this research, the different aspects important for the erosion of a vegetated cohesive shoreline are studied and the first steps towards a process based design tool are taken.

In order to give more insight in the behavior of different design choices in a lake environment, the model of Duró et al.(2020) is modified for a setting with cohesive bed at a lake. Duró et al.(2020) developed a model in order to calculate the shore morphology based on the induced bed shear stresses of ship waves along the river Maas, without accounting for sediment accumulation in milder conditions. In the modified model, sediment accumulation is also neglected, resulting in conservative results. The main modifications concern the shore morphology based on the induced bed shear stresses from regular waves (instead of ship waves), a steeper slope and the presence of vegetation.

The model development and validation is done in four steps. First, the wave reduction through vegetation is implemented and validated based on both kelp data and a comparison with the model results of Mendez and Losada (2004). This comparison shows a good resemblance during bore propagation, but a difference in wave breaking is visible, as the experiments with kelp data use different wave spectra. Second, the amount of induced bed shear stresses from the waves is compared with the model results of SWASH. It shows that the amount of induced bed shear stresses fits quite well during the bore propagation, but shows differs from the SWASH results at the start of the run-up when the slope deviates from 0.02 meter vertical/meter horizontal, resulting in restrictions for the models use. This can become a problem when the morphology of the shore will be considered. Third, the morphology is validated in the original model, from which can be concluded that, as long as the induced bed shear stresses are correct, the calculation of the morphology is correct as well. Fourth, a sensitivity analyses is done in order to estimate the influence of the main calibration parameters on the maximum induced bed shear stresses. The effect of changing the values of the input parameters is investigated, in order to check how an uncertainty in the input values would affect the model inaccuracy. For this step, the characteristics of common reed, *Phragmites Australis* (hence after *P. australis*), are used. The soil reinforcement by the roots of *P. australis* is also added to the model.

Most of the used formulas are derived and calibrated for slopes around the 0.03 m/m. When the slope steepens, waves will break differently which is not included in the model. For this reason it can be expected that the deviation in the calculated run-up shear stresses is related to the use of a process based model. Process based models reproduce the physical processes as long as they are used in the conditions for which they are derived, which constitutes a problem at the moment morphology changes the conditions, resulting in an overestimation of the shear stresses at the start of the run-up, so the morphological module is not longer applicable. It is possible to implement different empirical relations for the different stages of the morphology, which all need a separate validation and/or calibration. However, this is a

time consuming process and will always keep an uncertainty when the conditions differ. Another solution could be found in the use of a numerical part in the model. It can be expected that a higher accuracy can be reached with the implementation of the numerical shallow water equations, as these equations account implicitly for the difference in morphological stages and the resulting types of wave breaking. This has been done in models like X-Beach (Roelvink et al., 2015). This will remove the benefits of the simplicity of a process based approach, that allows an easily implementation for additional processes, but will increase the accuracy of the model. Also, the computation time will increase.

Once the model is fully developed and validated for the different morphological phases, it may constitute an useful tool for designs. Processes can easily be added, resulting in a model with many opportunities, such as implementing the growing process of sowed vegetation or adding a wave damping structure at the start of the terrace slope. Another benefit is the variety of output results that can be generated. As the model has been build in Matlab, it can easily run multiple times with a varying input, so an estimate can be made for the changes of any input value. As only the main processes are included, multiple results are often generated within a minute.

The model results show that the dominant processes for erosion can be found at the point of wave breaking and at the start of the run-up, as both combinations give the highest wave height compared to the local water depth. This can be used for a strategic placement of vegetation in order to dampen the wave impact and reinforce the soil through the roots. There are situations in which a partially vegetated shore is sufficient to withstand the daily wave attack. This allows the vegetation to grow naturally to full strength, which is required in a storm situation. In this way a financial benefit can be reached as well as a healthier vegetated shore, as a large part of the vegetation has grown naturally.

Contents

1

Introduction

1.1. Background

Shores along lakes are among the most valuable areas of the landscape in terms of recreational and ecological values (Comoss et al., 2002). The shore vegetation plays an important role as an ecosystem engineer (Bouma et al. 2005) which is difficult to replace by traditional shore protection methods (Cacabelos et al., 2016).

Due to the importance of the shores, local authorities of countries such as The Netherlands, Germany, Switzerland and the V.S are responsible for protecting the reed and defending the natural coastline from erosion, since the 1960s (Ostendorp et al., 1995).

When looking at the traditional way of solving erosion problems along the shoreline, many hard solutions like rip-rap and sheet piles are found. This can be explained by the ease of hard structures to adapt to different situations and the extensive amount of research made accessible in user-friendly manuals, such as the Rock manual. However, the use of those traditionally hard structures also has a downside. Multiple studies suggest that a traditional structure cannot replace the different functions of a natural habitat and has unforeseen negative influences on the local ecology (Borsje et al., (2011); Cacabelos et al., 2016). Comoss et al. (2002) stated that the erosion protection techniques which are traditionally used, are costly and can detract from the natural environment. Traditionally structures mainly fail to provide the habitat heterogeneity found on most natural shores, even when local materials are used (Cacabelos et al., 2016).

Currently the main focus on vegetation in shore protection is reducing the hydrodynamic loads (Dalrymple et al., 1984; Mendez and Losada, 2004). In addition to protection agianst these loads, the vegetation creates a bio diverse space for many other species. For example, it forms the shelter and spawning location for different kinds of fish (Nash et al., 1999), allows some turbulence in order to refresh the water (Bouma et al., 2005) and traps nutrient rich sediment (Koch, 2001) which is used by many different submerged vegetation.

A clear example of the importance of the use of vegetation as shore protection can be found along Lake Erie (Comoss et al., 2002). In previous years the erosion along Lake Erie was countered by the placement of large stones as riprap along the shoreline which resulted in a fragile ecosystem with a non-natural appearance. A low cost renovation project was conducted with innovative erosion protection measures. The project goal was to combine the beneficial use of dredged material, indigenous vegetation and landscaping to reduce sediment loading into Lake Erie, and to protect the recreational aspects of Presque Isle State Park, which lays along Lake Erie (Figure 1.1). As a result, a large amount of natural values are added to the shore due to the decrease of nutrient run-off and soil entering lake Erie.

(A) Before renovation   (B) After renovation
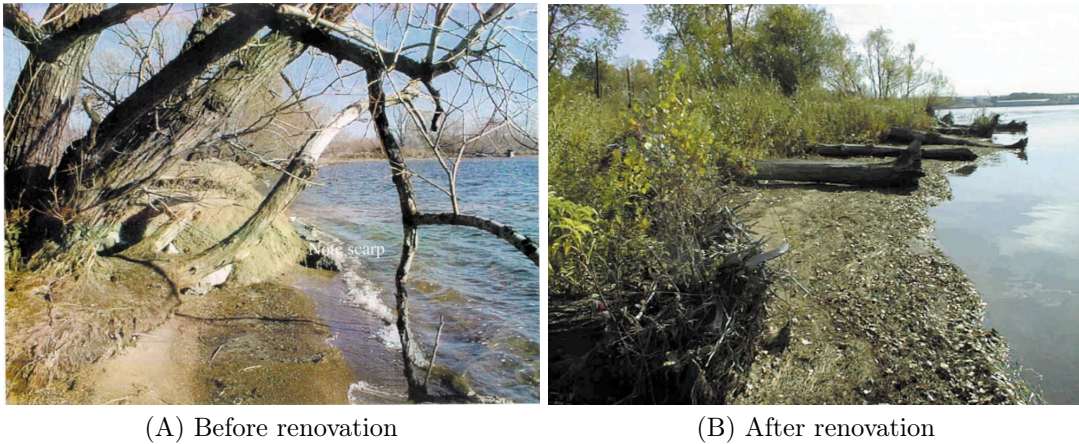
Figure 1.1: Shoreline along Presque Isle State Park before and after renovation in which the natural environment stands central (Comoss et al., 2002).

1.2. Problem description

Designing a nature based shore protection brings multiple challenges in the design process. One of those challenges is the ecological boundary condition for different species (Ministerie van Verkeer en Waterstaat,1999b). Another challenge is the restricted amount of monitoring data, which is needed for successful implementations (Borsje et al., 2011). Furthermore the amount of given protection by a successful implementation has a high uncertainty.

Multiple recent studies focus on the impact of vegetation on the shore hydrodynamics in order to give a better estimation of its role in shore protection (Chen et al., 2018; Nepf, 2011; Sonnenwald et al., 2018). The research was conducted in order to quantify the influence of different vegetation parameters, such as density and stem arrangement, on the capability of vegetation on wave damping and sediment trapping. This way a dynamic interaction between ecology and engineering can be established. There is still a need for a generic framework in order to decide which species of ecosystem engineers can be used in which situation (Borsje et al., 2011).

1.3. Research question

For shore protection, soft, nature based solutions are preferred as they are favorable for the local habitat, water quality, the appearance of the shore and can be very cost efficient if applied correctly (Comoss et al., 2002). The use of vegetation to reduce bed shear stresses has already proved its potential, but for an optimal use the scientific basis is not yet sufficient. This could reduce the natural aspect (Sayah et al., 2004). In order to improve the design of shore protection in a natural way, insight is needed in the influence of different design choices. Consequently, the following research question is formulated:

How to estimate the contribution of reed-like vegetation, specifically *P. australis*, towards the shore protection along a lake against hydrodynamic loads using a process based model.

In order to answer the main question the following sub questions are formulated.

1. Which effects of reed-like vegetation are important to consider based on the shore hydrodynamics and erosion processes?
   For the use of a process based model the different processes affected by the presence of vegetation need to be added separately. Therefore it must first be understood in which way the vegetation effects the shore hydrodynamics and which of those effects are important to reproduce the erosion processes.

2. How can the model of Duró et al.(2020) be used to estimate the induced bed shear stresses at a reed-like vegetated shore in a lake situation?
   The original model of Duró et al. (2020) is developed to estimate the final morphological state along the Maas based on the induced bed shear stresses of ship waves. It can be questioned how and if vegetation can be added and in which way the model needs to change in order to calculate the shore processes along a lake.

3. Which parameters, concerning the hydrodynamics, morphodynamics and vegetation characteristics, have a high influences in a reed-like shore protection?
   When modelling and/or designing a vegetated shore, knowledge about the importance of the main parameters is needed in order to determine which parameters and/or measurements are in need of additional care. This way a higher accuracy can be reached without investigating all the parameters in detail.

1.4. Methodology

In order to get a better understanding of the influence and the limitations of vegetation, a literature study is conducted for the required background information. The model of Duró et al. (2020) is modified in order to show the induced bed shear stresses, so the interaction between vegetation and the resulting shore erosion for a lake can be studied. The modified model of Duró et al. (2020) is specified for common reed, *P. australis.*

The implementation for vegetation in the modified model of Duró et al. (2020) is validated based on the shallow water model of Mendez and Losada (2004), experimental data from Dubi (1995) and Wu et al. (2011). The amount of induced bed shear stresses has been compared with the model results of SWASH. Since the morphology module of the model of Duró et al.(2020) has been tested and validated, a correct morphology has been expected when the amount of induced shear stresses is correct.

Multiple model runs are made in order to show the sensitivity of the induced bed shear stresses resulting in shore erosion to the different aspects included in the modified model of Duró et al. (2020). A distinction has been made between the model sensitivity and the sensitivity of the hydrodynamic and shore properties

1.5. Reading guide

In order to answer the main question " *How to estimate the contribution of reed-like vegetation, specifically P. australis, towards the shore protection along a lake against hydrodynamic loads using a process based model.*" a literature study is conducted (Chapter 2) in order to get a better understanding of the hydrodynamic processes responsible for erosion along the shore and the influence of vegetation on those processes. Besides the role of vegetation in shore protection, a short elaboration is conducted on different wave breaking structures which could assist the protecting role of vegetation. At last different models resolving the morphology shore changes have been compared in order to choose the basis for this research.

In Chapter 3 different aspects concerning the wave attenuation through vegetation in a lake environment are added and tested towards the model of Duró et al. (2020). The model is specified in order to show how the influences of common reed, *P. australis*, can be estimated. The following chapter discusses the results of the tested aspects and the resulting consequences. Based on those findings conclusions are made concerning the restrictions of the model. Keeping those restrictions in mind, a sensitivity analysis is made in order to determine the dominant processes for the final shore equilibrium. In Chapter 6 a final elaboration is given on the overall model resulting in an answer on the main research question.

2

Literature Background

Natural shores often disappear or degrade through a lack of attention for the combined impact of the ecological and hydrodynamic forces. Examples of actions which result in a reduction, or even disappearance of the nature based shores are an uniform design along the shores, heavy shore protection measures, reduction or removal of the natural water level variation, wave attack, lowering of the water quality, poor maintenance and various kinds of recreation (Rijksoverheid, 2011). In order to keep, or even increase the ecological quality of a lake the attention of a healthy shore zone is needed. To succeed, insight is needed into the different processes along the shore, for both the ecological and for the hydrodynamic aspects (Rijksoverheid, 2011).

In this chapter a short overview is given in order to capture the main processes on the hydrological side concerning: shore attack, the role of vegetation and finally different additional measures to protect the shore on a nature based way.

2.1. Shoreline hydrodynamics

2.1.1. Lake circulations

The water flow in a lake can be driven by various mechanism. The best known mechanism in lakes are the wind and heat driven motions (Cushman-Roisin, 2012).

Wind driven circulation

The friction induced by the wind on to the water surface leads to surface stresses. Those surface stresses results in a current in the same direction as the wind. Through boundary conditions a return current will be created. The surface stresses will interact with the layers below which results in turbulent mixing in the vertical layers (Cushman-Roisin, 2012).

Heat driven circulation

The heat fluxes in a lake are created by the temperature variations during the day/night cycles and the summer/winter cycles. During heating a vertical stratification will accrue. As a result the intermediate and the bottom waters are shielded against the wind driven influences. When the water surface temperature drops a downward water flux will occur which results in the mixing of the different water layers. Through this process the oxygen rich layers on the surface will be mixed with the lower, oxygen poor layers. This results in the ventilation of the water in the lake (Cushman-Roisin, 2012).

2.1.2. Wind waves

Wind waves are generated by the friction between wind and the water surface. When the wind has an infinite length to interact with the surface in order to create waves (fetch length) and the waves are not restricted by the depth the relation between wind velocity and wave height/length can be described with a simple, empirical relation (Equation 2.1 and 2.2).

In the case of a limiting depth or a limiting fetch the relation becomes more complex. The resulting relation is still empirical and has been shown in Equation 2.3 and 2.4. These relations are called the Sverdrup-Munk-Bretschneider equations (Schiereck, 2001).

Unlimited water depth and fetch length:

$$\frac{gH_s}{u_w^2} = 0.283 \tag{2.1}$$

$$\frac{gT_s}{2\pi u_w} = 1.2 \tag{2.2}$$

Limited water depth and fetch length:

$$\frac{gH_s}{u_w^2} = 0.283 tanh\left[0.578\left(\frac{gh}{u_w^2}\right)^{0.75}\right] tanh\left[\frac{0.0125\left(\frac{gF}{u_w^2}\right)^{0.42}}{tanh\left[0.578\left(\frac{gh}{u_w^2}\right)^{0.75}\right]}\right] \tag{2.3}$$

$$\frac{gT_s}{2\pi u_w} = 1.20 tanh\left[0.833\left(\frac{gh}{u_w^2}\right)^{0.375}\right] tanh\left[\frac{0.077\left(\frac{gF}{u_w^2}\right)^{0.25}}{tanh\left[0.833\left(\frac{gh}{u_w^2}\right)^{0.375}\right]}\right] \tag{2.4}$$

where: H_s = Significant wave height generated by the wind
          T_s = Significant wave period generated by the wind
          u_w = Wind velocity
          h = Water depth
          F = Fetch length

2.1.3. Ship waves
The disturbance of the water by a ship can be divided in the following category's:

- Primary Wave

- Secondary wave

Primary Wave
The influences of the primary wave depend on the ships characteristics and its surroundings. The primary wave originates from the depression of the ship, the smaller the channel in comparison with the ship width, the larger the depression and the return current. in comparison to a ship, a lake has a large width, thus the primary wave will be negligible (Schiereck, 2001).

Secondary wave
The size of secondary waves depend on the ships geometry. When a ship is less streamlined, so has a higher blocking factor, higher waves will be generated. The pressure pattern resulting from the water displacement of the ship shows a wave train, formed by a number of periodic waves. An empirical approach to determine the wave height has been shown in Equation 2.5 (Schiereck, 2001).

$$\frac{H}{h} = \zeta \left(\frac{s}{h}\right)^{-1/3} Fr^4 \tag{2.5}$$

where: H = Wave height

h = Water depth

ζ = Coefficient to represent the ships geometry, reasonable upper limit is 1.2

s = Ship-shore distance

Fr = Froude number, for modurate speed Fr = 0.75 can be assumed.

2.1.4. Flow induced bed shear stresses

For laminar flow the bed induced shear stresses are proportional to the velocity. When the flow becomes turbulent, the velocity term becomes quadratic.

laminar flow

$$\tau \sim u \tag{2.6}$$

turbulent flow

$$\tau_b = c_f \rho \bar{\bar{u}}^2 \tag{2.7}$$

where: τ_b = Bed shear stress

c_f = Bottom roughness

$\bar{\bar{u}}$ = Velocity averaged over time and depth

In order to model bed erosion an often used approach is using the differences between the bed shear stresses and the critical shear stresses. The critical shear stress depends on the bed properties and is often formulated in a single value. As erosion is a process that evolves gradually an often used equation for erosion is as followed:

$$E = M(\tau_b - \tau_c)^n \tag{2.8}$$

where: E = Amount of erosion

M and n = model variables

τ_b = induced bed shear stress

τ_c = critical shear stress

2.1.5. Wave induced bed shear stresses in shallow water

Near shores shallow waves can be expected. Since the waves are short, a boundary layer can not be developed and the horizontal orbital velocity's of the surface waves remain almost constant in size until the bottom, this has been illustrated in Figure 2.1. To calculate the wave induced surfaces friction the following formula's can be used (Schiereck, 2001):
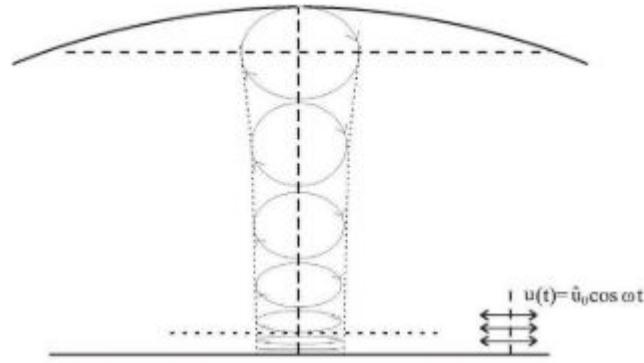
Figure 2.1: Illustration of the orbital velocity below shallow waves, resulting in an orbitol velocity near the bed. (Bosboom and Stive, 2012)

$$\hat{\tau}_w = \frac{1}{2}\rho_w c_f \hat{u}_b^2 \tag{2.9}$$

$$\hat{u}_b = \omega a_b = \frac{\omega a}{sinh(kh)}; \qquad \omega = \frac{2\pi}{T}; \qquad k = \frac{2\pi}{L} \tag{2.10}$$

where: $\hat{\tau}_w$ = Amplitude of the shear stress induced by waves
   ρ_w = Water density
   c_f = Bottom roughness, estimated to be 0.045 for the shore by Lohrmann, (2018)
   $\hat{u}_b$ = Amplitude of the bed velocity
   a_b = Horizontal amplitude of the wave on the bed surface
   a = Wave amplitude ($H/2$)
   h = Water depth
   T = Wave period
   L = Wave length

For the bottom roughness Jonsson(1966)(cited from Schiereck, 2001) experimented with the turbulent flow over a rough bed and formulated an expression that has been reformulated by Swart (1991) (Equation 2.11). With very short waves values between the 0.1-0.3 are possible, with 0.3 as a maximum value for the bottom roughness. Those value's are a lot higher than for uniform flow (g/C^2), where the values are in the order of 0.001 (Schiereck, 2001).

$$c_f = exp\left[-0.6 + 5.2(a_b/k_r)^{-0.19}\right] \qquad with : c_{fmax} = 0.3 \tag{2.11}$$

where: k_r = Roughness equivalent of the bottom
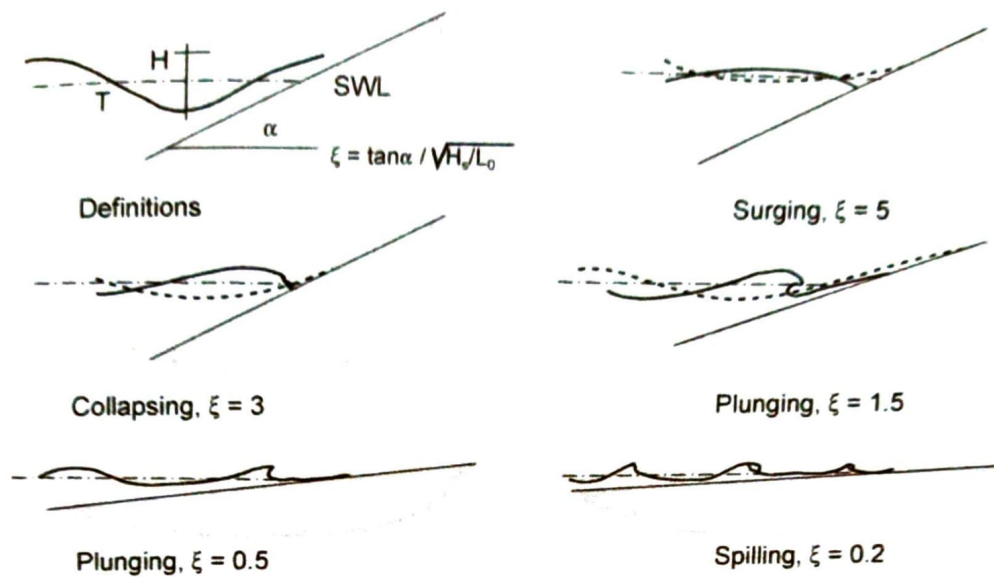
Figure 2.2: Different types of wave breaking for different Iribarren numbers (Schiereck, 2001)

2.1.6. Breaker type

The impact of a wave on a slope does not only depend on the incoming wave characteristics, but also on the breaker type of a wave. The breaker type of a wave has been described with a non-dimensional number, also called the Iribarren number (Battjes, 1974) (Equation 2.12). For surging waves ($\xi = 5$) the wave moves up and down the slope without air entertainment (Figure 2.2 b) which results in a minimal impact on the shore, therefore the waves in the range of $\xi = 3 - 5$ are often called surging breakers. In the range of $\xi = 2.5 - 3$ the waves start to break. When the waves break on the slope ($\xi \approx 0.5 - 3$) it encloses an air pocket which results in an impact on the slope similar to a water jet. When the slope decreases further ($\xi < 0.3$) the formed water jet is projected forward and spilling waves are formed (Schiereck, 2001). The main breaking types are illustrated in Figure 2.2.

$$\xi = \frac{tan(\alpha)}{\sqrt{H/L_0}} \tag{2.12}$$

where: ξ = Iribarren number
α = slope
H = Wave height
L_0 = offshore wave length

2.1.7. Wave run-up

During a wave period the water level along the slope will increase and decrease. The maximum water level on the slope is called the wave run-up and the lowest point is called the maximum wave run-down. The size of the run-up and run- down is important concerning the energy dissipated by a certain area of the shore. (Schiereck, 2001). The total wave run-up on a slope exist of 3 components, the static set-up, dynamic set up and the incident wave run-up.

$\bar{\eta}$, static set-up

When waves are propagating towards the shore a horizontal flux will be generated consisting of the transport of momentum ($\rho\bar{u}$) and a wave induced pressure force (p_{wave}). By integrating the horizontal flux over the depth the transport over the entire plane can be obtained.
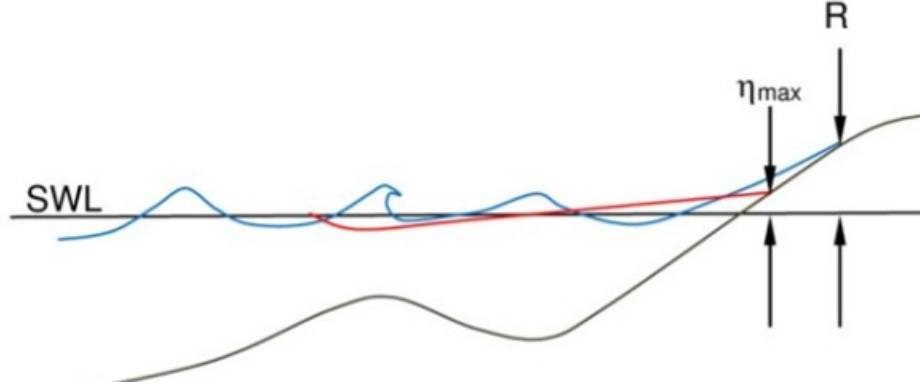
Figure 2.3: Components contributing to the total wave run-up are the maximum wave setup (η_{max}) and the wave runup (R) (Melby et al., 2012).
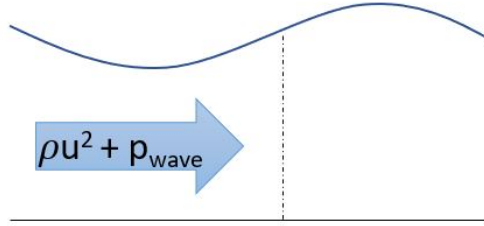
Figure 2.4: Transport of momentum (ρ u) with the partial velocity u, combined with the induced wave pressure (p_{wave}), results in a horizontal transport of wave-induced momentum.

Integrating over time results in the total wave average momentum transport S. As it consists of the transport of the x momentum in the x direction the subscript xx has been added (Bosboom and Stive, 2012).

$$S_{xx} = \overline{\int_{-h}^{\eta} (\rho u_x dz)} + \overline{\int_{-h}^{\eta} p_{wave} dz} \tag{2.13}$$

$$\text{where:} \quad \begin{aligned} S_{xx} &= \text{Radiation stress} \\ h &= \text{Water depth} \\ \eta &= \text{Wave setup} \\ p_{wave} &= \text{Pressure induced by waves} \end{aligned}$$

So the force induced by the radiation stresses at an alongshore uniform coastline can be described as followed:

$$F_x = -\frac{dS_{xx}}{dx} \tag{2.14}$$

On a slope an equilibrium between the radiation stress gradient and pressure term can be written as followed (Bosboom and Stive, 2012):

$$-\frac{dS_{xx}}{dx} = \rho g(h + \overline{\eta}) \frac{d\overline{\eta}}{dx} \tag{2.15}$$

When waves decrease inside a vegetated field the radiation stresses will decrease as well what results into a force directed towards the direction of propagation. So, following the same logic as in Equation 2.15, the decrease in radiation stresses will lead to an increase in water level

elevation. At the same time a water level set down will take place caused by the drag force induced by the vegetation. In order to calculate the wave set-up through the interaction of waves with a vegetated field Dean and Bender (2005) derived the following equation:

$$\frac{d\eta}{dx} = \frac{1}{\rho_w g(h+\bar{\eta})} \frac{C_D \rho g D H^3}{12\pi S^2 h} \left(\frac{3}{2} - 1\right) \qquad (2.16)$$

where: C_D = Drag coefficient of the vegetation
ρ_w = Water density
g = Gravitational constant
D = Stem diameter
H = Wave height
h = Water depth
η = Set-up
S = Hart to hart distance between stems

$\hat{\eta}$, dynamic set-up
Through the smaller oscillating motions in waves induced by wave groups and infragravity waves, a second compound of the wave induced set up arises, the dynamic set-up. The effect of the smaller oscillating motions on the set-up through vegetation has not yet been investigated as it knows a small influence. For this reason this aspect will be neglected in this study, as the contribution is often small compared with the static set-up.

R_u, incident wave run-up
The incident wave run-up on a smooth slope for breaking waves ($\xi = 2.5 - 3$) can be described with the use of the Hunt's equation (Equation 2.18) who used the Iribarren number (Equation 2.17)) and the incident wave height. For the range of ($\xi = 2.5 - 3$) the wave run-up reaches the highest value's (Schiereck, 2001) but many different derivations can be found in the literature as can be seen in the paper of Didier et al. (2016).

$$\xi = \frac{tan(\alpha)}{\sqrt{H/L_0}} \qquad (2.17)$$

$$\frac{R_u}{H} = \xi \qquad (2.18)$$

where: ξ = Iribarren number
α = Slope angle
H = Wave height
L_0 = Offshore wave length
R_u = Vertical wave run-up

2.2. Shoreline morphodynamics
In recent years the hard, traditionally measures in order to control bank erosion have taken place for approaches in which is searched for the balance between technical and ecological requirements were some natural processes are allowed. When erosion of a bank is allowed, an understanding is needed of the final extend of the bank retreat. In order to increase habitat suitability, a diverse morphology is preferred. Wave attack increases the shore variability, but through the induced shear stresses, resulting in sediment re-suspension and the mobilization of nutrients and chemicals, the quality of the local ecosystem will be decreased.

In order to define potential ecological improvements and evaluate management strategies a good understanding of the shore profile evolution is needed (Duró et al., 2020).

2.2.1. Equilibrium profile

When an unprotected shore is encountered by a wave attack the largest interaction between the waves and the shore will take place at the terrace. Through the shear stresses induced by the terrace the wave energy will decrease. The shear stresses induced by the wave results in erosion along the terrace, while at the same time the breaking of waves add sediments to the Terrace. When the waves reach the upper bank the induced impulse forces will erode the upper bank, the eroded soil will partly be re-distributed over the terrace as well. As a result the Terrace length will increase and thus the waves reaching the upper bank will decrease. At a certain point the shear stresses induced by the waves will no longer be sufficient to erode the Upper bank and Terrace, so an equilibrium profile will be reached (Duró et al., 2020).
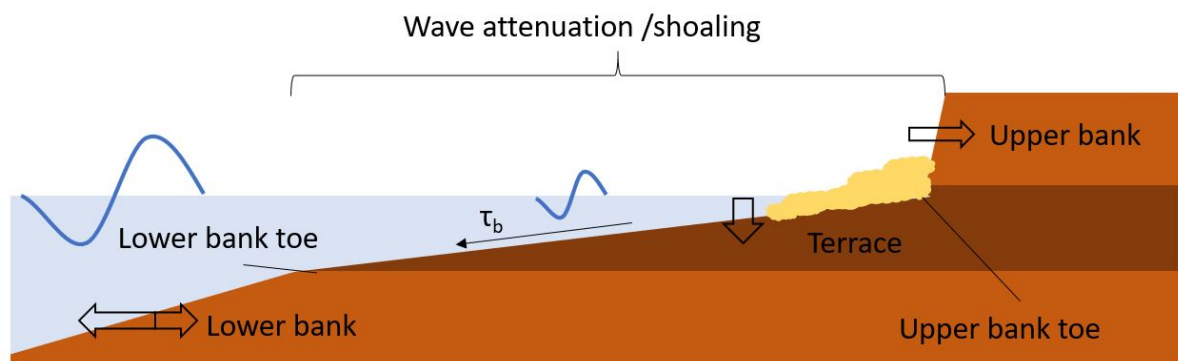
Figure 2.5: Schematic bank profile showing the induced bed shear stresses τ_b, location of wave attenuation/shoaling and the movement directions of the lower bank, terrace and the upper bank by erosion.

2.2.2. Differences in bank retreat

When two different stretches of shores are affected by the same circumstances the resulting erosion rates and equilibrium profiles can still differ. Important factors in the erosion rate of a shore are the lithology and either the vegetation (Section 2.3) or the gravel armouring at the upper-bank toe, depending on which one is used. This combination determines the impact of the secondary waves.

Lithology layers can lay random in the ground but have a high influences on the erosion rate of the shore. When an area is not subject to erosion it shelters the surrounding areas as well. Sharp angles along the shoreline can be expected, these will eventually become smooth over time. In order to capture the influences of the different soil cohesion's three cohesion groups have been distinguished (C1 for low, C2 for middle and C3 for a high cohesion) which have been compared with the waterlevel above the lower bank toe and the terrace length. These parameters obtained along the Maas, summarised with the use of a Kernel density function, represent two of the main parameters defining the terrace. In Figure 2.6 it can be seen that their is indeed a general correlation, so a high impact of the soil cohesion on the rate of erosion of the shore can be expected.
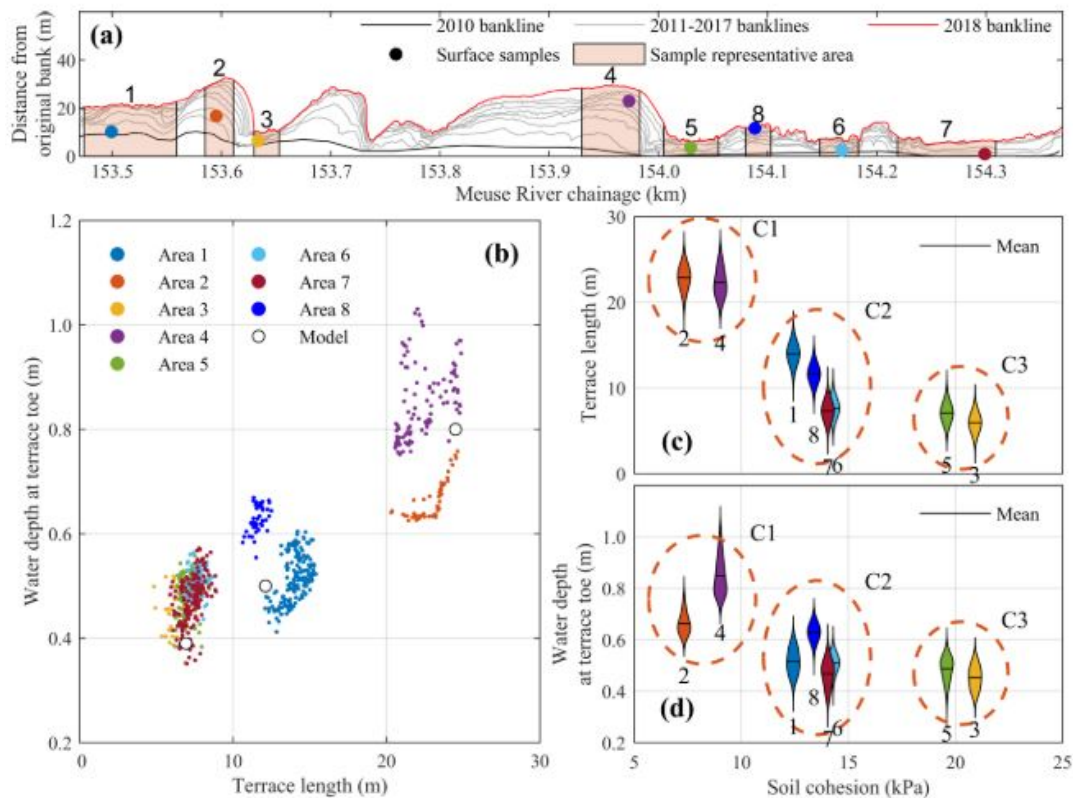
Figure 2.6: Different terrace characteristics defined by different lithologies after seven years of development (Duró et al., 2020). (A) semplel locations, (B) Toe depth and terrace lenght for the different locations after 7 years, (C)Terrace lenght with corresponding soil cohesion, (D) Toe depth with corresponding soil cohesion.

2.3. Vegetation as shore protection

Vegetation plays an important part for the shore protection, as it reduces the forces attacking the shore and increases the shore strength. But it is also important for the ecological functions, as it forms the bridge between land and water. A shore has also a large influence on the experience of the landscape (Ministerie van Verkeer en Waterstaat,1999b).

2.3.1. Time depended solution

There are a lot of different species of vegetation, all with their own characteristics in space and time. An important point to consider is the fact that plants need to grow. For example, for newly grown vegetation a wave attack in the first year is undesirable while a frequently wave attack with waves of 0.25m does not give any problem after two years (Ministerie van Verkeer en Waterstaat, 1999a). In the first two years a temporal construction can be needed to protect the shore and the newly grown vegetation.

Over time the characteristics of the vegetation can change through the closing up of the shore resulting from extensive growth or souring of the bed. This will change the amount of protection of the shore, so mostly maintenance is needed to keep the intended characteristics. There are multiple options for a maintenance planning. For example, small maintenance once a year to keep the plants pioneer characteristics, or once in the few years removing a lot of the created slib and the larger plants (Sollie et al.,2011).

2.3.2. Drag coefficient

In order to include the characteristics of a certain vegetation field on the energy reduction many formula's include the drag coefficient C_D, as can be seen in Equation 2.27. An analytical description of the process of the interaction between waves and vegetation requires

reproducing the physical processes. Multiple studies have been conducted in order to describe those physical processes, in which the flow can be reduced with a factor 2 to 10 by the presence of vegetation (Koch et al., 2006).

The vegetation is subject to a drag force induced by the velocity differences between the vegetation and the surrounding flow. The different stem characteristics influencing the amount of drag force are Form and Friction drag (Appendix A.1.1), resulting Reynolds number (Appendix A.1.2), surface roughness (Appendix A.1.4) and the influences through vortex shedding (Appendix A.1.5).
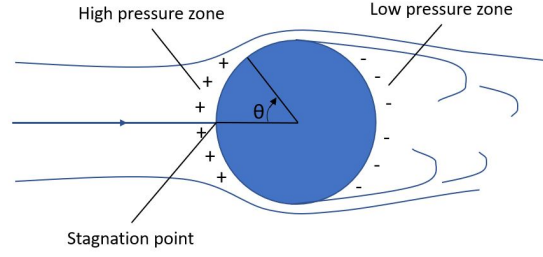
Figure 2.7: Drag induced on the vegetation resulting from the pressure differences.

Not only the stem characteristics influence the amount of damping of the vegetation, but also the interaction between the stems are of importance. Lima et al. (2006) (cited in Anderson et al., (2011)) concluded that the canopy drag was on average four times higher than the summation of the individual drag forces. One of the most important parameters is the stern density, which has a large influence on the blockage and the sheltering effect (Appendix A.2.1).

Since many different processes influence, the canopy drag coefficient it is difficult to derive an equation that will encounter all the processes based on the indifidual (Appendix A.1) and canopy characteristics (Appendix A.2). Often a formula has been calibrated in order to describe the canopy drag (as in Equation 2.19 derived by Sonnenwald et al. (2019)). Also analytical approaches have been used (as in eq 2.20 derived by Etminan et al. (2019)) in order to derive a canopy drag coefficient.

$$C_D = 2\left(\frac{6475D + 32}{Re_D} + 17D + 3.2\phi + 0.50\right) \tag{2.19}$$

where: C_D = Drag coefficient
D = cylinder diameter
Re_D = Cylinder Reynolds number
ϕ = Solid volume fraction

$$C_{D,c} = 1 + 10Re_c^{-2/3} \tag{2.20}$$

With:

$$U_c = \frac{1 - \lambda}{1 - \sqrt{\frac{2\lambda}{\pi}}} U_p \tag{2.21}$$

where: $C_{D,c}$ = Drag coefficient based on the constricted cross-section velocity

Re_c = Reynolds number based on the constricted cross-section velocity

U_c = Constricted cross-section velocity

λ = Canopy density or solid fraction

U_p = Pore velocity

The influence of the oscillatory motions in waves add an additional difficulty for the deriving of the canopy drag coefficient. Chen et al. (2018) has given an overview of the different formula's found in literature (Appendix A.2) in order to include the orbital waves motions. It can be noted that none of the formulations is derived analytically so the dependency of the tested environment should be considered. From the table one of the most promising equations for regular waves is from Losada et al. (2016), as it is tested for real vegetation and knows a R^2 of 0.60.

$$C_D = 0.08 + (50,000/Re)^{2.2})$$ (2.22)

2.3.3. Wave damping
One of the most used characteristics of vegetation in hydraulic engineering is the effect of wave damping. Vegetation exerts resistance forces on the flow, which removes part of the wave energy. The amount of removed wave energy is difficult to estimate as not only the individual characteristics are important, but also the group dynamics. This is illustrated by the fact that the friction added to the water by vegetation is approximately four times higher than the summation of the individual stem resistances. This suggests that the stem interaction has an even higher importance than the individual stem resistance (Anderson et al., 2011).

There are a lot of different studies conducted in order to describe the wave dissipation of vegetation. This results in a lot of different equations that can be used but several overall trends can be distinguish (Anderson et al., 2011):

- The total wave dissipation will be increased by a longer vegetation field.

- The total wave dissipation will be higher with a higher stem density.

- The total wave dissipation will increase slightly with larger incident wave heights.

- An increase in water depth leads to a decrease of wave dissipation.

- A clear trend with respect to the wave period is not observed.

Different kinds of vegetation influence the waves in different ways. An example is the oscillatory movement of vegetation with blades in lower orbital velocities, where the blades will be swaying in phase over the entire wave circle, while the blades extend in the direction of the flow by higher orbital velocity's, what leads to a reduction in drag and less attenuation. The in-phase movement at low frequency's (0.38 Hz) and out of phase movement at higher peak frequency's (0.67Hz) leads to an expected shift in the probability density function of a wave field, but a significant shift was not observed (Anderson et al., 2011).

Also the stiffness of vegetation has large influences on the interaction between the vegetation and the waves. Vegetation with a low stiffness will move with its surroundings while vegetation with a high stiffness will deflect the currents and waves with an angle of 90 degrees. A prediction has been made that the dissipation of flexible stems was approximately 30% of the dissipation of stiff stems(Mullarney et al.(2010, cited in Anderson et al., (2011)). Often the bulk drag coefficient C_d has been used to represent the specie specific characteristics, which is empirically determent (Anderson et al., 2011).

The effects of individual stems are a result of plant material properties, surface textures and architecture. Those factors are determent by the kind of specie, but also by the environment, which the specie is adapted to. A vegetation field may vary even more in terms of composition and structure. As they are in competition with different species and need to interact with the fauna community (Anderson et al., 2011).

Considering all variations formulating a single parameter is nearly impossible, so the large amount of equations concerning the interaction between waves and vegetation is not a big surprise.

According Bradley and Houser(2009) the wave attenuation in different literature has been described by the exponential Equation 2.23.

$$\frac{H_t}{H_i} = e^{-k_i \delta x} \tag{2.23}$$

where: H_i = Incoming wave height
H_t = Transmitted wave height
δx = Distance between H_1 and H_2
k = Attenuation coefficient, vegetation related, varying between 0.01 and 0.05
(Kobayashi et al., 1993; Möller et al., 1999) referenced by Bradley and Houser (2009)

In Equation 2.24 the wave dissipation is described specific for reeds. To account for the seasonal influences the factor p has been introduced (Ministerie van Verkeer en Waterstaat, 1999a):

$$H_t/H_i = 1 - p(1 - exp(-0.001(N)^{0.8} * B_{eff})) \tag{2.24}$$

where: H_i = Incoming wave height
H_t = Transmitted wave height
N = Number of stems per m^2
p = Seasonal influence
for reeds: first quart 0.2, second quarter 0.8, third quarter 1, forth quarter 0.6

$$B_{eff} = B(cos\beta)^{-1} \tag{2.25}$$

where: B = width of the vegetation
β = angle of attack

Dalrymple et al. (1984) studied the wave dissipation through an array of vertical cylinders, representing a vegetation field. He derived an analytical formula in which the wave energy dissipation is the result of the horizontal drag force. For this equation the assumption has been made that all the energy of the mean flow is converted to turbulent energy (Stam, 2018).

$$E = \frac{1}{8}\rho_w g H^2 \tag{2.26}$$

Neglecting the inertia forces in the vegetation and using the dispersion relation for waves Dalrymple (1984) expressed the energy dissipation by waves as followed (Mendez and Losada, 2004):

$$E_{diss} = \frac{2}{3\pi}\rho_w C_D b_v N \left(\frac{kg}{2\sigma}\right)^3 \frac{sinh^3(k\alpha h) + 3sinh(k\alpha h)}{3kcosh^3(kh)} H^3 \tag{2.27}$$

$$H = \frac{H_0}{1 + \beta x} = K_v H_0 \tag{2.28}$$

$$\beta = \frac{A_0 H_0}{2} = \frac{4}{9\pi}C_D b_v N H_0 k \frac{sinh(k\alpha h)^3 + 3sinh(k\alpha h)}{(sinh(2kh) + 2kh)sinh(kh)} \tag{2.29}$$

where: ρ_w = Water density

b_v = Plant area per unit height of each vegetation stand normal to u

N = Stem density

k = wave number

g = Gravity constant

σ = Angular wave frequency

α = Relative vegetation height

H = Wave height

H_0 = Wave height in previous grid

A downside of Dalrymple et al.'s (1984) formula is the neglecting of the reflection induced by the vegetation and assumed that the horizontal movement of the stems is minimal compared with the orbital wave velocity, so the vegetation can be represented by a rigid stems. This assumption results in a large induced drag force on the waves (Bradley and Houser, 2009). A more detailed derivation can be found in Appendix B.1.1.

2.3.4. Soil strengthening

The soil below the vegetation will be strengthened through the presence of the roots. Just like the resistance against wave attack the amount of soil strengthening will depend on the kind and age of the vegetation(Ministerie van Verkeer en Waterstaat, 1999a). Increasing the slope stability is an often used application for the roots reinforcement. An important thing to keep in mind is the fact that the roots become thinner and sparser with increased depth. (Yan et al., 2010). A Rule of thumb for the soil reinforcement for sand can be taken as a factor 2.5 on the maximum allowable velocity. (Ministerie van Verkeer en Waterstaat, 1999a). Beside the strengthening of the soil a reduction in bottom pressure, so a reduction in shear stresses is present (Ministerie van Verkeer en Waterstaat, 1999a).
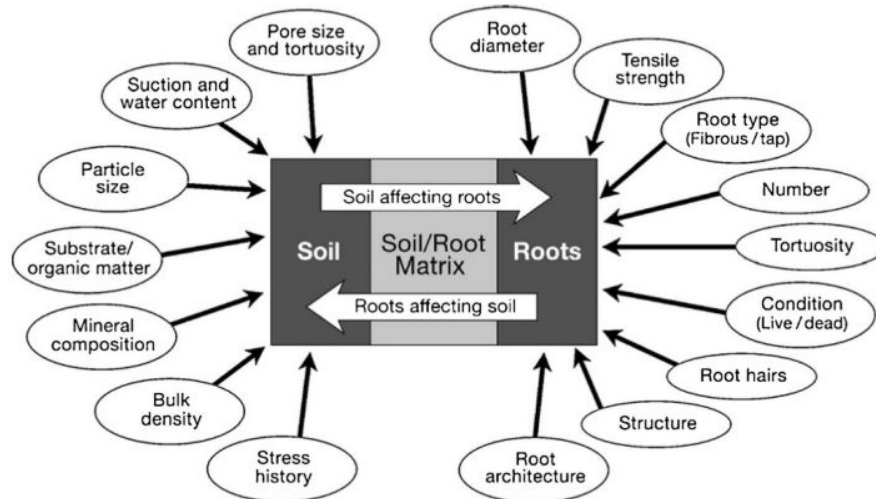
Figure 2.8: main factors affecting soil and root strength (Cazzuffi et al., 2014)

In Figure 2.8 it can be seen that the induced strength of the soil by vegetation depends on many characteristics. In Figure 2.8 the main components are schematised but many different factors determine the magnitude of the reinforcement. The most important characteristics are the strength properties and the root distribution in the soil. Those characteristics are influenced by (Cazzuffi et al., 2014):

- Characters of the root system: geometrical, biochemical, genetic and morphological.

- Mechanical characteristics of the root system: tensile strength and stiffness.

- Geotechnical and biochemical characteristic of the soil in contact.

- Land use management.

- Environmental characteristics: growing location, organic matter content, interaction between different plants, climate characteristics, age, tree health.

To estimate the root cohesion (additional resistance against shear stress) Cazzuffi et al. (2014) proposed Equation 2.30, With the simplification of only vertical roots in Equation 2.31.

$$\Delta c = K * \sum_{i=1}^{N} [T_{R_i} \frac{A_{R_i}}{A}] \tag{2.30}$$

$$\Delta c \approx 1.2 T_R \tag{2.31}$$

where: K = Correction factor for the slope of the roots crossing the shear plane

T_{R_i} = The average root tensile strength per average cross sectional area of diameter class i

A_{R_i} = Cross sectional area of the root class i

A = Specimen area

T_R = Mobilized tensile force in roots per unit area of soil

Yan et al. (2010) considers not only the additional shear strength Δc but also the increase in bearing capacity of the soil by herbaceous roots, which are usually fibrous roots with diameters less than 1 mm which decreases even when the soil depth increases(Yan et al., 2010). Due to constrains of the lateral expansion of the soil mass, so increasing σ_3 and σ_3' while σ_1 stay's constant, results in the increase of the bearing capacity. He assumes that the stability of the slope soil mass is mainly determent by three factors as shown below, what results in Equation 2.32.

- τ_0, Shear strength of the original soil

- τ_x, increment of shear strength contributed by the roots

- Δc, additional cohesion contributed by the roots

$$\tau = \tau_0 + \tau_x + \Delta c \tag{2.32}$$

$$\tau_0 = c_0 + \sigma tan\phi_0 \tag{2.33}$$

$$\tau_x = \sum_{j=1}^{n} T_j cos\theta_j \left(\sum_{j=1}^{n} T_j sin\theta \right) tan\phi \tag{2.34}$$

where: c_0 = Cohesion without roots

σ = Soil strength without roots

ϕ_0 = Internal friction angle without roots

θ = Angle between roots and the horizontal plane

ϕ = Internal friction angle of the soil mass

T = Tensile strength of a single root

Yan et al. (2010) conducted experiments with different root density's to determine τ related to σ and showed that the increase of root density has an enormous effect on the cohesion, but little effect on ϕ (see Table 2.1). ϕ tells something about the contact area between the roots and the soil, which stay's small. Further, c tells something about the strength of the soil, which is dominated by the roots. For the cohesion Yan et al. proposes the following Equation 2.35:

$$\Delta c = kV_t - b \tag{2.35}$$

where: K and b = cohesion effect coefficients which are root specific

V_t = the root density

Table 2.1: Influance of the root density on different soil strenght parameters for Vetiver Grass (Yan et al., 2010)

influence root density			
Root density [kg/m^3]	cohesion c[KPa]	internal friction angle ϕ [degree]	linear equation of the shear strength
0	10.0	22.4	$\tau = 0.413\ \sigma +10.0$
24.89	17.5	23.1	$\tau = 0.428\ \sigma +17.5$
41.48	24.3	25.2	$\tau = 0.471\ \sigma +24.3$
58.14	33.8	26.7	$\tau = 0.503\ \sigma +26.7$

2.4. Vegetation Parameters, *Phragmites australis*

Many different kinds of vegetation can be found in the shoreline, each with their own characteristics. Common reed (hence after *P. australis*) is one of the most common kind of vegetation along the European wetlands, such as the Dutch lakes (Clevering, 1999). For this reason the model parametrization has been based on the characteristics of *P. australis*, although the parameters could easily be adjusted for different kinds of vegetation. In this section a literature study is conducted in order to find the specific characteristics of *P. australis* at look at their changes over time and space. In order to calculate the wave attenuation through *P. australis* an elaboration is made on the vegetation specific drag factor. At last the soil reinforcement by *P. australis* is studied.

2.4.1. Vegetation Characteristics

Designing ecosystem engineering measures requires constructing with living organisms, that grow and change depending on their environment. This means that the strength and resistance of the vegetation depends on the environmental factors, such as the wave climate and seasonal fluctuations. The age of the vegetation plays an important role as well.

The resistance against wave attack shows a strong development in the first 3 years after sowing. In the first year the vegetation needs to be protected as the stems are week and the root structures are still fragile. After 2 years *P. australis* can resist waves with a height of 0.25m on a daily basis or waves with a height of 0.4m for short periods (Ministerie van Verkeer en Waterstaat, 1999a).

Coops and Velde (1996) tested the influence of two different wave conditions as well as the seasonal influence in order to determine the main factor leading to the growing locations of *P. australis* and its resulting characteristics. These experiments are conducted with *P. australis* which has been grown for 3 years in a water depth of 0.5m and a wave climate with waves of 0.23m .

The maximum hydrodynamic load resisted by the vegetation depends on the mechanical property's of the stems, such as bending stiffness. The measured bending stiffness is directly related to the season, where the dead stems (February) and young shoots (June) know a lower elastic modules (*E*) than the fully grown stems in August(Coops and Velde, 1996). This is shown in Figure 2.9. Also the water depth influences the stem properties. *P. australis* is found in water depths until the 75cm (Vretare et al., 2001).

	Phragmites australis	
	June	August
Living stem density (m^{-2})	70.6 ± 6.8	45.3 ± 3.7
Total stem density (m^{-2})	166.5 ± 11.2	139.5 ± 13.0
Stem length (m)	1.81 ± 0.11	2.32 ± 0.17
Stem diameter (m)	0.0060 ± 0.0004	0.0068 ± 0.0003
Stem wall thickness (m)	0.0014 ± 0.0002	0.0012 ± 0.0001
Stem dry weight (g)	6.22 ± 1.43	12.21 ± 2.13
EI (N m^2)	0.22 ± 0.06	0.55 ± 0.16
E (GPa)	3.62 ± 0.72	6.93 ± 1.58

Figure 2.9: Seasonal influences on the characteristics of P. australis (Coops and Velde, 1996)

In both the wave exposed sections as well as the controlled sections the found mechanical properties are around the same value(Coops and Velde, 1996). Figure 2.10 illustrates the influences of the wave climate on the total stem length.
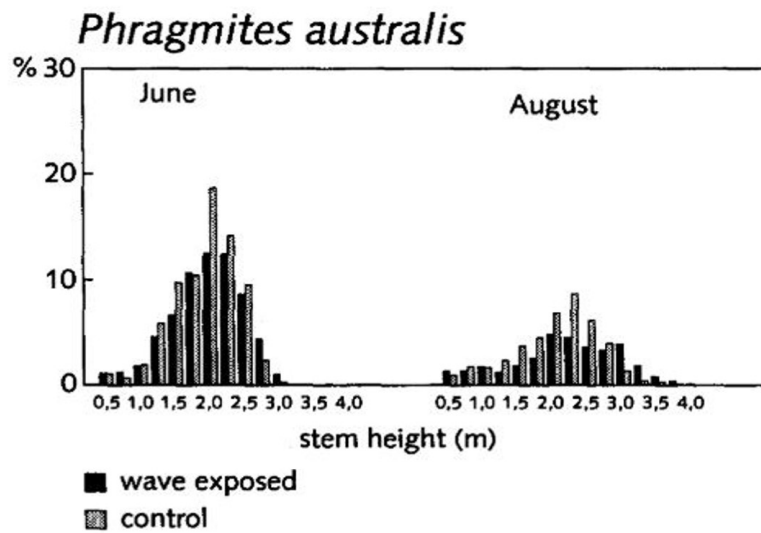
Figure 2.10: Vegetation height in wave exposed environment vs unexposed environment(Coops and Velde, 1996).

Looking at a more natural system in order to determine the expected range of stern densities, it can be seen that *P. australis* belongs to the class of strongly competitive species. In some cases it is even regarded as environmental weed (invasive native) (Uddin and Robinson, 2017). In the research of Uddin and Robinson (2017) the competitive character is investigated by looking at the stem density of 3 populations of *P. australis* in a field investigation (Figure 2.11). In the stage with the highest amount of *P. australis* the stem density reaches a value of 285 stems/m^2, but even in this stage there is still space available for other species (Figure 2.12).
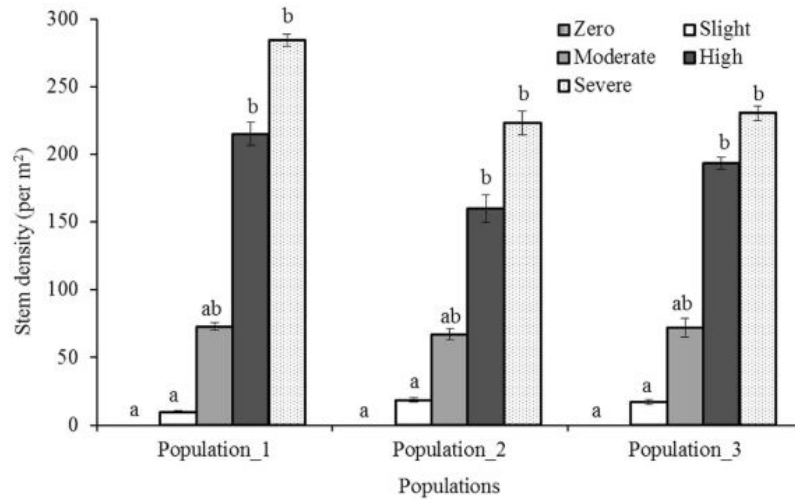
Figure 2.11: Stem density along density gradient of 12m for three different populations of P.australis resulting from an increasing dominance of P.australis (Coops and Velde, 1996).
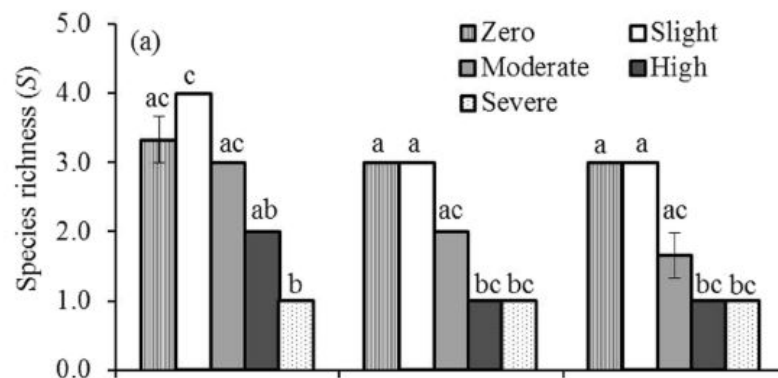
Figure 2.12: Density depended impact of P.australis on the specie richness of 3 different stretches of P.australis (Uddin and Robinson, 2017). The density of P.australis is is defined in 5 category's: Zero, Slight, Moderate, High and a Severe amount of P.australis

It can be concluded that the seasonal influence has a high impact on the mechanical properties of *P. australis*. As long as the wave climate stays below the critical value of 0.25 m and an incidental attack of 0.4m, the influence of the wave climate is negligible. It is interesting to see that the the value of $D*N$, the main variable determining the wave attenuation through vegetation, stays relatively constant through the year (1.00 in June, 0.95 in August). High uncertainties in the determining of the overall density of *P. australis* in a natural situation can be expected, since there is a high dependency on the surrounding factors, both a-biotic as biotic (Uddin and Robinson, 2017). But it can be expected that, if an area consist mainly of *P. australis*, higher density's than 285 stems/m^2 are reached.

2.4.2. Drag Coefficient
In order to calculate the wave damping the drag coefficient is used (Subsection 2.3.3). The drag coefficient describes the forces that the vegetation induced on the surrounding waves and currents. This means that the drag coefficient does not only depend on the characteristics of the vegetation, but depends on the characteristics of the surroundings as well (Appendix A shows the different elements contributing to the drag coefficient and Appendix A.2.3 shows different derivations for the drag factor).

Many formulations have been derived in order to calculate the drag coefficient. Those relations are often empirical and can therefore only be used for the vegetation species (or vegetation species with comparable characteristics) and conditions for which they are derived (Appendix A). Wu et al. (2011) has conducted an extensive amount of research in order to derive a formulation describing the relation between the Keulegan–Carpenter number (KC) and the drag coefficient for multiple species such as S.Alterniflora (Figure 2.13), which has comparable characteristics with *P. australis* (emerged vegetation with N= 405 and D_v = 6.5mm). This formulation is used in order to derive the drag coefficient in the modified model of Duró et al. (2020).

$$CD = 1.767 + \left(\frac{76.04}{KC}\right)^{1.641} \quad R^2 = 0.84 \tag{2.36}$$

$$KC = \frac{u_{c1}T}{D} \tag{2.37}$$

$$u_{c1} = \frac{H}{2}\omega\frac{cosh(k\alpha h)}{sinh(kh)} \tag{2.38}$$

where:
C_D = Drag coefficient
KC = Keulegan Carpente number
u_{c1} = characteristic velocity acting on the plant
T = Wave period
D = Stem diameter
H = Wave height
k = Wave number
α = Relative vegetation height
h = Water depth
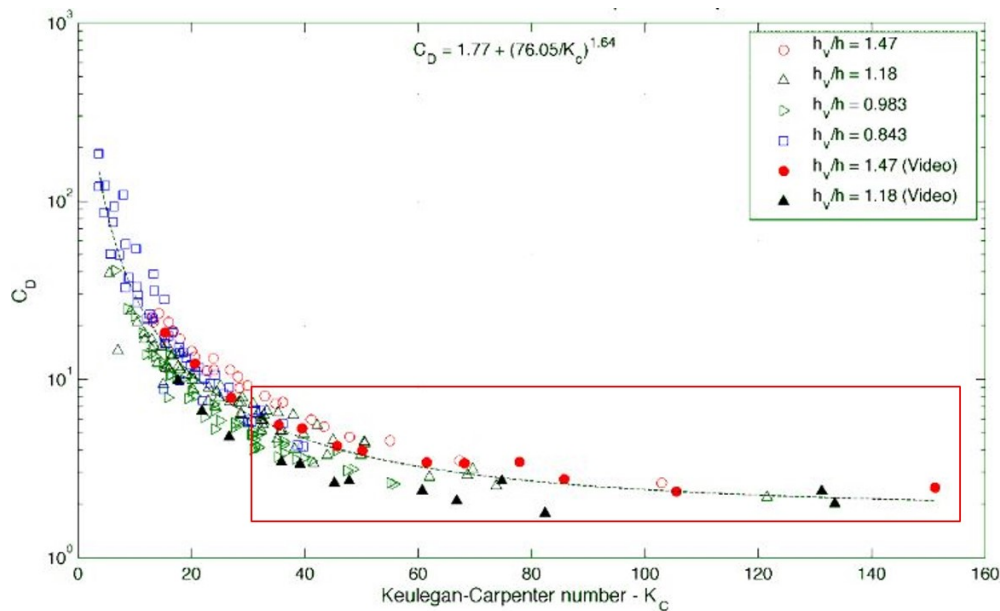
Figure 2.13: Relation between Keulegan-Carpenter number and the Drag coefficient for S. Alterniflora (Green) (Wu et al., 2011). In this figure the measurements and resulting relation between the Keulegan-Carpenter number and the Drag coefficient followed by Wu et al.(2011) is shown. In the model only a small range of this formula is used, highlighted in the red box. It must be noted that the model only accounts for emerged vegetation, so the data points concerning a h_v/h value below the 1 are not relevant.

2.4.3. Soil reinforcement

Roots play an important role against the erodibility of the vegetated soil. According to Ministerie van Verkeer en Waterstaat (1999a) the critical velocity in order to erode the soil increases with a factor of 2.5 for sandy soils.

de Baets et al. (2008) looked into the different mechanical characteristics of Mediterranean plant root systems, leading towards the soil resistance against erosion. One of the most important characteristics is the roots tensile strength, as soils are often strong on compression but week on tensile forces. Adding the tensile strength of the roots to the compression strength of the soil leads to a strong, reinforced soil. Besides the tensile strength, the morphological characteristics of the root systems, such as the root distribution over depth, root orientation and the different diameter classes, play also an important role by the total soil reinforcement (Figure 2.14). In order to calculate the root reinforcement tensile strength including those morphological characteristics ,de Baets et al. (2008) derived the following formula based on the root diameter (D):

$$T_r = a * D^{-b} \tag{2.39}$$

For *P. australis* de Baets et al. (2008) found the value *a*=34.29, *b*=0.78, *n*=20 and a root diameter range of 0.10-7.91m. The following formula is derived in order to calculate the additional cohesion of a silty loam soil by the presence of roots:

$$C_r = 1.04 * \frac{\sum T_i n_i a_i}{A} \tag{2.40}$$

where: T_R = Root tensile strength
D = Stem diameter
C_r = Cohesion added by the roots
A = Considered area
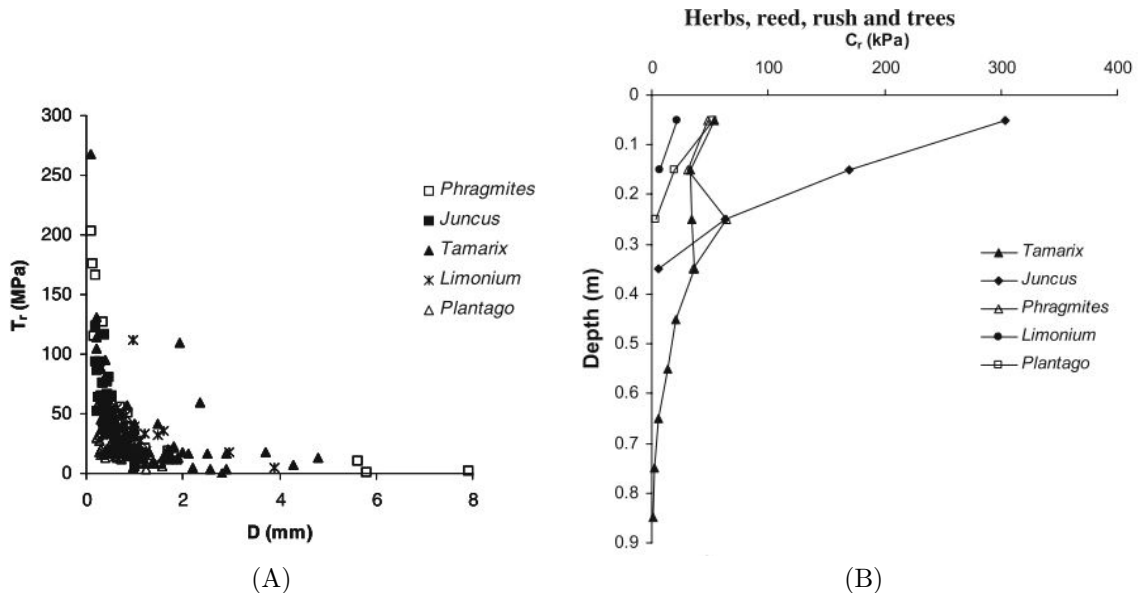
Figure 2.14: P. australis tensile strength (A) and increased cohesion over depth (B) (de Baets et al., 2008).

2.4.4. Root Distribution

Not only the erodibility of the top layer of the bed but also the soil reinforcement below the top layer plays an important role in the overall stability of the soil. Due to the high density of *P. australis*, a part of the wave impact will be reflected, leading to a high turbulence area in front of the vegetated field, which could lead to the formation of a scour hole. Without the roots to stabilise the soil behind the scour hole the soil would probably collapse. For this reason it is important to know the extent of soil reinforcement by the roots.The roots of *P. australis* can be found in depths around the 0.7m (Moore et al., 2012), but looking at the distribution of the biomass (Figure 2.15) the soil is reinforced sufficiently up too a depth of 0.2m.
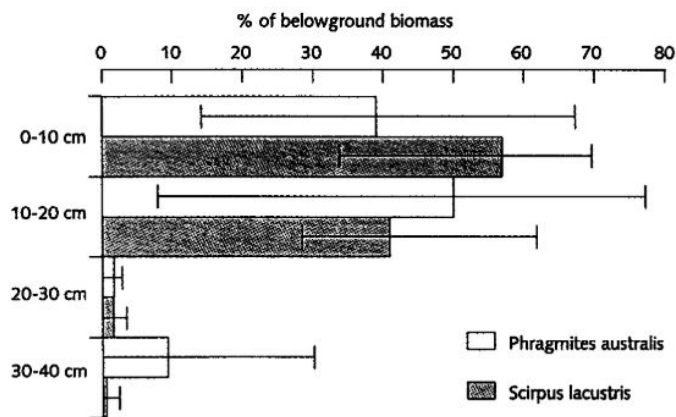
Figure 2.15: Distribution of roots biomass over depth as percentage dry weight biomass (Coops et al., 1996)

2.5. Shore Protection structures

In some situations the energy dissipation through vegetation has not enough influence to protect the shore. It can also happen that the wave climate is to strong for the vegetation to grow on its own and an additional structure to reduce the waves is needed. The two most common nature friendly energy reducing structures are rows of poles and brushwood structures. Also temporary structures are often used to support the newly grown vegetation. In this section a brief overview has been given concerning the design rules for those nature friendly structures.

2.5.1. Rows of pols

The wave height passing through a **single row** of pols can be calculated with the formula of 2.41. In this equation a pole height of 0.5*normative wave height is considered (10 to 30 cm above the surface) (Ministerie van Verkeer en Waterstaat, 1999a).

$$H_t/H_i = \sqrt{(1 - W^2)} \tag{2.41}$$

$$W = D/S \tag{2.42}$$

where: H_t = Wave height through structure
H_i = Incoming wave height
D = Pole diameter
S = Hart to hart distance

When a **double row** of poles has been used the wave height through a structure can be reduced with:

$$15\% \text{ by } S/D = 1.1$$
$$5 \text{ to } 10\% \text{ by } S/D = 1.2$$

For the total length of a pole the following rule of thumb can be used: "1/3 of the pole is above the soil, 2/3 below"(Ministerie van Verkeer en Waterstaat, 1999a). In the case of a double row of poles most time an entrance is created to refresh the water behind the row of poles. When a double row of poles is not sufficient for the reduction in wave height it is possible to fill the space between the rows of poles with different kind of materials. The amount of vertical poles can be reduced, as the main function changes from wave reduction to forming the frame of the new Brushwood Structure.(Ministerie van Verkeer en Waterstaat, 1999a)

2.5.2. Brushwood Structures

When rows of poles are not longer adequate for the wave and current reduction a brushwood structure is often a preferable solution in shallow waters. Different parameters are adaptable, like the width of the structure and the density of the used material. Besides the protective role a brushwood structure can also function as a place for flora and fauna to settle.

It is important to keep in mind there needs to be a flow through the structure for water refreshment. Reed, particularly in the early years, is sensitive to the amount of oxygen that is used around the roots, especially if the water level variations are minor. The placement of structures can act as a trap for organic material, which can choke the new vegetation. It is therefore advised to keep, for example, a 5m gap every 25m (Pelsma et al., 2009).

In the research of Sayah and Schleiss (2005) the transmission coefficient of the waves (K_T) on a brushwood fences has been evaluated using the following variables:

- The relative freeboard of the structure (R_c/H_i)

- The relative structure height (h/H_i)

- The relative wave number (kd)

- The wave steepness (H_i/gT^2)

- The porosity of the structure (p)

In the experiments they noted that the structure responds differently in relation to its immersion. The efficiency of the transmission decreases rapidly when the structure is totally submerged. Not only the relative freeboard, but also the wave steepness and the porosity plays a major role in the transmission of waves. The influence of the relative wave height and the wave number are small, so will be neglected. The width of the structure in the test was constant, but the porosity replaces to some extent the width. This equation has been tested for the following ranges:

- The relative freeboard is between -2 and 2m

- The wave steepness is between 0.001 and 0.008

- The porosity is recommended to be higher than 0.1 (lower porosity's are practically impossible to construct).

Resulting in the transmission coefficient (Equation 2.43) with an accuracy of 95 % in a range of 0.24 (Sayah and Schleiss, 2005).

$$K_T = 0.01(\frac{R_c}{H_i})^2 - 0.11\frac{R_c}{H_i} + 0.69p^{-0.04} - 12.40\frac{H_i}{gT^2}(\pm 0.24) \tag{2.43}$$

where: R_c = Structure free board
H_i = Incoming wave height
p = Porosity
g = Gravity constant
T = Wave period

In the research of Water Land en Dijken (2018) the use of brushwood structures to protect the shore made of rows of poles with willow trees his evaluated. This investigation shows that less than 10 % of the brushwood structures that were placed in the past five years were damaged. In almost all the cases it did not lead to functional failure, as the vegetation has become strong enough to hold on its own. By the structures more than 5 years old 52% was damaged. It is possible that the quality of those structures was less, but a live time of 5 years for a brushwood structure seems like a conclusion that is more likely.

2.5.3. Bed Protection
New sowed vegetation can be very vulnerable, both against erosion and animals. Especially a design without revetment (above or below water), where the main protection depends on the vegetation what still needs to grow, is very vulnerable in the first state. For a bed protection on a nature friendly shore the ecological value needs to be considered. Sufficient refreshment for the roots is one of the most imported aspects to consider with the construction of a bed protection as already seen in Subsection 2.5.2.

Bed protection is often used for the bed protection near structures where velocity's can increase drastically. One of the most traditional bed protections in the Netherlands is a fascine mattress. A fascine mattress concists of faggots with twigs between. The faggots are in the Netherlands often made of willows, but the use of all strong, flexible material is possible. Stones are used to sink the mattress to the bed. The spaces between the twigs will not fulfill a filtering fiction, as the are to open. (Schiereck, 2001). Using a fascine matrass of a decaying product may be useful to stimulate the growth of new vegetation.

Another option is to use the nature itself. Ecosystem engineers are capable to reduce current and change their surroundings into a complete different environment. A downside of the use of ecosystem engineers is the starting situation. As it is a natural solution, growing time is needed, and a sufficient start environment is needed(van de Ven, 2018).

2.6. Existing models
The calculation and modeling of near shore processes has been the topic of many studies. This section provides an overview of existing models reproducing nearshore processes over a coastal profile in order to determine which model could be used to answer the main question "How to estimate the contribution of reed-like vegetation, specifically *P. australis*, to wards the shore protection along a lake against hydrodynamic loads using a process based model".

X-Beach has been developed in order to asses the influence of storm impact's while SWASH has been written with the focus on the rapidly varying flows near the shore. Both models have initially been derived for coastal situations with sandy shores. The model made by Duró et al. (2020) focused on riverbanks under ship wave attack, so the erosion processes applied are based on the erosion of cohesive soils.

2.6.1. Xbeach

X-beach is an open source numerical model developed to estimate the near shore and coastal response to storm and hurricane conditions. Initially the model included wave breaking, surf and swash zone processes, dune erosion, overwashing and breaching on sandy barrier island systems (Roelvink et al., 2009)(McCall et al., 2010). In the meantime many processes have been added such as vegetation (van Rooijen et al., 2016). Also many processes have been improved over the past few years (Roelvink et al., 2018) (van Dongeren et al., 2013).

X-Beach resolves the dominant, physical processes explicitly and uses only empirical relations when the processes are not well understood or if an explicit computation is to expensive (Roelvink et al., 2018). As the dominant physical processes are calculated explicitly the model is relatively flexible and has been proven in many different situations.

X-Beach has been developed in order to asses storm impacts on low lying sandy coasts in order to make (re-)designs for coastal protection measurements and re-evaluate the existing coastal protection measures (Roelvink et al., 2009). Until this point, models predicting the influence of extreme storm events on dune erosion mainly included an uniform coast which was insufficient in order to model the more complex systems of many coastlines (Roelvink et al., 2009).

2.6.2. SWASH

SWASH is a numerical method which resolves the nonlinear shallow water equations including vertical acceleration in which mass and momentum are conserved. With this method the non-hydrostatic, free-surface, irrotational flow has been calculated in one and two horizontal dimensions. The model uses a vertical boundary fitted grid with a compact finite difference scheme (Zijlema and Stelling, 2008; Zijlema et al., 2011), which is a method to solve the compressible Navier Stokes equation (Boersma, 2005).

SWASH has been developed in order to describe the complex changes of a rapidly varying flow, as often found in coastal systems. This way the different processes near the shore, such as wave breaking in the surf zone and run-up in the SWASH zone, can be studied and predicted. Both processes play an important role in the area of coastal engineering as they are essential for both sedimentation and erosion (Zijlema and Stelling, 2008; Zijlema et al., 2011).

2.6.3. Model description of Duró et al(2020)

The model of Duró et al. (2020) is a process based model. As input for the approaching wave and soil characteristics are needed. In the model the bed shear stresses induced by primary and secondary waves during propagation, breaking and run up have been included.

The model has been developed in order to account for the effect of ship waves propagating along a shore of a cohesion soil. As the model has been based on energy relations and empirical formulations new processes can separately be implemented which makes it a flexible model that can be adapted to different situations.

In the rest of this subsection the processes and equations used in the model of Duró et al. (2020) will be explained in detail.

Rate of erosion

In order to change the profile a terrace morphology needs to be updated. This is done with a formula in the form of Partheniades (1965) erosion formula (Equation 2.44), where the erosion rate ϵ can be used to calibrate the system. The critical bed shear stress (τ_c) can be calculated with the use of the soil cohesion (C_0), the used formula in this model has been derived by Kimiaghalam et al. (2016) (Equation 2.45) (Duró et al., 2020).

$$\frac{\delta Z_b}{\delta t} = \epsilon(\tau_b - \tau_c) \tag{2.44}$$

$$\tau_c = 0.89 C_0 - 0.1 \tag{2.45}$$

Primary wave draw-down

In the model it is assumed that the water level gradient during primary wave draw-down is constant with a given depression H_p and terrace length L. In order to estimate the flow velocity's induced by the primary wave draw-down the following momentum balance is used (Duró et al., 2020):

$$\frac{d(Z_b + h)}{dx} + \frac{d(U^2/2g)}{dx} = \frac{U^2}{hC^2} \tag{2.46}$$

With:

$$\frac{d(Z_b + h)}{dx} = -\kappa \frac{H_p}{L} \tag{2.47}$$

The use of a maximum linear water level gradient combined with the assumption of a steady flow seems to be conservative. To compensate for the overestimated velocity's κ, the attenuation coefficient, will compensate. In the first stages a maximum depression will not be reached at the terrace toe before the primary waves reach the upper bank toe, so the maximum energy gradient will be lower than the energy gradient estimated with H_p, so $H_{p,eff}$ will be used (Duró et al., 2020).

$$H_{p,eff} = H_p \frac{T_{UBt}}{T_p/2} \tag{2.48}$$

With the time needed for the primary wave to reach the upper-bank toe:

$$T_{UBt} = \int_0^L \frac{x}{\sqrt{ghdx}} \tag{2.49}$$

The friction losses are calculated with the use of Chézy formula, assuming flow resistance on a certain section equal to the flow resistance of a situation with uniform flow, depth and velocity. With the use of the White-Colebrook formula (Equation 2.50) and the Nikuradse roughness height K_s the induced bed shear stresses can be calculated (Equation 2.51) (Duró et al., 2020).

$$C = 18 log \left(\frac{12h}{k_s} \right) \tag{2.50}$$

$$\tau_b = \frac{g}{C^2} \rho U^2 \tag{2.51}$$

Primary wave surge

The propagation of the primary wave is modeled as a bore during the rising limb (Equation 2.52). The corresponding water level is given by the maximum depression resulting from the primary wave recession (H_p). The bore height (stern wave) upper limit has been given by $H_b = 1.5 * H_p$. After breaking a dissipation model is used for fully developed bores (Equation 2.55) (Duró et al., 2020).

$$\frac{dEC_g cos(\theta)}{dx} = D_b \tag{2.52}$$

$$E = B_0 \rho g H_b^2 \tag{2.53}$$

$$C_g = \sqrt{gh} \tag{2.54}$$

$$D_b = \frac{1}{4}\rho g \frac{1}{T_b} \frac{H^3}{h} \tag{2.55}$$

The shape of the primary wave bore is assumed constant with resulting in a variance in wave surface elevation B_0 of $1/12$. Due the shallow water the rear slope steepens and the bore period can be taken as $1/3$ of the primary wave period. The breaker period for nonlinear waves is taken ($\gamma = H_{br}/h_{br} = 5/9$). The mean velocity under the through can be given by (Duró et al., 2020):

$$\overline{u_w^2} = \beta^2 C_w^2 \left(\frac{H_{br}}{h}\right)^2 B_0 \tag{2.56}$$

$$\beta^2 = 0.8 - 0.5 tanh\left[2.5\left(\frac{h}{h_B}\right)^2\right] \tag{2.57}$$

$$C_w^2 = C_b^2 = gh\frac{d_c d_t}{h^3}\frac{(d_c + d_t)}{2} \tag{2.58}$$

Finally the bed shear stresses can be calculated as followed:

$$\tau_b = \frac{1}{2}f_b \rho U^2 \tag{2.59}$$

$$\frac{0.5}{\sqrt{f_b}} = -2log\left(\frac{k_s}{14.9h} + \frac{2.51}{Re2\sqrt{f_b}}\right) \tag{2.60}$$

Wave run-up

At the moment that $h/h_{br} < 0.15$ assuming energy dissipation concerning the approach of a steady bore becomes unrealistic. In order to calculate the maximum run up above the location where the bore collapse the formula of Bergsma et al. (2019) can be used (Duró et al., 2020):

$$R_v = \frac{(Fr_{b,c} + 0.889)\sqrt{gH_{b,c}}}{2g} \tag{2.61}$$

The upper limit of the measurements concerning induced bed shear stresses due run up can be described with the following relation:

$$\frac{\tau_{b,max}}{(\rho U_{b,c}^2)} = 0.01\left(1 - \frac{x_R}{R_h}\right) \tag{2.62}$$

With x_R the horizontal run up length.

Secondary waves

Using the formulation for bore propagation (Equation 2.52) with $B_0 = 1/8$ for sinuous waves the dissipation, shoaling and refraction can be calculated.The group celerity C_g (Equation 2.63) and the wave celerity $C_w = L_s/T_s$ can be calculated with the use of the dispersion relation for linear waves (Equation 2.64) (Duró et al., 2020).

$$C_g = C_w * n = \frac{C_w}{2}\left(1 + \frac{2\pi}{L_s}\frac{2h}{sin\left(2h\frac{2\pi}{L_s}\right)}\right) \tag{2.63}$$

$$L_s = \frac{gT_s^2}{2\pi}tanh\left(\frac{2\pi}{L_s}2h\right) \tag{2.64}$$

As breaker criteria for secondary waves $\gamma = H_s/h_B = 0.8$ can be used. However, only after breaking dissipation is considered. When $h/h_B < 0.15$ the run up shear stresses can be computed (Duró et al., 2020).

Morphological update
The development of the shore profile is determined based on a single wave height ,one for the primary waves and one for the secondary waves, and accounts every time step for a single wave event, like the passing of a ship. After every time step the induced shear stresses will be calculated and the terrace slope will be updated with the use of Equation 2.44. The model stops when the morphological values are zero or when a set amount of iterations has been reached. The grid size used to compute the hydrodynamics is 0.02m and the grid size for the morphological update is 2m. For the bed shear stress (τ_b) the highest bed shear stress on every spacial step has been used, looking at the bed shear stress resulting from the primary wave drawdown, the primary wave bore, and the secondary waves. Only slopes between the 0.00 (S_{min}) and 0.1 (S_{max}) will be used in order to prevent negative slopes or scarps (which will be unrealistic through the smoothing in practice) (Duró et al., 2020).

2.6.4. Discussion on model choice
In order to answer the main question "How to estimate the contribution of reed-like vegetation, specifically *P. australis*, to wards the shore protection along a lake against hydrodynamic loads using a process based model" a lake environment is needed in which is accounted for morphological changes. In the model of X-beach extreme events are simulated for a coastal environment. This means that the formulations for sediment transport are based on sandy foreshores, while a lake is more often found in an area consisting of cohesive soils. In SWASH the main focus lays on the correct calculation of the velocity's in the different layers. Sediment transport has been included, but it does not incorporate a morphodynamic module.

The choice is made to work with the process based model of Duró et al.(2020). This model has specifically been written in order to calculate the morphodynamic changes for cohesive soils. A process based model is preferred, since it gives a clear insight in all the separate processes, has a higher flexibility concerning the implementation of new processes and different result can be extracted directly from the calculations . In order to simulate a lake shore based on erosion from wind waves, a large part of the formulations concerning the primary wave surge and draw-down have been removed, but could easily be added in a further research.

3

Model setup and validation

In this chapter the setup and validation of the modified model of Duró et al. (2020) is shown and explained. This is done in 3 steps. First, the wave height propagation through vegetation is implemented and validated based on the model results of Mendez and Losada (2004) and the measurments of Wu et al. (2011) and Dubi (1995). When the wave height is validated the corresponding induced bed shear stresses can be investigated. This has been done in the second step, where the induced bed shear stresses are compared with SWASH. The third step consist of the morphology changes, which are the result of the difference between the maximum induced bed shear stresses and the critical shear stresses depending on the soil characteristics. As the morphological model is already validated by Duró et al. (2020) it is assumed that a correct calculation of the induced bed shear stresses leads to a correct morphology. Multiple aspects were tested in order to strengthen this assumption.
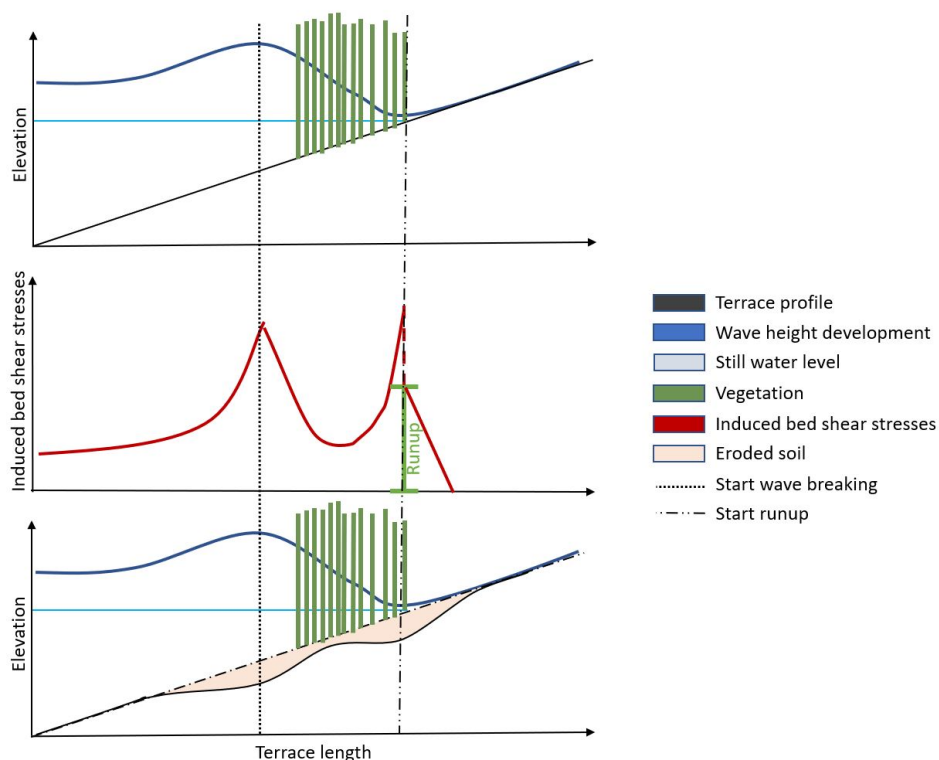

Figure 3.1: Overview Chapter 3, Model setup and validation. The setup and validation of the modified model of Duró et al. (2020) is done in three steps. First, the wave height development through the vegetation is studied (Section 3.1). Second the induced bed shear stresses (Section 3.2) and at last the morphology (Section 3.3).

3.1. Implementing Energy dissipation by vegetation

The wave height propagation over the terrace in the model of Duró et al. (2020) is calculated based on the wave energy balance. In this section the energy dissipation by vegetation is added to the model and is validated.

3.1.1. Energy dissipation by vegetation

In order to calculate the contribution of energy dissipation by the vegetation the formulations of Dalrymple et al. (1984) are used in the model (Equations 2.27 , 2.29 and 2.28). Initially a wave height along the terrace will be guessed which is used for the initial calculations. The amount of energy dissipation by the vegetation will be calculated after the update of the wave length and celerity, but before the wave height update itself. The calculations concerning the wave properties, dissipation by vegetation and the wave height update will be repeated until the difference between the guessed wave height and the calculated wave height is negligible. The full set of used equations can be found in Appendix B.2.

Changes in model concerning vegetation on a slope
1. Formula of energy dissipation by vegetation and damping coefficient (Equation 2.27, 2.29 and 2.28).

2. Input parameters for Vegetation ($CD, b_v, N, \alpha(i)$) and the minimal and maximal growing depth of the vegetation.

3. Update wave parameters k and σ

4. Lowering the energy flux with $Ediss * dx$.

In order to check the correct implementation of the formulas derived by Dalrymple et al. (1984) a comparison has been made between the model results of Mendez and Losada (2004), which uses the same equations in order to calculate the wave attenuation by vegetation. After it is confirmed that the equations are implemented correctly the model is validated with the use of kelp data from Dubi (1995) and Wu et al. (2011). Both experiments look at the wave attenuation through vegetation on a constant slope.

3.1.2. Validation based on the model of Mendez and Losada(2004)

Mendez and Losada (2004) studied the wave height evolution over a plane sloping beach where the effects of vegetation, shoaling and wave breaking were added in different stages. This is done with the use of the shoaling coefficient K_s according to Green's law and a damping coefficient K_V representing the vegetation. Mendez and Losada, (2004) also developed an energy dissipation model for random wave transformation and for random breaking waves.

This subsection compares the model of Duró et al. (2020), including a vegetation module, with the shallow water approximation for monochromatic waves of Mendez and Losada (2004), to validate the main process of wave transformation are well implemented. In order to show the influence of the vegetation, the different vegetation characteristics were combined in a single parameter A1 (Equation 3.3). Similarly the parameter A2 (Equation 3.4) has been introduced in order to combine the effect of the wave height, slope and vegetation characteristics.

$$K_S = \frac{h_0^{1/4}}{h^{1/4}} \tag{3.1}$$

$$K_v = \frac{1}{1 + 2\frac{A_1}{m}H_0(K_s - 1)} \tag{3.2}$$

$$A1 = \frac{2C_D b_v N \alpha}{3\pi} \tag{3.3}$$

$$A_2 = \frac{A_1 * H_0}{m} \qquad (3.4)$$

where: h = Water depth
         m = Slope
         H = Wave height
         C_d = Drag coefficient
         b_v = Plant area per unit height of each vegetation stand normal to u
         N = Number of vegetation stems per m^2
         α = Relative vegetation height

Small changes are in order to compare the models based on the same variables. The model of Mendez and Losada (2004) uses a constant parameter to describe the vegetation (Parameter A_1), for this reason the relative vegetation height (α) is assumed to be constant. This will give some small differences in results compared to a relative vegetation height depending on a set vegetation height and the local water depth. For this reason the relative vegetation height is set as a constant for the model comparison, but is used as a variable for the other validations. In practice the relative vegetation height is difficult to determine, as changes in water depth due to erosion or tidal variations, will play a part.

Another difference can be found in the use of Greens law, which assumes shallow water conditions while the used model uses the transitional water depth (Appendix B.2.2).

The last difference concerns the angle of wave attack, which is not included in the model of Mendez and Losada (2004). The angle will be set to zero in order to make the comparison between the models and the kelp data. Overall both models are based on the same principals, so similar results can be expected. The differences between the models are illustrated in Figure 3.2.
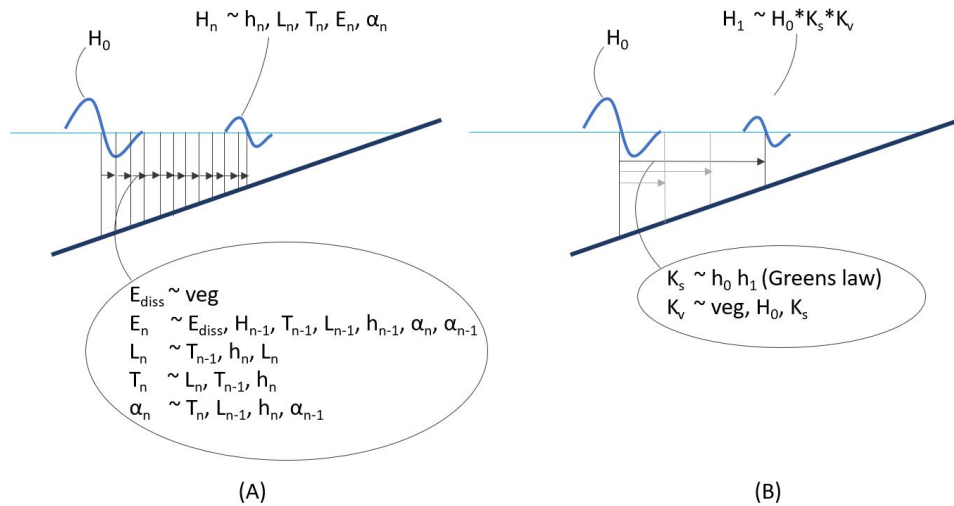

Figure 3.2: Modeling differences between the used model (A) and the shallow water model of Mendez and Losada (2004)(B).

Results
In Figure 3.3 both the model results as well as the results of the model of Mendez and Losada (2004) are plotted for various values of A2.
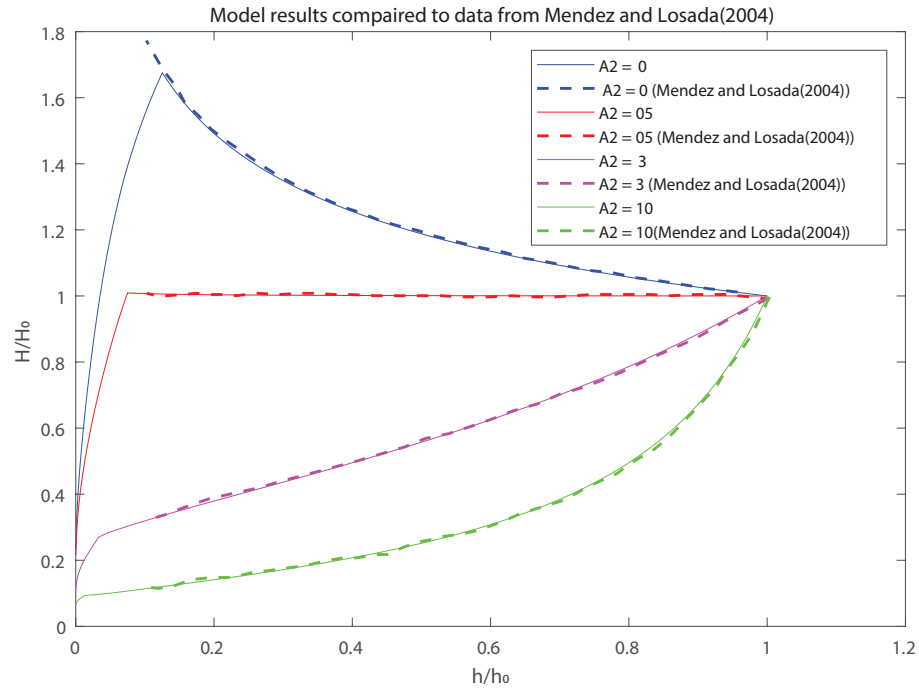
Figure 3.3: Comparing Model results with the model results of Mendez and Losada (2004) showing the relation between wave height, vegetation characteristics and slope for shallow water waves (without wave breaking)

In order to determine the sensitivity of the different parameters contributed to the $A2$ value Figure 3.4 shows different combinations of $A1$, wave height (H) and the slope (m) resulting in an $A2$ value of 3. Plots with different wave periods are shown as well in order to explore their influences. The wave period has not been considered in the first, simplified model of Mendez and Losada (2004) which is based on the shallow water approximation, but has a large influence on the resulting wave height evolution. In Figure 3.4 it can be seen that a deviation in wave period, especially when the wave period becomes smaller, leads to a deviation of the model made by Mendez and Losada (2004). This sensitivity can be expected as the wave height depends indirect on the wave period.

- $T \rightarrow L \rightarrow c \rightarrow$ Total energy flux $\rightarrow H$

- $T \rightarrow L \rightarrow k \rightarrow$ Energy dissipation by vegetation $\rightarrow H$

Further explanation can be found in the paper of Dubi and Torum (1994). In his paper the theoretical force induced by vegetation is plotted for different wave periods which can be seen in Figure 3.5. Overall the force induced by vegetation shows an almost constant relation with the wave height, except for the wave periods below the 2 seconds. Here, the forces induced by the waves on the vegetation increases compared to the other wave periods. This is the result of the higher velocity's and shorter wave periods (Equation 3.5). As the total wave force increases it can be expected that the wave height reduction, compared with the same situation but a different wave period, has less influence.

$$F = F_\lambda |1 - A_m| u_\lambda \tag{3.5}$$

$$A_m \sim \omega, N \tag{3.6}$$

where: F_λ = Empirical constant for equivalent drag force coefficient at elevation λ

A_m = Velocity amplification ratio

u = Particle velocity
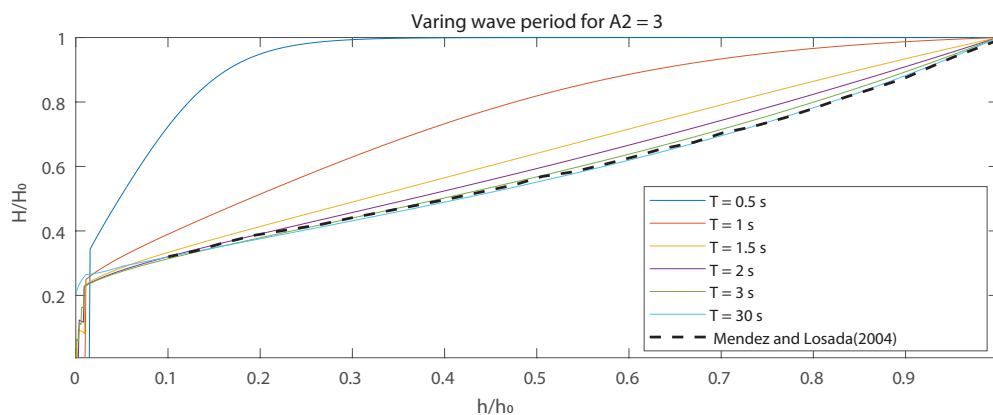
(A) serie MODA2 3 H027 T *X*
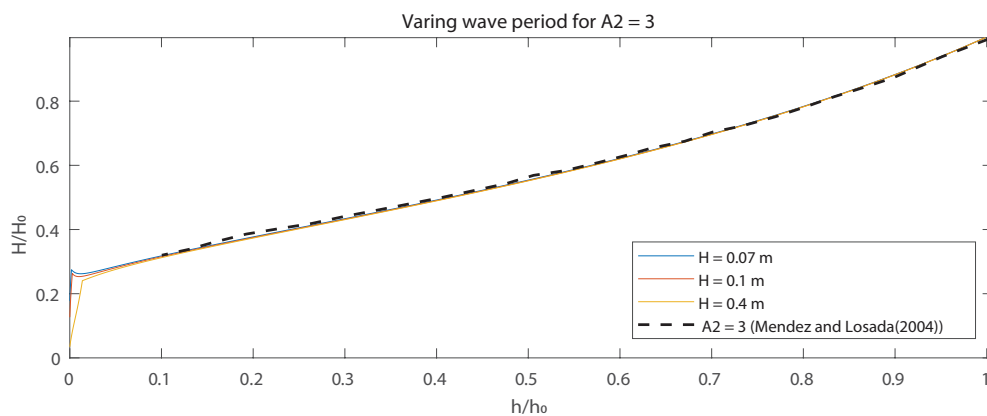
(B) serie MODA2 3 H *X* T10
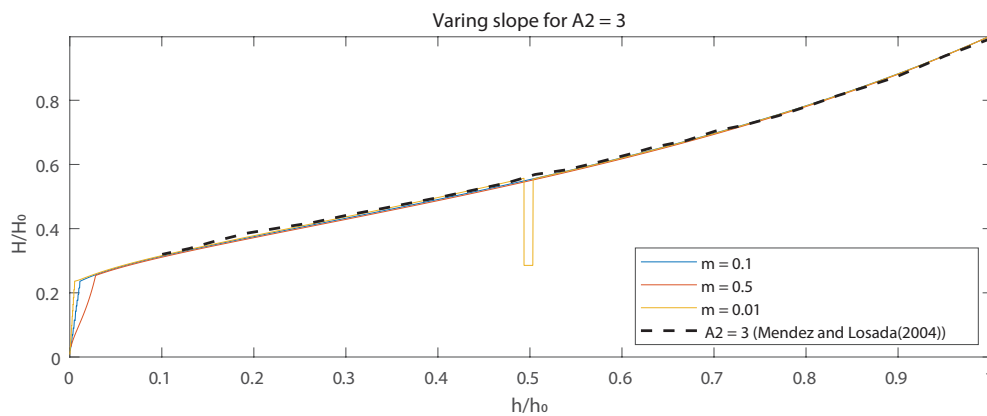
(C) serie MODA2 3 m *X*

Figure 3.4: Different compositions for A2 = 3 with (A) Wave Period variations [0.5 - 30s] for $H = 0.3$m and $m = 0.033$. (B) Wave height variations [0.07 - 0.4m] with $T = 10$s and $m = 0.03$. (C) Slope variations 0.1 - 0.01 with $T = 8$ and varying H. The precise parameters can be found in Table C.11.
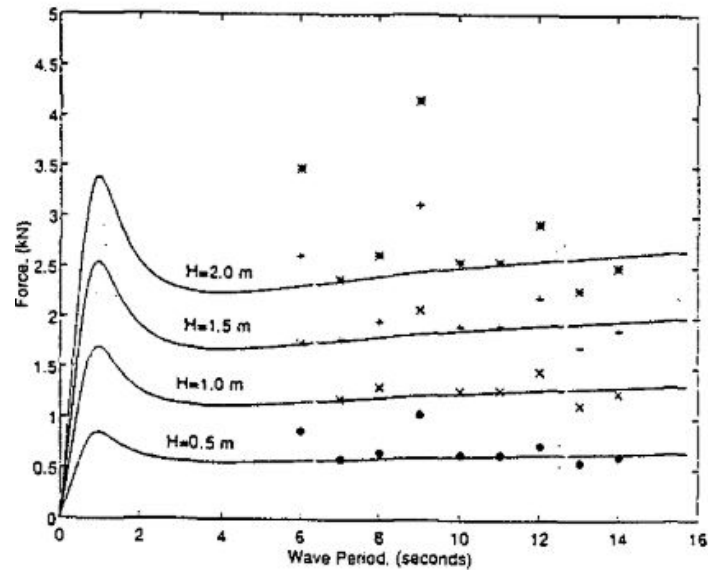
Figure 3.5: Theoretical force model fitted to measured force by Dubi and Torum (1994). Results related to Equation 3.5.

In order to minimise this effect a large wave period is chosen for the plots of Figure 3.3. In order to normalise the graph the wave height at the second grid cell is used in order to remove the initial error. Another remarkable result is the instability observed in plot MODA2 3 m001 (Figure 3.4). This is further discussed in Appendix C.3.

Aside from these minor differences the overall results look similar, so it can be concluded that the equations are implemented correctly.

3.1.3. Validation based Kelp data from Dubi (1995)

Derived Kelp data

The model made by Mendez and Losada (2004) is validated using data from experiments from artificial kelp measured by Dubi (1995). Mendez and Losada (2004) derived the drag coefficient for those experiments through calibration. The artificial kelps are *L. hyperborea* with the following properties:

1. b_v = 0.025m

2. d_v = 0.20m

3. N = 1200 units/m^2

4. $\alpha = d_v/h$

The test is conducted in the following hydrodynamic conditions:

1. T_p = 1.26 - 4.42 s

2. h = 0.4 - 1m

3. H_0 = 0.045 - 0.17 m

In order to derive the kelp data a random wave field is simulated with the Jonswap spectrum with γ_j = 3.3. The free surface is measured with wave gauges at eight locations. In this model a single wave height is used, so the used wave height is based on the initial wave height showed in the plots of Mendez and Losada (2004). The initial water depth and wave period are given.

Comparison Model with Kelp data
Two series of plots are made, the first series with alpha based on the local conditions (initial plantheight/ water depth) and the second series with alpha based on the initial conditions (initial plantheight/ initial water depth), as is done in Section 3.3 and 3.4.

In Figure 3.6 it can be seen that the use of a constant alpha gives often an overestimation of the wave height, as the relative vegetation height is smaller at the offshore side than at the shore side. As the model mainly focuses on emerged vegetation this aspect was not invstigated in more detail.

Overall the plotted graphs fit quite well through the kelp data, as the average wave height differences are around the 0.005m ($\approx$ 4 %) over a terrace length of 7m. Differences can be explained by an inaccuracy in the measured initial wave height, which shows an offset of 0.005m. The parameters representing the kelp characteristics can also differ from the true kelp, especially the estimation of the drag coefficient is quite difficult which is shown in appendix A.

3.1.4. Validation based on data from Wu et al.(2011)
Model of Rooijen et al.(2016)
In the study of van Rooijen et al. (2016) the influences of the attenuation of sea-swell, IG waves and wave setup is added to two modes in X-beach, the sea-swell wave phase-resolving (nonhydrostatic) and the phase- averaged (surfbeat) mode. The extension of those modes is validated with the use of data from flume experiments by Wu et al.(2011) with mimic vegetation for different configurations. The Kelp data is used to validate the model with the plotted graphs of van Rooijen et al. (2016) as a reference to illustrate the average trend through the data.

The used L.hyperborea have the following characteristics:

1. b_v = 0.025m

2. d_v = 0.20m

3. N = 1200 stems/m^2

4. $\alpha = d_v/h$

5. CD = 0.2 Calculated with formulas formulated by Mendez and Losada(2004)

The following waves are generated:

1. H = 0.14 m (JONSWAP, with γ = 7.0)

2. L = 2.5 s
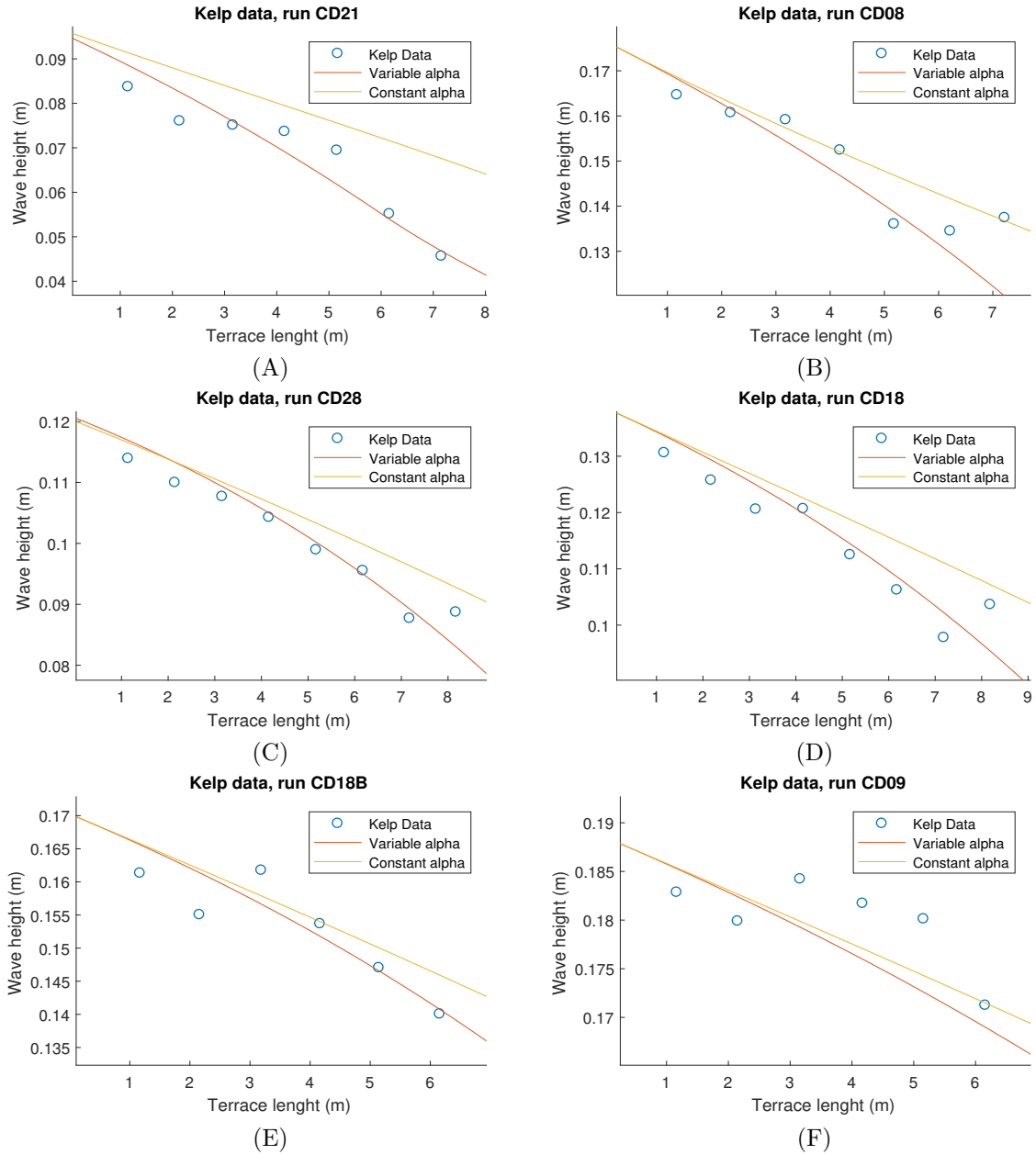
Figure 3.6: Comparison between kelp data from Dubi (1995) and the model results for a constant and a variable alpha. The used input data for the model results can be found in Table C.12.

Results
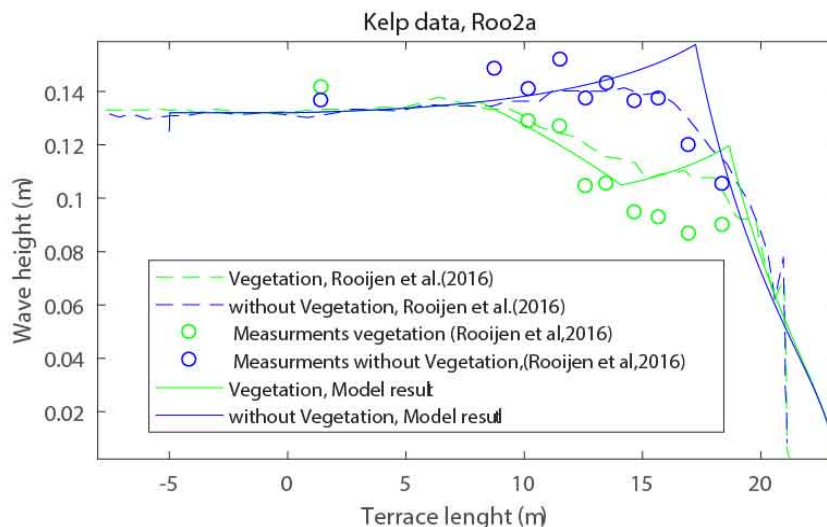
Figure 3.7: Comparison in wave height development. A compairison is made between the model results of X-beach van Rooijen et al. (2016) (dashed line), the expanded model of Duró et al. (2020)(solid line) and the field observations of Wu et al. (2011)(dots). The situation with vegetation is shown in green, without vegetation in blue.

Looking at the differences between the Kelp data, the X-beach results of van Rooijen et al. (2016) and the model results of the modified model of Duró et al. (2020) (Figure 3.7) it can be seen that the energy dissipated by the vegetation is well represented, as the decrease in wave height through vegetation matches the data points(Figure 3.7). A large overestimation of the wave shoaling can be found in both the plots with and without vegetation just before breaking. As the model represented in this thesis uses a single wave height, a sharp transition in wave height at the breaking point can be expected. The Kelp data is generated with the use of a Jonswap wave spectra, so the energy dissipation through wave breaking will occur over a larger area, as the larger waves break in deeper water than the shallower wave in the spectrum, what results in a smooth transition.

The first point of wave breaking happens at $H_b/h = \gamma = 0.4$ which can be expected if a wave spectrum is used where $2 * H_s = H_{max}$, when H_{max} breaks at $H_b/h = \gamma = 0.8$. H_s will break at $H_b/h = \gamma = 0.4$. A further investigation into the different graphs can be found in Appendix C.1

Consideration of the use of a wave spectrum

The Jonswap wave spectrum is often used to describe wind waves in a coastal setting. Its suitability representing lake conditions has not been tested. Considering the differences in wave generation and propagation between an open ocean and a constricted lake the Jonswap spectrum was not applied in the present study. Another reason for the use of monogramatic waves can be found in the goal of the model. The model is written in order to calculate the final morphological state which mainly depends on the highest waves. When also the intermediate morphological stages need to be calculated the use of a wind wave spectrum is needed. In order to include the effect of ship waves representative wave data should be collected.

Summary

The implemented energy dissipation by vegetation is compared to the model results of Mendez and Losada (2004) and Kelp data from Dubi (1995) and Wu et al. (2011). The data is used to compare the model results focusing on wave propagation seaward from the breaking zone.

A deviation from the normalised wave height based on the shallow water approximation of Mendez and Losada (2004) can be found when the wave period reaches values below the 2 seconds (Figure 3.4.C). This might be due the fact that the wave period has not been considered for the first phase in the work of Mendez and Losada (2004). In Figure 3.6 it can be seen that the wave height evolution compared to the kelp data derived by Dubi (1995) fits in the most cases quite well. An explanation for the deviation can be found by the uncertainty in the used initial wave height, wave period and representation of the kelp characteristics.

The model was also able to reproduce the wave attenuation through vegetation measured by Wu et al. (2011) (Figure 3.7). However, an overestimation of the wave height before wave breaking can be found in the model of Duró et al. (2020), which is also visible in the results where vegetation is added. An in-depth elaboration on this aspect can be found in appendix C.1.

3.2. Induced bed shear stresses

The induced bed shear stresses are the result of the oscillatory motions induced by the wave (Subsection 2.1.5) and the velocity's induced by run-up (Subsection 2.1.7). After the validation of the wave height propagation (Section 3.1) it can be investigated if the corresponding induced bed shear stresses are calculated correctly.

The morphodynamic model of Duró et al. (2020) is validated for primary and secondary ship waves acting on river banks. For that reason we are mainly interested in the changes in magnitude of the induced shear stresses in the shallower areas and through the vegetation, under the assumption that the shear stresses in front of the vegetation are correct. In order to validate the shear stresses calculated with the presented model, a comparison is made with the shear stresses calculated by SWASH.

3.2.1. Energy dissipation by bed shear stresses

The interaction between the bed and the waves goes both ways. The friction with the bed dissipate energy from the waves and enhances the erosion of sediment. Wave dissipation by friction was modelled using the equation of Roelvink et al. (2015) (Equation 3.7). The energy dissipation through bottom friction is neglected in the original model, as it has only a small influence (Appendix C.1.2) but is added in the modified model of Duró et al. (2020).

$$D_f = \frac{2}{3\pi} \rho_w f_w \left(\frac{\pi H_{rms}}{T_{m01} sinh(kh)} \right)^3 \tag{3.7}$$

where: D_f = Energy dissipation through bottom friction
ρ_w = Water density
H_{rms} = Root mean square wave height
T_{m01} = Mean absolute wave period
k = wave number
h = Water depth

3.2.2. Comparison of bed shear stresses with SWASH

In order to validate the induced bed shear stresses calculated with the vegetation extended model of Duró et al. (2020), a comparison is made with the bed shear stresses calculated with SWASH. Liao (2015) showed that SWASH could reproduce the vertical flow structure under wave action in the nearshore, including the processes of asymmetric oscillatory flow, wave grouping-induced flow and undertow correctly. The bed shear stresses calculation of SWASH is successfully applied to investigate the importance of different bed load transport processes by Engelstad et al. (2019). Considering the lack of validation data for the shear stresses, and that SWASH has been extensively validated under different conditions, SWASH is used for qualitative validation of the model modified model of Duró et al. (2020) .

In SWASH the bed shear stresses are calculated based on the shallow water equations, were the bottom frictions forms one of the boundary conditions of the calculated domain. In this way, a friction velocity can be calculated (u_*) which is representative for the magnitude of the induced bed shear stresses (Appendix C.2). Since the calculation approach from SWASH (based on the boundary layer between the bottom and the waves) and the model of Duró et al. (2020) (based on the orbital wave motion) differ, a different result of shear stresses can be expected. However, the relative growth and reduction of shear stresses should be the similar. For this reason it is expected that, even as the results show a difference of a factor 5/2, the presented model the resulting morphology is correct. This should validate the shear stress calculation.

The wave height in SWASH displayed oscillations (Figure 3.8(C) and (D)), due to reflection in the model, since the length of the oscillations is equal to the wave length itself (2m). The same fluctuations are visible in the model results of Phan et al.(2019), which still results in a good fit with the measurement data. The induced bed shear stresses show similar fluctuations, as shown in Figure 3.8 (E) and (F)). As those fluctuations have also the same length as the waves, they can be related to the oscillatory wave motions. But were the plotted wave height is a average over 15 seconds the friction velocity is taken at a single moment. This follows from the [QUANTity duration] function in SWASH (Figure C.21, Section C.4), which is applicable on the wave height and setup, but not on the bed shear velocity. The model of Duró et al. (2020) was able to reproduce a similar behaviour of the shear stresses, without fluctuations.

Comparing the model results, it can be seen that the peaks of induced bed shear stresses calculated with SWASH (*5/2) fits well with the results of the extended model of Duró et al. (2020) (Figure 3.8).

3.2.3. Bed slope and run-up

The calculated bed shear stresses starts to deviate from the SWASH results when the bed slope deviates from the 0.02 (Figure 3.10). The comparison of bed shear stresses with SWASH shows that, in the non vegetated situations of the model of Duró et al. (2020), the highest amount of shear stresses takes place in an earlier stage (Plots (A), (C), (E) and (G) of Figure 3.10). This can be explained by the location of the breaking point. As the waves of SWASH starts to break in an earlier stage (Appendix C.1.4) the highest turbulence also occurs in an earlier stage. As the maximum amount of shear stresses in both plots are equal it can be assumed that the same amount of erosion will take place along the slope. However, this can not be said for the shear stresses induced by the run-up at the end of the terrace. The amount of induced bed shear stresses through the run-up in SWASH experiences a high dependency on the slope and/or terrace length, while the amount of induced shear stress by run-up calculated with the model of Duró et al. (2020) shows only a dependency on the incoming wave height and local water depth. In order to understand the difference in calculated shear stresses the equations used in the model of Duró et al. (2020) are re-evaluated and are compared with the findings in SWASH.
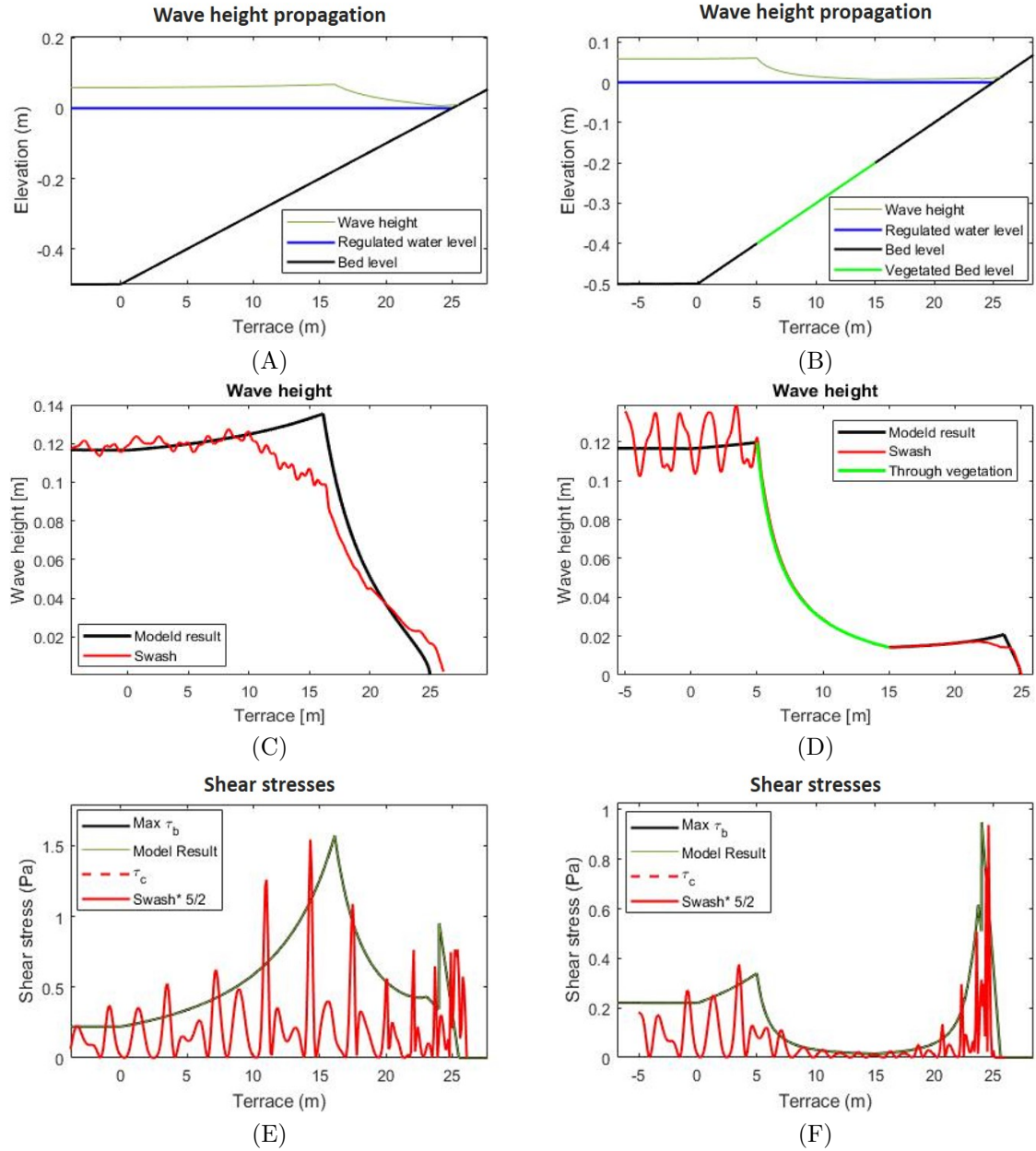
Figure 3.8: Comparison of the induced bed shear stresses between the SWASH results and the modified model of Duró et al. (2020).Plots (A) and (B) illustrate the wave propagation resulting from the model and show the bed level changes over the terrace length. In Plots (C) and (D) a comparison is made between the wave height development calculated with both models. Plots (E) and (F) show the corresponding bed shear stresses calculated by both models. This is done for a situation without vegetation (Plots (A), (C) and (E)) and a situation with vegetation (Plots (B), (D) and (F)).

Run-up Calculation

The formulation of the run-up consist of three different parts. First, an estimation has to be made at what point the bore propagation ends and where the run-up starts. When this point is known, the total height of the run-up can be estimated, from which the total run-up length can be calculated. Finally, the amount of induced shear stresses at the start of the run-up can be calculated which will be interpolated towards the end, at which the bed shear stresses are zero.

It is assumed that the collapsed bore propagates until a depth of 0.15 times the breaking depth. After this point further propagation of the bore becomes unrealistic (Putrevu and Svendsen, 1991). In the model of Duró et al.(2020), this is the point at where bore propagation ends and the run-up starts.

The formulation for the run-up height in the model of Duró et al. (2020) is based on the research of Bergsma et al. (2019). In this research a formulation is derived which accounts for the energy losses through the imperfect conversion of potential energy to kinetic energy. This is done with the introduction of the factor α, which has an average observed value of 0.889 for the tested location. The tested location has an upper beach slope of 0.1 and an inter tidal terrace with a slope of 0.01. In the case of a perfect conversion of potential energy to kinetic energy the value of α reaches its maximum value of 2.

$$R_v = \frac{(c_b + \alpha\sqrt{gH_b})^2}{2g} \tag{3.8}$$

$$\alpha = \sqrt{\frac{2R_h}{H_b}} - Fr_b \tag{3.9}$$

where: R_v = Vertical run-up height
      c_b = Water celerity at start run-up
      α = Factor accounting for imperfect energy conversion
      g = Gravity constant
      H_b = Wave height at start run-up
      Fr_b = Froude number at start run-up

In order to calculate the amount of shear stresses induced by run-up the model of Duró et al. (2020) uses a non-dimensional relation derived by Pujara et al. (2015) (Equation 3.10) . This non-dimensional relation accounts for different types of wave breaking.

$$\frac{\tau_b}{0.5\rho_w c_b^2} = 0.01\left(1 - \frac{x_r}{R_h}\right) \tag{3.10}$$

where: τ_b = Induced bed shear stresses
      ρ_w = Water density
      c_b = Water celerity at the start of the run-up
      x_h = horizontal distance from start location run-up
      R_h = Horizontal run-up

The water depth where the wave breaks (and the run-up starts) depends on the incoming wave. The wave celerity depends only on the water depth, which influences the wave length

and the wave period. So even when the relations for the bed shear stresses accounts for the different breaking types and an imperfect formulation for the transformation from potential energy towards kinetic energy, the amount of induced bed shear stresses does not change with a changing slope and/or terrace length.
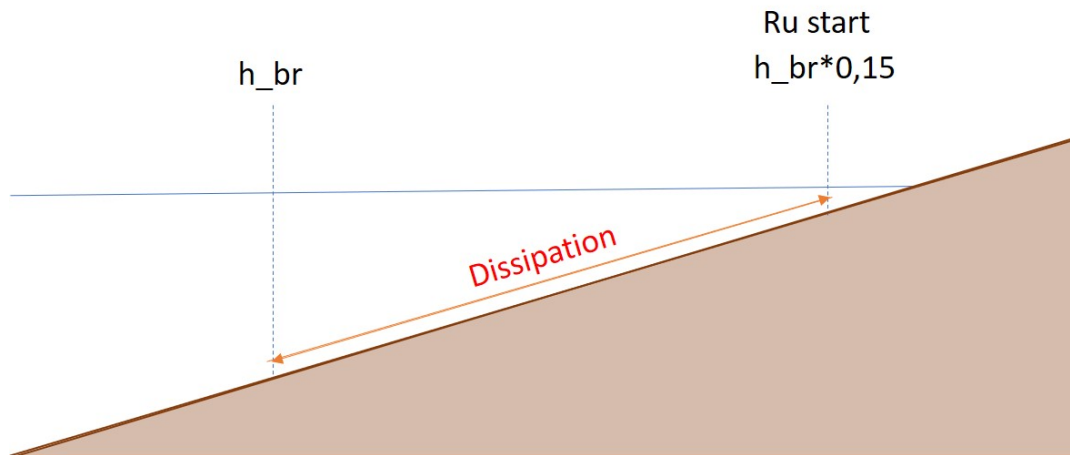

Figure 3.9: Run-up formulation. The start location of the run-up is defined as the water depth equal to 0.15 times the wave breaking depth. Therefore the start location of the run-up is not dependent on the induced dissipation between those two points. The velocity used to calculate the induced bed shear stresses is the wave celerity at the start location of the run-up (Ru start).

Run-up evaluation
Most of the Equations used in the model of Duró et al. (2020) are derived for a plane sloping beach, were spilling waves are dominant. Even as all the tested situations have the same breaking type (spilling waves), a deviation of the induced shear stresses could be expected when the slope deviates from the 0.03 (common value for a plane sloping beach). In the case of a longer terrace length an uncertainty can be found in the α value found by Bergsma et al. (2019) which determines the total run-up height. The main inaccuracy can be found in the estimation of the bed shear stresses at the start of the run-up for which the formulation of Pujara et al. (2015) (Equation 3.10) is used. This formulation depends mainly on the bore velocity at the start of the run-up (C_b). Since energy dissipation is only accounted for in the calculation of the wave height and not in the calculation of the bore celerity itself, this could be the reason for the overestimation at the end of an (unrealistic long) terrace length (Figure 3.10. In practice the maximum design slope is a lot steeper, as space is often restricted (Ministerie van Verkeer en Waterstaat, 1999a). For this reason, an overestimation of the run-up velocity's by slopes shallower than 0.02, gives a model restriction which does not undermine the goal of the model but should still be acknowledged for further development of the induced processes.

This is not the case for a vegetated shore (Figure 3.10 (G) and (H)). This is the result of the delay in wave breaking, resulting in a delay of the starting point of the run-up were lower wave celerities are present. It is interesting to see that the calculated shear stresses through run-up are underestimated in the situation with a slope of 0.04 (Figure 3.10 (C) and (D)). This can be explained by the fact that the velocity in vegetation can both increase (as vegetation is responsible for a restricted area) and decrease (as vegetation is also responsible for energy losses). But could also be the result of a small deviation of total run-up height, which is only now remarkable since the total terrace length is smaller. A more detailed explanation on the influence of velocity on vegetation can be found in Appendix A.2.2. In the case of a slope of 0.3 the wave breaker type of the waves change towards plunging waves (with an Iribarren number of 1.3)(Schiereck, 2001). In this situation the responsible part of the overestimation is not the run-up (light blue dotted part of the model result) but the induced shear stresses by wave propagation (Figure 3.10 (A) and (B)). As the kind of impact changes, it can be questioned to
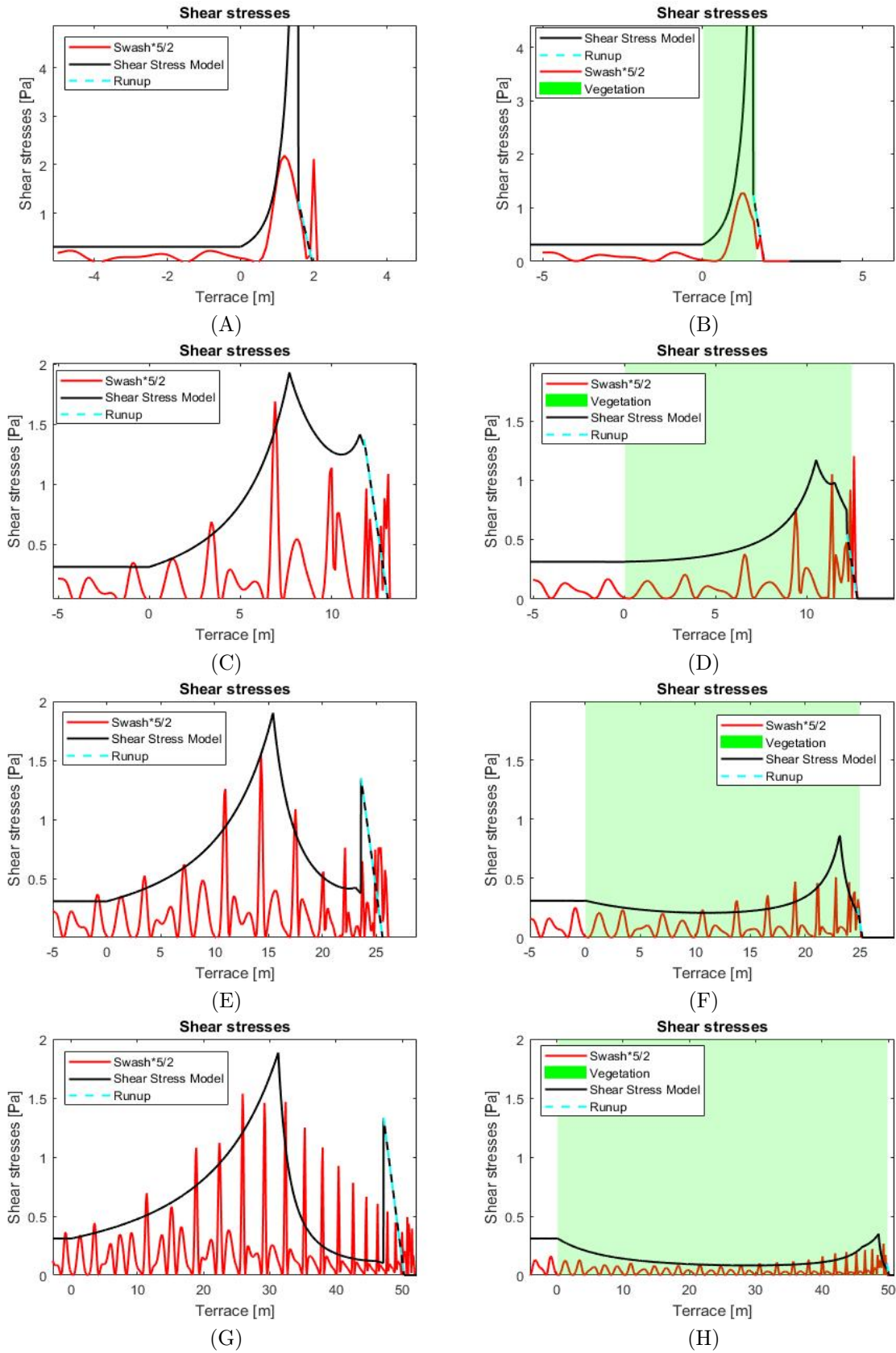
Figure 3.10: Comparison of the induced bed shear stresses for different slopes calculated with the model and with SWASH. The comparison of induced bed shear stresses is done in a vegetated (A, C, E and G) and non vegetated (B, D, F and H) situation with a slope of 0.3 (A and B), 0.04 (C and D), 0.02 (E and F) and 0.01 (G and H).

what extend the calculated shear stresses of SWASH are correct, as the results of SWASH are calculated based on a shear velocity (u_*) and not on the stresses resulting from direct impact of a wave. The model of Duró et al. (2020) works similarly thus its result are subject to the same doubts. Concluding, it can be said that the model of Duró et al.(2020) is not applicable in a situations without surging waves (Iribarren number lower than 0.3).

3.3. Terrace Morphology

The morphology is calculated based on the difference between the induced bed shear stresses and the critical bed shear stresses. The induced bed shear stresses are validated in Section 3.2. For the critical bed shear stresses the values found by Duró et al. (2020) are used. In this section the used equation and parameters for the morphology are described and their influence is estimated.

The model of Duró et al. (2020) has been developed and validated to calculate the shore erosion based on the induced bed shear stresses of primary and secondary ship waves. For this reason, it has initially been assumed that as long as the induced bed shear stresses are correct, the model is capable of predicting the morphological equilibrium of the shore. An in-depth elaboration of one of the largest assumptions concerning the terrace update and its influence will be conducted, in order to test the assumption of a correct calculation of the terrace morphology. In order to estimate the sensitivity of the shore to erosion, a look is taken towards the range of expected soil cohesion which can be found in the Netherlands.

3.3.1. Maximum slope formulation

Near the shore, not only the process of erosion, but also the process of calving plays a role (Figure 3.11). In this process the shore steepens until its stability is threatened and a part of the shore could collapse. In the model of Duró et al. (2020) this effect is not modeled. In order to account for this effect, a maximum slope is defined in order to prevent sharp slopes at the end of the terrace. When the final terrace length is calculated, a sharp transition at the end of the terrace can be expected, but this process is not modeled.

Figure 3.11: Scour process at the end of the slope (de Vree, 2020). This picture illustrates the effect of the scour process at the end of the slope. Here it can be seen that a steep cliff can be formed when the soil in front of the cliff erodes away. The roots of the vegetation can stabilise the cliff, blocking further scour.

The value of the maximum slope was set to 0.1 in the model of Duró et al. (2020) (Figure 3.12.C) which resulted in a maximal inaccuracy of 10% for the calculated bank retreat when compared with data of the Maas under ship wave attack. In order to estimate the influence of this simplification in the modified model of Duró et al. (2020) a field or lab investigation is needed. Especially as a deviation from this number leads to significant different results in induced bed shear stresses (Figure 3.12). Figure 3.12 confirms that the deviation of the total terrace length is indeed within the 10% for the first 800 waves.

The largest increase of shear stresses by the eroded slope originates from the bore propagation which reaches shallower water, but is not yet converted towards run-up (Figure 3.12). Putrevu and Svendsen (1991) stated that the shear stresses based on the orbital motions are not realistic after a water-depth of $0.15*h_{br}$. It can be expected that this value is estimated based on experiments and that a different value is needed in a different situation. Especially as the Irribarren number of the waves changes from 0.2 to 0.4, which means that the wave breaking type changes from spilling waves (which have an Irribarren number of 0.2) to surging waves (which have an Irribarren number of 0.5). The influence of a different type of wave breaking can be found in the way the forces of the breaking waves are induced on the shore. For this reason, a different wave breaking type needs a different formulation for the amount of induced shear stresses (Schiereck, 2001). If the value determining the start of the run-up (in this case 0.15) would indeed increase, meaning that the bore propagation ends and the run-up starts at an earlier stage , the peak resulting from the induced bed shear stresses through bore propagation just before the start of the run-up would be removed. When the wave run-up starts at an earlier stage the resulting bed shear stresses through run-up will increase, what can be expected for the steepening of the slope.

3.3.2. Soil Characteristics

The critical shear stress is calculated with the use of Equation 3.11 based on the research of Kimiaghalam et al. (2016). The soil characteristics measured in the NL were used as a reference for the range of parameters that can be expected.

$$\tau_{cr} = 0.89 * Cohesion - 0.1 \tag{3.11}$$

The soil characteristics of the Netherlands can roughly be divined into 4 area's: sand, clay, peat and loam (Figure 3.13). It can be seen that the reaches with multiple lakes are characterised by a soil existing mainly of clay and peat. In the research of Duró et al. (2020) soil samples along the Maas are measured with a resulting cohesion parameters in the range from 7.33 until 20.92. The Maas lays primarily in an area characterised by clay, as is visible on the map in Figure 3.13. For peat Rahgozar and Saberian (2016) found a cohesion parameters in the range of 10.4 to 11.2 kPa. When sand was added to the mixture (a dosage of 400 kg/m^3) the found parameters for cohesion increased to the range from 12.9 until 13.1 kPa. Using the formula given in Equation 3.11, critical shear strengths in the range of 6.4 up to 18.5 can be found.

In order to account for the presence of vegetation de Baets et al. (2008) derived an Equation accounting for the soil reinforcement of *P. australis* by increasing the soil cohesion. The derivation and Equation can be found in Subsection 2.4.3)

(A)

(B)

(C)

(D)

(E)
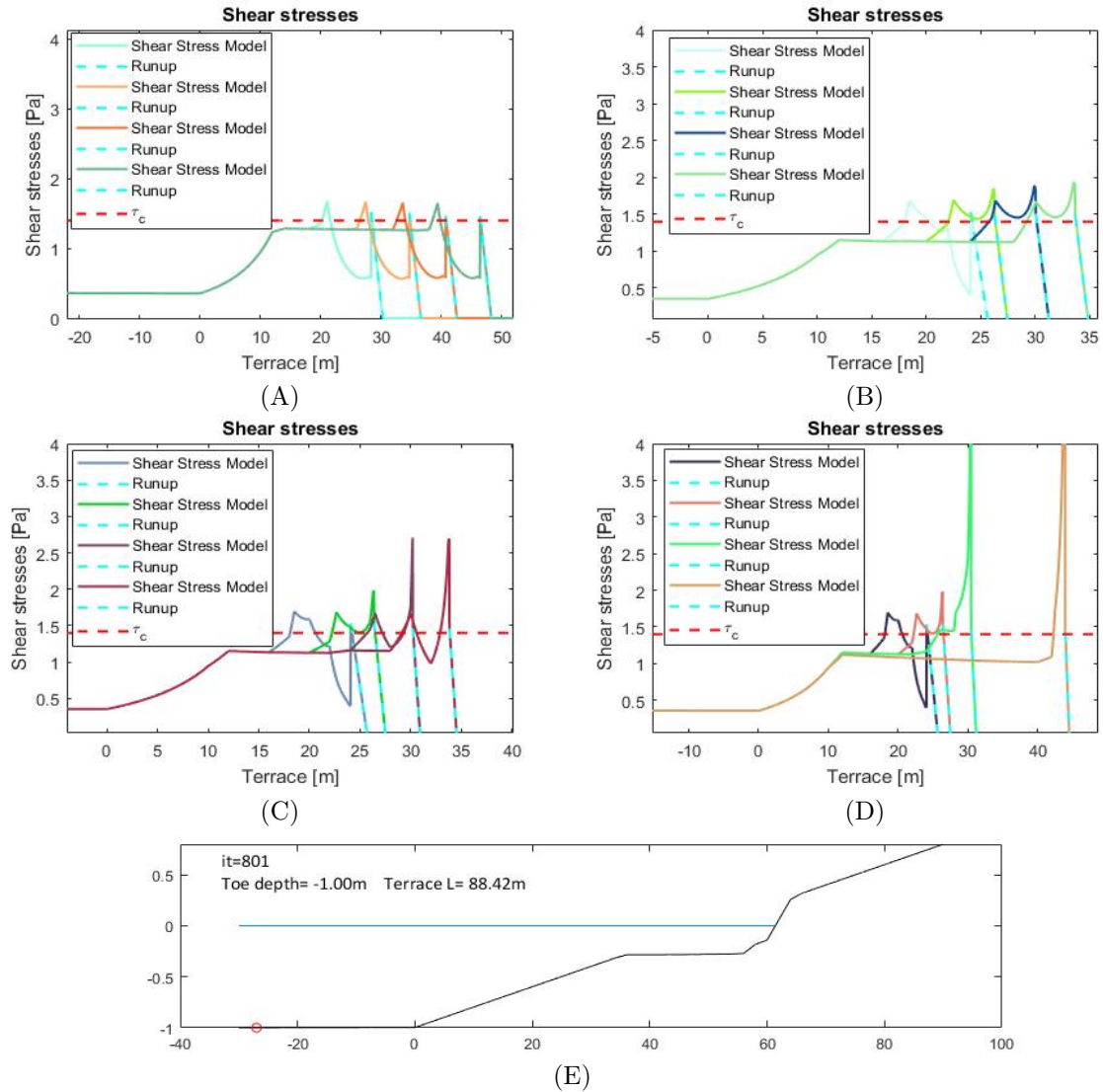
Figure 3.12: . Influence of the maximum slope formulation without vegetation. Induced bed shear stresses related to shore development for every 200 iterations with a maximum of 801 iterations. The used maximum slope formulation are (A) 0.025, (B) 0.05, (C) 0.1 and (D) 0.15 for τ_c=1.4, H=0.15, T=2, m=0.02. Plot (I) illustrates the shore state after 800 iterations for Plot (C)
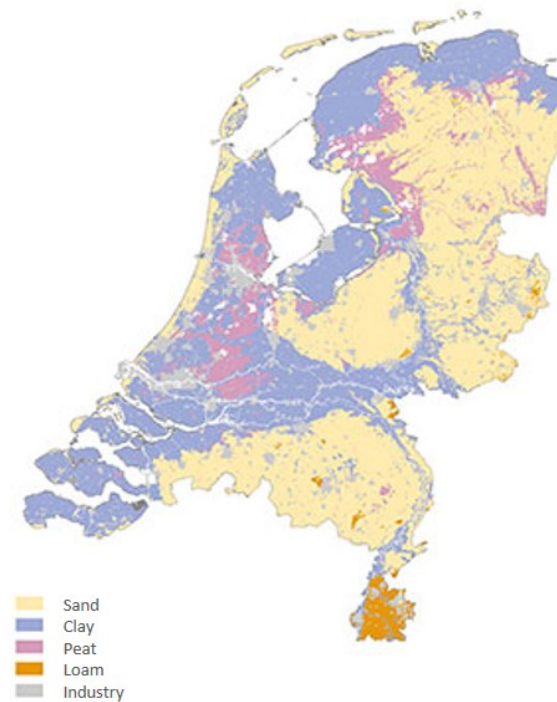
Figure 3.13: Soil classification of the Netherlands (RIVM, 2019).

3.3.3. Lake morphology

Combining the findings of Section 3.2 about the induced bed shear stresses and Subsection 3.3.2 about the soil characteristics found in the Netherlands, an estimation can be made of the impact of the used formula's in real situations.

The goal of the development of the modified model of Duró et al. (2020) is to quantify the contribution of *P. australis* along a lake against hydrodynamic forcing. In order to compare a situation with and without *P. australis*, the hydrodynamic loads have to remain in the range that *P. australis* will grow. Another restriction is given by the slope. By designing the least amount of space is preferred, but the slope has to be steep enough in order to develop a rich habitat. Often a slope of 0.3 is taken as a boundary (Ministerie van Verkeer en Waterstaat, 1999a). In Subsection 3.3.1 it is established that the model is not capable of modeling other wave types than spilling waves.

In order to calculate the maximum shore attack, waves with a wave-height of 0.4m and period of 3.5 are taken. Assuming only spilling waves are allowed (Iribarren number of 0.3) the maximum initial shore steepness equals 0.1. In this situation for a non-vegetated shore a small, almost negligible amount of erosion takes place (Figure 3.14 (C) and (D)). If vegetation is included the amount of induced bed shear stresses stay's below the critical shear stress (Figure 3.14.B).

For regular wave attack, *P. australis* can resist a wave attack with a wave height of 0.25m, in which case the shore will not erode when the slope equals 0.1. Even without vegetation the shore shows no erosion in those conditions. As the shore attack based on the maximum daily situation does not lead to erosion for the shore with the lowest cohesion found in Subsection 3.3.2, it can be assumed that the main erosion taking place along shallow shores is driven by biotic processes which disturb the soil, such as fish rooting the soil, which are not represented in this model.

(A) Without vegetation

(B) Without vegetation

(C) Without vegetation

(D) with common reed

(E) morphological change in shear stresses

(F) Final terrace profile
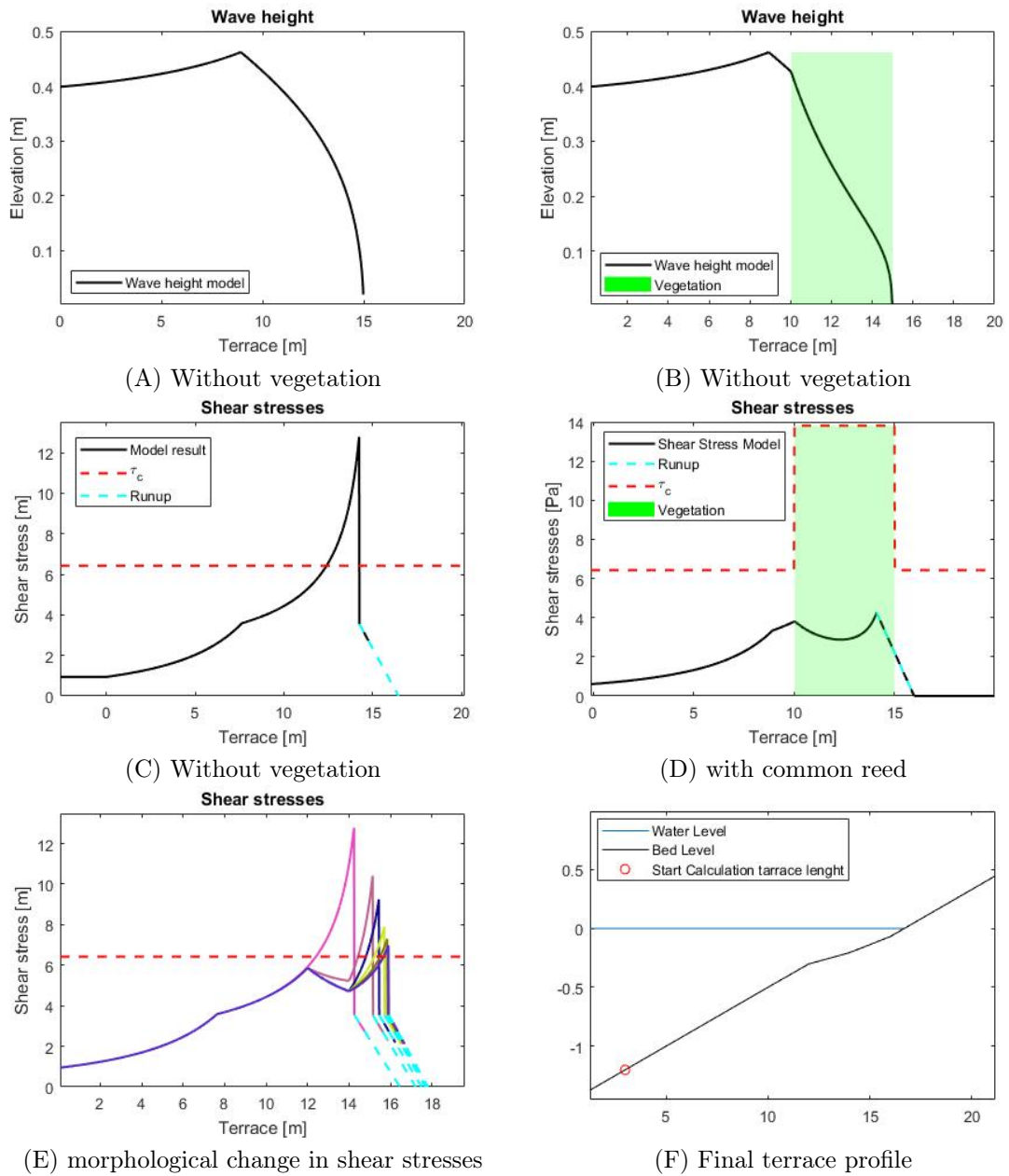
Figure 3.14: Maximum amount of shear shear stresses in a condition with spilling waves ($\xi= 0.3$ and m=0.1) in which common reed can stand ($H = 0.4$ and $T = 3.5$). The influence of the presence of vegetation is illustrated by showing the wave height development and the related induced bed shear stresses and critical bed shear stresses in a situation without (A and C) and with (B and D) vegetation for the lowest found cohesion by Duró et al. (2020). In Plot (E) the change in induced bed shear stresses due to morphological changes is shown. Plot (F) shows the equilibrium profile for the case without vegetation. In a situation with vegetation no morphological changes are present.

4
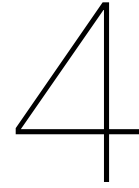
Model Results

In this chapter different input parameters, which can be used for design choices concerning a vegetated shore, are tested (Section 4.1). In order to estimate the sensitivity of these results towards one of the estimated and/or calibrated parameters, Section 4.2 shows the sensitivity of different parameters on the maximum induced bed shear stresses, after which the two parameters with the largest influence are elaborated into depth.

4.1. Results
In this section we investigated the influence of placement location (Figure 4.1), slope deviation (Figure 4.2) and the incoming wave period (Figure 4.3) on the wave height propagation and the induced bed shear stresses. In appendix C.4.1 the same is done with a single wave height for the vegetation growing depth, vegetation density, stem diameter, drag coefficient, breaking parameter and the start location of the run-up.

All aspects have been tested for wave heights in the range of 0.1 to 0.4m, as this is the range in which a healthy vegetation can grow. For every tested input parameter 8 plots are made showing the wave height propagation and the corresponding induced shear stresses. Below those plots, a summarising plot is made which shows for different tested variables the maximal induced bed shear stresses as a function of the incoming wave height.

The choice to change both the wave height and the tested input value is made as the wave height is one of the largest variables in the model and has a high impact on the maximum induced bed shear stress. Therefore it is important to understand how a change in the tested input parameter is affected by the different wave heights.
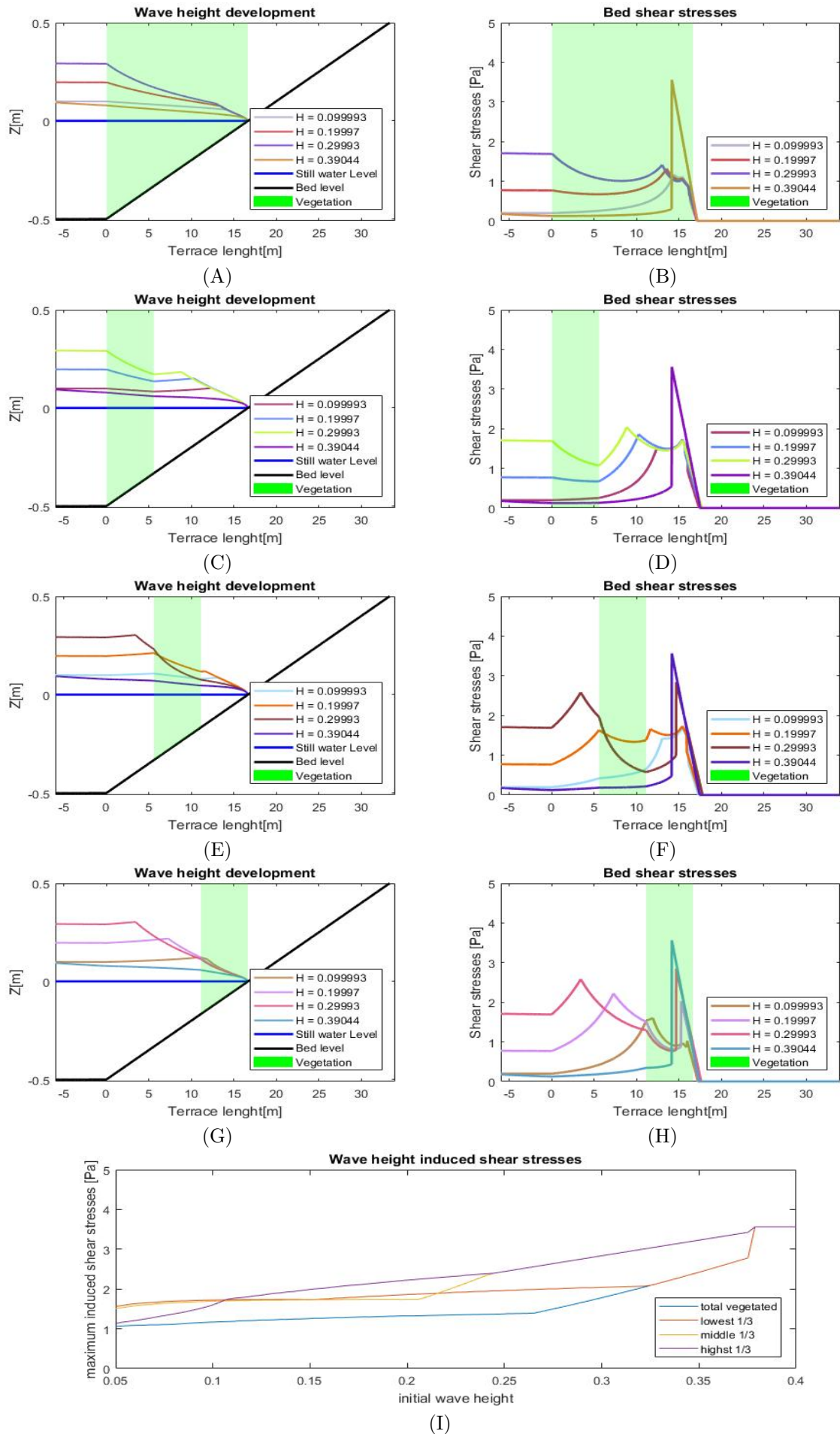
Figure 4.1: Wave height and shear stresses for different vegetated areas of P. australis across the shore, $T = 3$s and $m = 0.03$. In this figure four placements strategies for P. australis are tested. The influences of the different placements strategies is illustrated by the wave height development over the terrace length (A, C, E, G) with the corresponding induced bed shear stresses (B, D, F, H). In the final Plot (I), only the maximum induced bed shear stresses for the different placement strategies are shown based on different incoming wave heights.

Placement strategy
For a vegetated shore, it is not necessarily needed to place vegetation across the entire shore, also a partially vegetated shore is capable of reducing a large part of the wave impact. When a fully vegetated shore is only needed for storm conditions, it can be beneficial to start only with a partial vegetated shore and leave the vegetation to populate the rest of the shore naturally (Section 5.3).

The amount of wave reduction induced by the vegetation is highly dependent on the position of the vegetation across the shore profile (Figure 4.1). On average, the further a vegetation patch with a constant width is placed from the shore, the lower the maximum induced shear stresses become (Figure 4.1 (I)). This effect can be explained by looking at the location of wave breaking. When the waves break in front of the vegetation no energy is dissipated, so the wave could reach its maximum height, resulting in a maximum impact. Also the induced velocities by breaking are higher, resulting in higher shear stresses during run-up. When the waves break inside or behind the vegetation the point of wave breaking is delayed through the loss of wave energy. Because of this delay the water depth at the point of wave breaking is decreased, so the maximum possible wave height decreases as well. This results in a lower impact when the wave finally breaks. Aside from this the start location of the run-up is delayed, so lower shear stresses through run-up are induced. In the summarising plot (Figure 4.1 I) it can be seen clearly that the maximum induced bed shear stresses are almost constant for different initial wave heights, but show an increase when the vegetation starts behind the wave breaking point.

For wave heights above the 0.37m it can be seen that the placement location of the vegetation is no longer important. This can be explained by the fact that those waves will break before the vegetation is reached, so the location of wave breaking is in all the situation equal, resulting in an equal run-up induced shear stress.

(A)

(B)

(C)

(D)

(E)

(F)

(G)

(H)

(I)
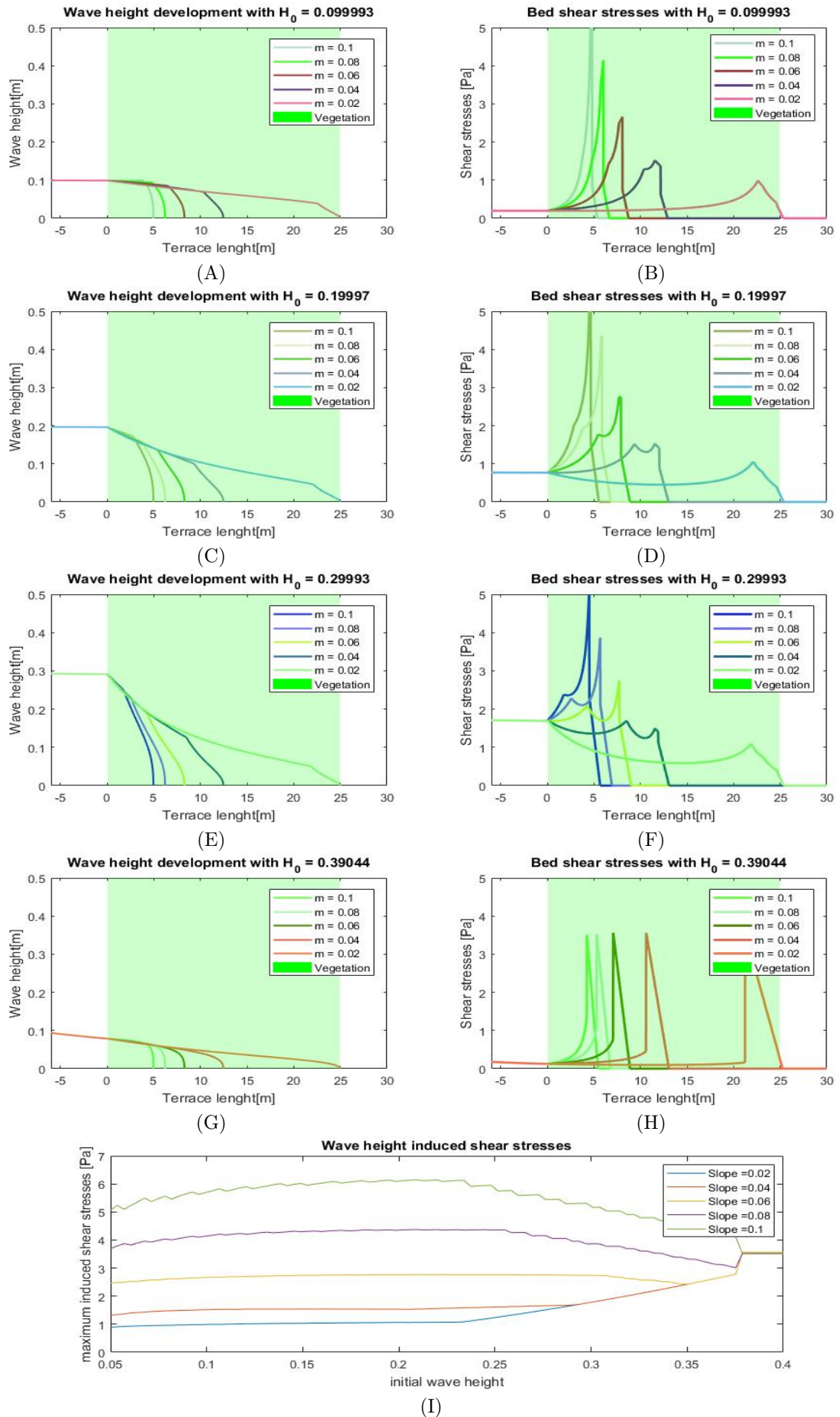
Figure 4.2: Wave height and bed shear stresses for different slopes with P. australis, $T = 3$s.
In this figure the influence of five different bed slopes are tested. The influences of the bed slope is illustrated by the wave height development over the terrace length(A, C, E, G), with the corresponding induced bed shear stresses (B, D, F, H). In the final plot (I), only the maximum induced bed shear stresses for the bed slopes are shown based on different incoming wave heights.

Slope
By the design of a shore the slope is one of the few variables which can be chosen freely. The slope has a high impact on the total horizontal vegetated area, and is therefore one of the main factors determining the amount of wave reduction the vegetation can reach. The influence of the incoming wave height is in general negligible, since a higher incoming wave will lose more energy until it reaches the same wave height as a lower wave before the shoaling effect starts to dominate. A combination of the higher incoming waves and a steeper slope can even lead to a reversed effect, where a higher incoming wave height leads to a lower maximum amount of induced bed shear stresses. This happens since the shoaling after wave breaking is responsible for the maximum induced bed shear stress. As the wave breaks in an earlier stage, the wave dissipation due to bore propagation removes waves energy, resulting in a lower wave height after wave breaking. This conclusion will also be dependent on an accurate prediction of the start location of the run-up. Further research should investigate this in more detail (Subsection 3.2.3 and 5.1.1).

(A)

(B)

(C)

(D)

(E)

(F)

(G)

(H)

(I)
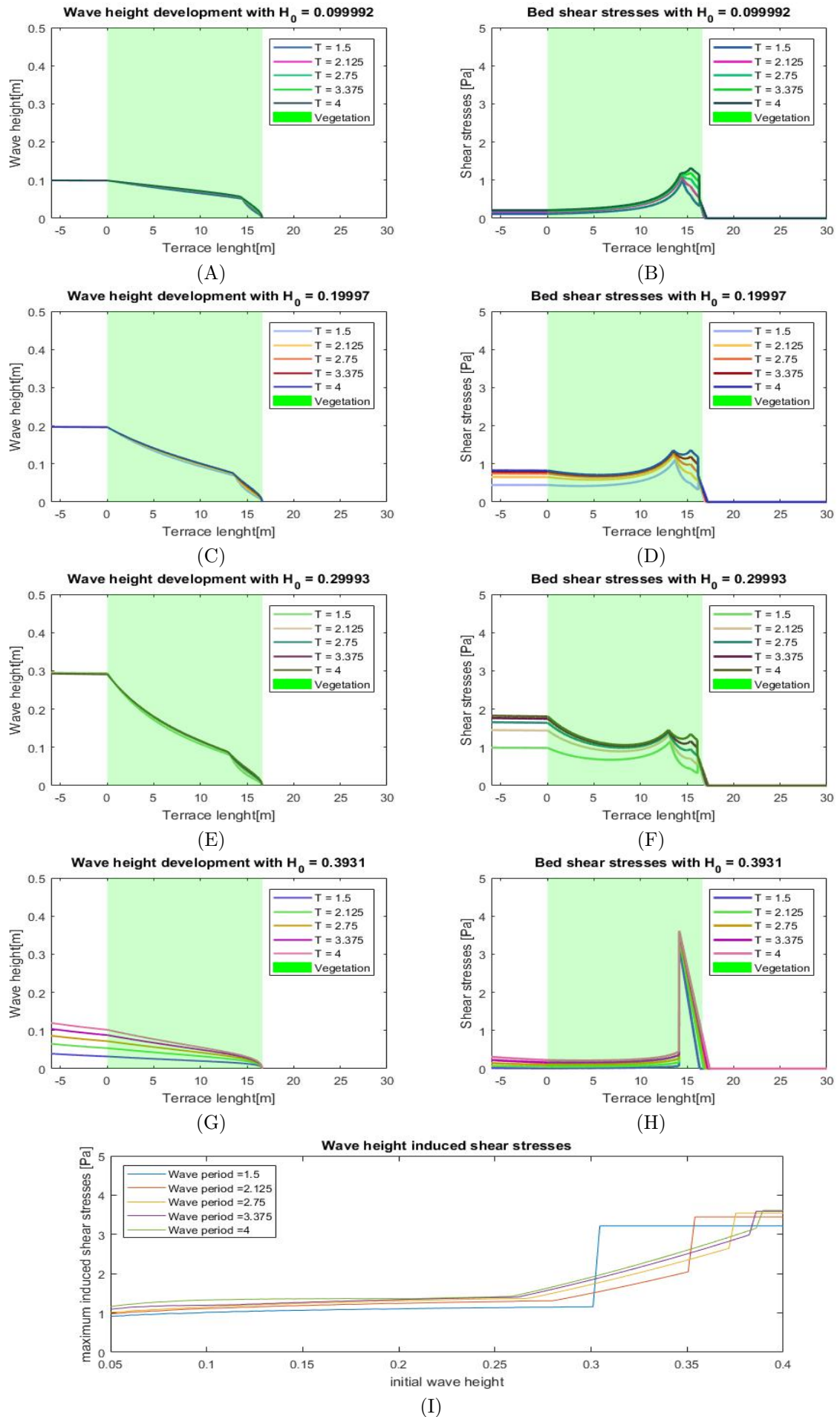
Figure 4.3: Wave height and bed shear stresses for different wave periods with P. australis, $m = 0.03$. In this figure five initial wave periods are tested. The influences of the different wave periods are illustrated by the wave height development over the terrace length(A, C, E, G), with the corresponding induced bed shear stresses (B, D, F, H). In the final plot (I), only the maximum induced bed shear stresses for the different wave periods are shown based on different incoming wave heights.

Wave period
The wave period is one of the parameters which is needed as an input value, but which is difficult to influence. But it is interesting to see the influence of a different wave period on the vegetation capacity to dampen the waves. From this analysis it can be concluded that the wave period had no impact on the vegetation damping capacity (Figure 4.3). The only influence of the wave period can be found in the final wave height, which is lowered when the combination of a wave height and wave period lead to an unrealistic situation, so the system balance itself.

4.2. Sensitivity analysis

The model is based on multiple empirical parameters, such as the breaking parameter γ and the start location of the run-up. Those parameters are estimated for situations similar to the conditions for which the modified model of Duró et al. (2020) has been developed. In order to estimate the sensitivity of the model towards those parameters the maximum shear stresses are calculated for the value of those parameters 10% lower and 10% higher than the used value in the model. The difference between the results has been translated towards a percentage of the total induced bed shear stresses for the original value.

The same is done for the sensitivity of the results towards the estimated input parameters, such as the incoming wave period and the slope of the shore. For the vegetation characteristics N (stem density) and dv (stem diameter) the choice is made to estimate those influences with a constant drag factor in order to give a better estimation of the impact of the two different processes (Figure 4.4).

In order to illustrate the impact of different parameters, the choice is made to show only the change in maximum induced bed shear stress, since the maximum induced bed shear stress determines if the shore is stable. The other variable is the initial wave height, as the wave height is one of the largest variables in the model and has a high impact on the maximum induced bed shear stress. Therefore it is important to understand how a change in the tested input parameter is affected by the different wave heights. The results are illustrated in Figure 4.4.

A difference is made between the maximum induced bed shear stresses during bore propagation and the maximum amount of bed shear stresses over the total terrace length. Figure 4.4.A includes the shear stresses induced during run-up and in the lower plot only the shear stresses of bore propagation have been accounted for. In Appendix C.4.1 the induced bed shear stresses for multiple values of the variables has been showed.

It can be concluded that the breaking parameter and the vegetation depth have a large influence on the maximum induced bed shear stresses (Figure 4.4 (A) and (B)). This is discussed in more detail in Section 5.2. All parameters concerning the damping characteristics of vegetation (stem density (N), stem diameter (D) and the drag coefficient (CD)) have the same sensitivity, which could be expected since the damping factor of the waves exist of a derivation of those three factors. The drag coefficient depends also on N and D, but in order to determine the sensitivity of the parameters separately the drag coefficient is taken as a constant. When the wave height increases (above the 0.33m) the change in induced bed shear stresses by the run-up become dominant, so a difference is seen between Figure 4.4 (A) and (B). The sensitivity for a change in vegetation depth, breaking parameter and the start location of the run-up increase, as they are important for the shear stresses resulting from run-up.

(A)

(B)
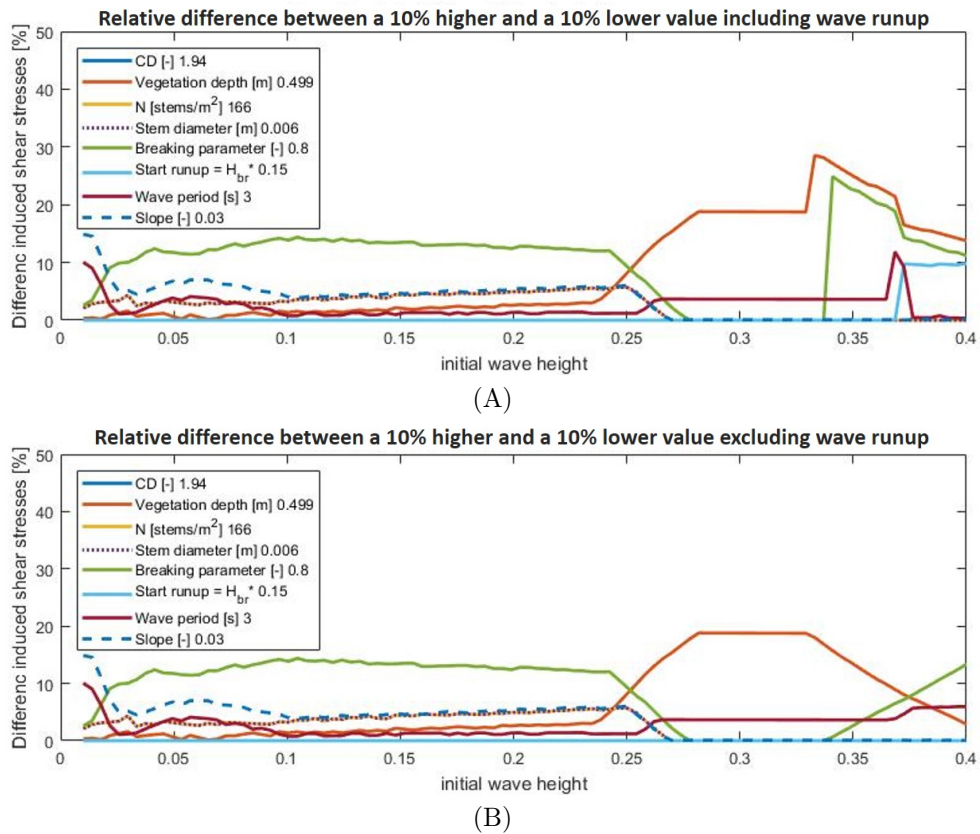
Figure 4.4: Sensitivity analysis of different model parameters as presented in Section 4.2. This figure shows the relative influence of a 10% higher and 10% lower value of the tested parameters on the induced bed shear stresses. The tested parameters drag coefficient (CD[-]), stem diameter (D[m]) and stem density (N [stems/m^2]) have exactly the same results. The other lines are the vegetation growing depth, breaking parameter (γ[-]), Start location of the run-up [-], wave period (T[s]), Terrace Slope(m[-]). This is done for all the wave heights ranging from 0.01 to 0.4m (vertical axis) in order to include the changing behavior of different parameters for different wave heights. As the model calculation of the induced bed shear stresses exist of 2 phases, bore propagation and run-up, the results of the sensitivity analyses are also deviated in a graph including the run-up and excluding run-up.

5

Discussion

The model was developed with a number of assumptions. This chapter discusses these assumptions, and the sensitivity of the model to changes in the input parameters. At the end, the potential of the model is discussed.

5.1. Limitations of the model

The model of Duró et al. (2020) is a process based model, so all the hydraulic processes must be added separately and are often based on empirical relations. Therefore one need to keep in mind for which situations the used formulas are derived and which processes are neglected. In this section an overview is given of the range of parameters for which the formulations are derived as described in Chapter 3. Aside from this, an estimate will be given concerning the influence of aspects which are not taken into account.

5.1.1. Restrictions concerning the parameter range

This subsection discussed the restrictions concerning the validity range for the water depth, wave heights, drag coefficient and the slope.

Water depth

The formulas describing the wave propagation (Appendix B) are based on the shallow water equations. This means that the equations can only be used when the water depth is shallower than 0.05 times the wave length (Schiereck, 2001). Wind waves comply with this limitation.

Wave height

The main restriction concerning the wave height can be found in the maximum allowable wave height in which *P. australis* can grow. As the model is designed to estimate the influence of *P. australis*, the model is not tested for wave heights above 0.4m. When the wave height increases further, the vegetation will be damaged and the calculated energy dissipation through the presence of vegetation will lead to unrealistic values, as the formulas account for a healthy populations.

Drag coefficient

Another restriction is the drag coefficient for *P. australis* (Equation 2.4.2). The used equation has been derived by Wu et al. (2011) for S. Alterniflora (Green) which has a high resemblance in characteristics with *P. australis*. The derivation relates the Keulegan-Carpenter number (KC) to the drag coefficient measured in the experiments. The range of used wave heights is 0.0092 up to 0.1634m, the tested wave periods are in the range of 0.7 up to 2s and the water depths range from a depth of 0.4m up to 0.7m. By a deviation of those parameters an inaccuracy can arise. As the estimated drag coefficient is related to the Keulegan–Carpenter number, the expected inaccuracy is small since the Keulegan–Carpenter is not restricted to a certain validation range.

Slope

In Subsection 3.2.3 an inaccuracy is found for slopes outside the range 0.02-0.04 m/m. In this subsection the possible reason is discussed followed by a recommendation concerning the limited range.

The induced bed shear stresses, which are the base of the morphology, are the result of the bore propagation over the terrace length. At the end of the terrace length the water depth decreases and at a certain point the assumption of bed shear stresses due to bore propagation is not valid anymore. This point has been established by Putrevu and Svendsen (1991) as 0.12 times the wave breaking depth, and is re-estimated by Duró et al.(2020) to 0.15. Since this number is derived empirically, it is assumed that this value will change with changing conditions. In the results a high dependency is found related to the end of the bore propagation, especially when the slope steepens. Therefore a more in depth study concerning this effect is needed.

A change in start location of the run-up can lead to significant changes in the induced bed shear stresses. If this value, for the relation between wave breaking depth and start run-up depth, is higher, the induced bed shear stresses of bore propagation end in an earlier stage. This could remove the sudden increase in bed shear stresses due to the shoaling effect just before the start of the run-up (green line in Figure 5.1). It would also mean that the run-up starts earlier, resulting in a higher run-up velocity followed by higher bed shear stresses (Subsection 3.2.3). Higher velocities at the start of the run-up would result in even higher jumps in induced shear stresses (Figure 5.1), which is not naturally.

The limitations of a single value for the transition depth can be seen in Figure 3.12 (Subsection 3.3.1), were a steeper slope results in a sudden increase of shear stresses. Therefore a dependency of the bed slope is expected and needs further investigation. At this point, the overestimation of the induced bed shear stresses at the end of the terrace length must be regarded with care. An overestimation can be expected when the slopes are steeper than 0.04, the height of the overestimation is case specific (Figure 3.10, subsection 3.2.3).

For the formulation for the run-up height, Bergsma et al. (2019) derived an equation based on data collected from a sandy beach with slopes varying between the 0.1 and 0.01. The induced shear stresses by run-up in this model are based on the wave celerity at the start of the run-up, which in the case of Bergsma et al. (2019) were spilling waves. As the equations are derived for spilling waves it can be expected that only the spilling waves can be modeled.

In follow-up studies it should be investigated if the change in physical processes for other types of waves affects the formulations for the start location of the run-up and the run-up height.

Overall the estimated ranges (summerised in Table (5.1) will be inside the expected range for a lake situation with a vegetated shore, except for the restrictions following by the changes in the slope. Within those restrictions the model can be used to give an overall idea for the influence of vegetation on shore protection, but is not ready to use for a specific location along a shore. Therefore the restriction by the slope is the limiting factor.

Table 5.1: Model restrictions concerning validated range

Parameter	unit	Minimal Value	Maximal value
Water depth (h)	m	-	$0.05\,L_0$
Wave height (H)	m	-	0.4
Slope	-	-	$0.5\,\sqrt{H/L_0}$
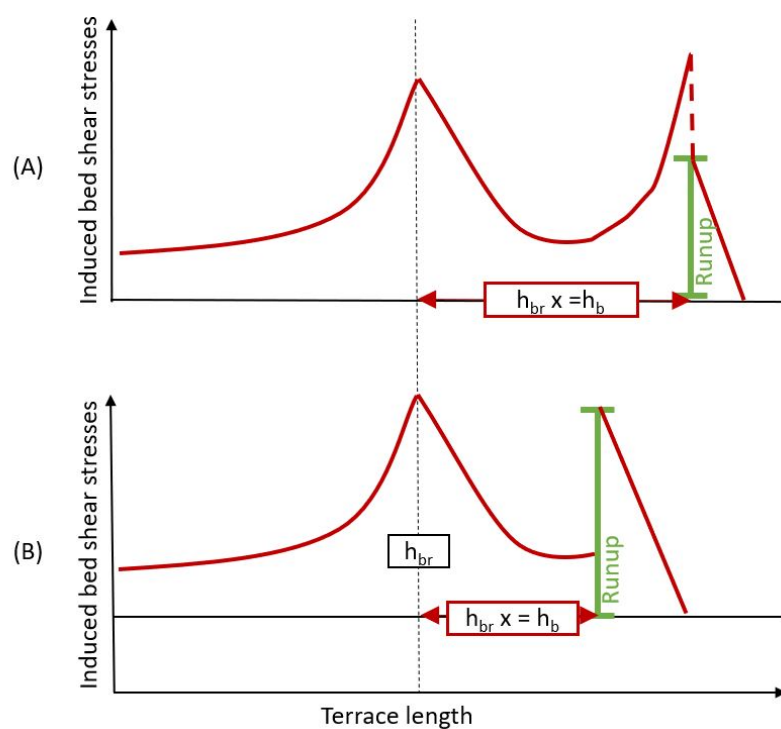
Figure 5.1: Changing transition point. (A) lower value for x. (B) higher value for x. A change of the transition point from wave propagation to run-up can lead to a large change in the maximum amount of induced bed shear stresses. At a certain point after wave breaking the shoaling effect starts to dominate over the dissipation processes, resulting in fast increase in induced shear stresses. At some stage this formulation gives an unrealistic result, this is were the run-up should start. The sooner the run-up starts, the higher the wave celerity is, resulting in a higher bed shear stress through run-up.

5.1.2. Aspects that are not taken into account

Reflection

In the current model the effect of reflection has not been taken into account. This choice is made since the model calculates the processes concerning wave propagation and energy conservation from offshore towards onshore, while reflection works the other way around. A feedback loop could be added, which makes it possible to include processes such as reflection, but due to the limited time this aspect is not included. In order get insight in the possible increase in wave height and induced bed shear stresses an estimate of the magnitude of the neglected reflection is made.

The impact of reflection is estimated with the model results of SWASH. This estimate is made for *P. australis* (common reeds). The chosen stem density and stem diameter correspond to the summer conditions of *P. australis*. These values were used, because the stems are the most flexible and developed in this period, and therefore less likely to break under wave attack while giving the highest reflection. The range of tested wave heights is between the 0.1 and 0.3m, as *P. australis* only grows until a depth of 0.4m with a constant water depth (Vretare et al. (2001), whereas waves larger than 0.3m will break. The drag coefficient is calculated with the formulas given in Subsection 2.4.2.

The reflected wave height is calculated based on the first oscillation in front of the vegetation modelled in SWASH. The vegetation is modeled on a slope of 0.02, starting at a depth of 0.5m. In front of the vegetation a straight foreshore of 10m is implemented. A total of 12 runs are made, of which model run 3, 6, 9 and 12 are shown in Figure 5.2.

Table 5.2: Indication of wave reflection in front of the vegetation for multiple runs. The increase in wave height in front of the vegetation ($H_{reflect}$) is modeled with SWASH for different combinations of the incoming wave height (H) and period (T). To relative the increase of the reflecting wave height it is expressed as the percentage increase in wave height.

Run	H[m]	T[s]	C_D	H reflect [m]	Increase in wave height[%]
Reflect 1	0.1	1	3.6556	0.00063	0.63
Reflect 2	0.15	1	2.7380	0.001	0.67
Reflect 3	0.1	2	2.6384	0.00234	2.34
Reflect 4	0.15	2	2.2163	0.00705	4.7
Reflect 5	0.2	2	2.0481	0.01425	7.125
Reflect 6	0.25	2	1.9625	0.02105	8.42
Reflect 7	0.3	2	1.9124	0.0594	19.8
Reflect 8	0.1	4	1.9163	0.00285	2.85
Reflect 9	0.15	4	1.8446	0.00585	3.9
Reflect 10	0.2	4	1.8157	0.0099	4.95
Reflect 11	0.25	4	1.8039	0.02105	8.42
Reflect 12	0.3	4	1.8154	0.0508	16.93

Table 5.2 shows that the reflected wave height increases exponentially with an increasing incoming wave height. A longer wave period results in the tested cases a lower reflection. This can be expected, because a shorter wave period brings a higher amount of energy flux (Figure 3.5, Subsection 3.1.2). The results of run 3 to 12 show a clear trend concerning the increase of the reflected wave height. For run 1 and 2, the wave period is in the range of 1 second, resulting in a negligible reflection.

The influence of the reflection is significant and should be taken into account, especially in the situation with a higher incoming wave height. Looking at the equations, a maximum increase of induced bed shear stresses of 43.5% can be expected. This can be explained with the knowledge that an incoming wave height of 0.3m increases 19.8% (Table 5.2) due to the reflection and the relation between the induced bed shear stresses and the wave height is quadratic since $\tau_b \sim H^2$.

(A) SWASH result Reflect 3

(B) SWASH result Reflect 6

(C) SWASH result Reflect 9

(D) SWASH result Reflect 12

(E) Modeled shore profile
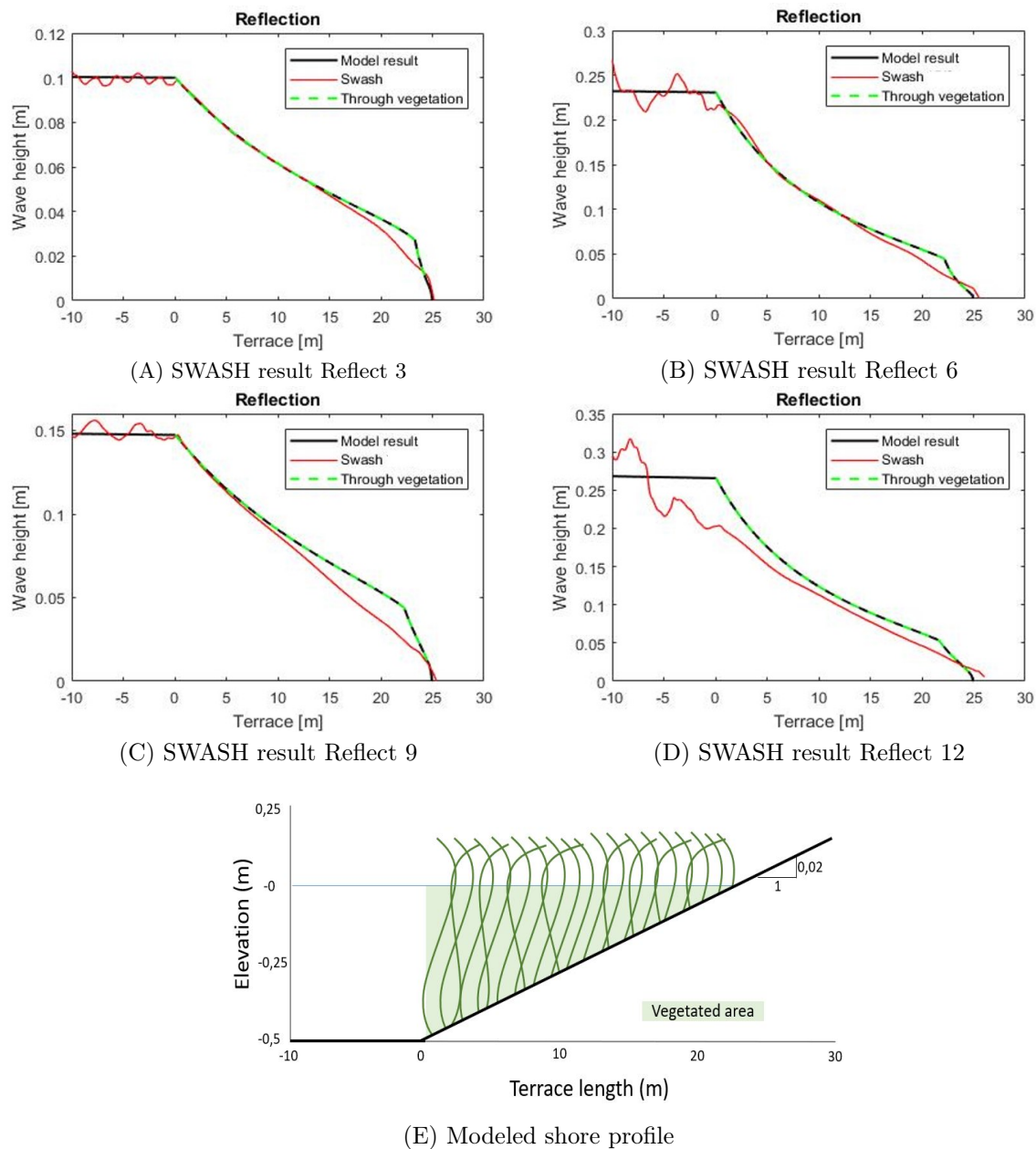
Figure 5.2: Modeling output of the magnitude of the reflection from Table 5.2. The magnitude of the reflection in front of the vegetation is modeled with the use of SWASH.

Set-up

Before an attempt is made to implement the equation to calculate the setup (Equation 5.1 (Dean and Bender, 2005)) an estimation is made of the the influence of the setup on the induced bed shear stresses. This is done by increasing the still water level over the cross section equally to the amount of setup calculated by SWASH.

The wave set-up can be calculated with the use of Equation 5.1 (Dean and Bender, 2005) but before an attempt is made to implement this process the influence of the set-up is estimated. This estimation is done by increasing the still water line manually until the same set-up is archived as found in SWASH.

$$\frac{\delta\eta}{\delta x} = \frac{1}{\rho_w g(h+\eta)} \frac{\rho_w \nu \beta H^2 C}{8h^2} \left(\frac{3}{2}-1\right) \tag{5.1}$$

$$\beta \equiv \sqrt{\frac{\sigma}{2\nu}} \tag{5.2}$$

$$
\begin{aligned}
\text{where:} \quad &\eta = \text{Set-up} \\
&\rho_w = \text{Water density} \\
&g = \text{Gravity constant} \\
&h = \text{Water depth} \\
&\nu = \text{Viscosity} \\
&H = \text{Wave height} \\
&\sigma = \text{Wave angular frequency}
\end{aligned}
$$

To get a feeling for the influence of the set-up resulting of the breaking waves the water level after wave breaking is increased. The amount of expected set-up is compared with the results from SWASH and the expected set-up given by the formulation of Bosboom and Stive (2012).

$$\eta_{max} = \frac{5}{16}\gamma_b H_{br} \tag{5.3}$$

$$
\begin{aligned}
\text{where:} \quad &\eta_{max} = \text{Maximum Set-up} \\
&\gamma_b = \text{Wave breaking index} \\
&H_{br} = \text{Wave breaking height}
\end{aligned}
$$

In Figure 5.3 it can be seen that the addition of wave set-up has almost a negligible influence on the wave height and induced shear stresses. In the last meter, a small difference can be found, as the wave height starts to increase a little at the end. It can be seen that the run-up starts a little later what results in the same amount of shear stresses, but only a meter later. From the estimation of the influence of the set-up it is concluded that its effect is negligible and is therefore not implemented.

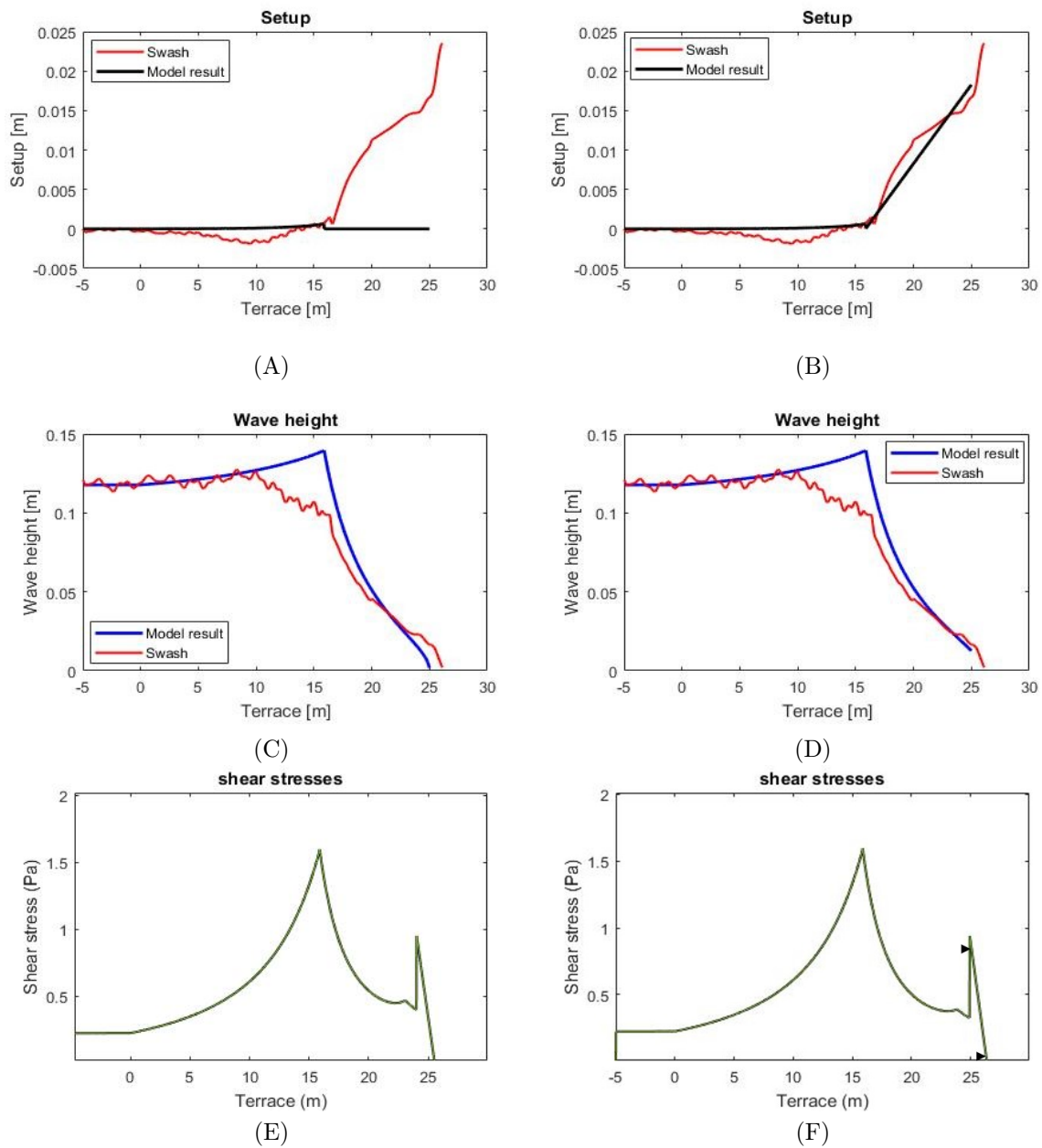Figure 5.3: Effect of implementing set-up over the cross section of the shore. Plot (A), (C) and (E) are without set-up. Plot (B), (D) and (F) are with set-up. Plot (A) and (B) show the induced set-up, (C) and (D) show the wave height development with and without the setup and E and F show the induced bed shear stresses with and without setup. In Plot (F) the difference in induced bed shear stresses is indicated with arrows.

Set-up inside vegetation

The influence of the set-up generated by the presence of the vegetation is estimated in the same way as the reflection (Subsection 5.1.2). The maximum set-up and set-down are estimated for the vegetated area until the start of the run-up (0.15*Wave breaking depth), as wave propagation from this point onward is unrealistic and the formulation will be translated towards the run-up formulation (Duró et al., 2020), where the set-up does not longer influence the amount of erosion (Subsection 3.2.3).

In the previous subsection it is shown that a set-up of 0.015m at the end of a slope gives a negligible effect in the bed shear stresses. The maximum found set-up through vegetation reaches a value of 0.0186m. Since this difference is too small to make a real difference it can be neglected as well. The set down reaches a maximum value of 4.601mm for the modelled conditions. It can be assumed that this is negligible as well, since the magnitude is smaller. Therefore the set-up/ set-down is not tested in more detail. However, when the vegetation type changes and the vegetation becomes denser or increases in diameter, the results can be different. It can be concluded that the reflection for *P. australis* is negligible, but for a different vegetation type the effect of the set-up has to be re-evaluated.

Table 5.3: Indication of the maximum set-up/set-down for multiple conditions. The set-up/set-down resulting from the presence of the vegetation (max set-down/set-up) is modeled with SWASH for different combinations of the incoming wave height (H) and period (T). Only values until the start of the run-up are considered, as only the bore propagation and start value of the run-up formulation are dependent on the set-up.

Run	H[m]	T[s]	CD	max set-down [mm]	max set-up [mm]
set-up 1	0.1	1	3.6556	1.594	1.352
set-up 2	0.15	1	2.7380	3.849	2.306
set-up 3	0.1	2	2.6384	2.98	0.489
set-up 4	0.15	2	2.2163	2.228	1.679
set-up 5	0.2	2	2.0481	0.223	3.776
set-up 6	0.25	2	1.9625	-	6.67
set-up 7	0.3	2	1.9124	-	14.27
set-up 8	0.1	4	1.9163	4.601	-
set-up 9	0.15	4	1.8446	4.405	-
set-up 10	0.2	4	1.8157	1.827	1.497
set-up 11	0.25	4	1.8039	-	19.84
set-up 12	0.3	4	1.8154	-	18.6

(A) SWASH result set-up 3

(B) SWASH result set-up 6

(C) SWASH result set-up 9

(D) SWASH result set-up 12

(E) Modeled shore profile
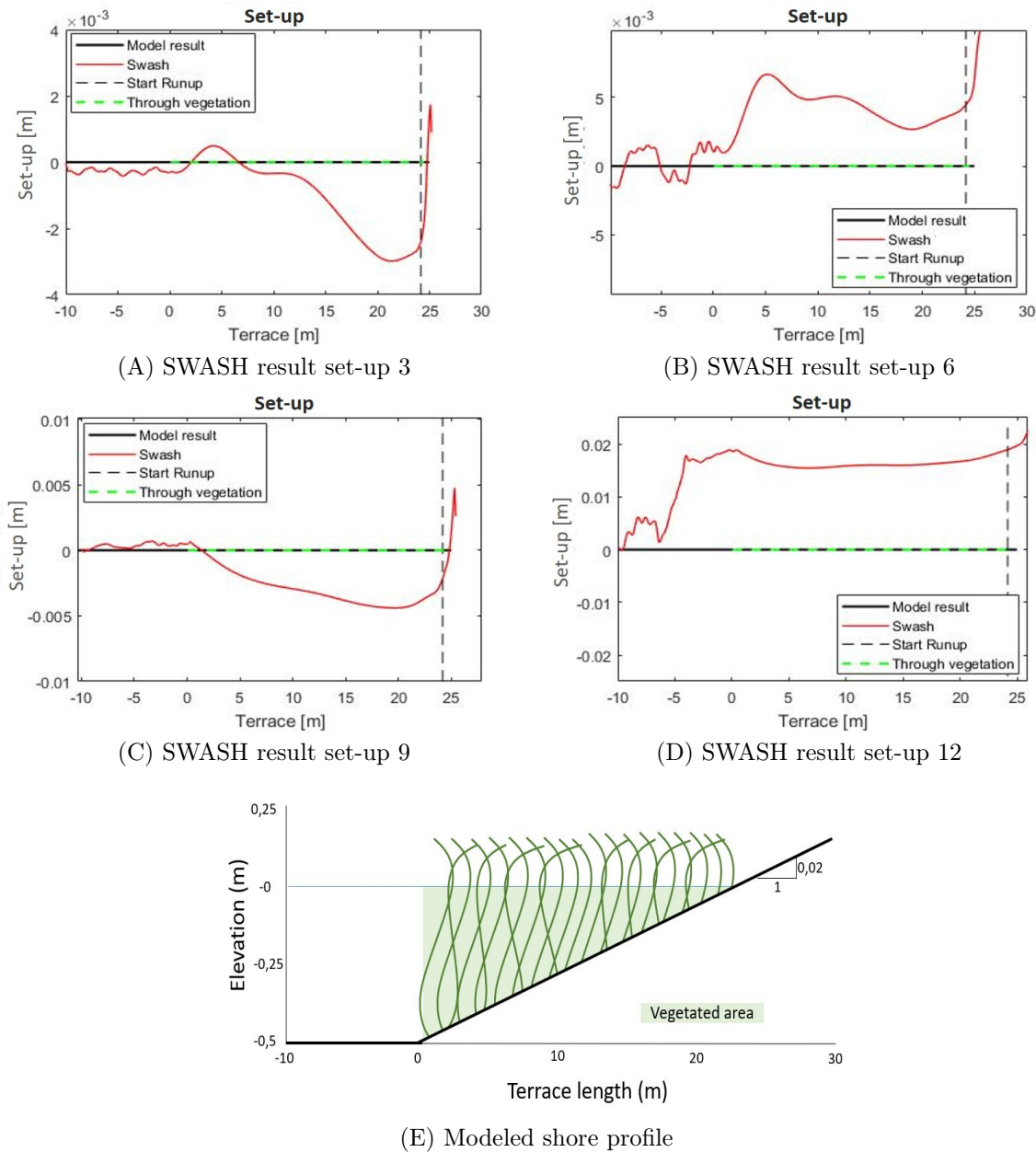
Figure 5.4: Modeling output of the magnitude of set-up from Table 5.3. The magnitude of the set-up inside the vegetated area is modeled with the use of SWASH. For the estimation of the set-up only values until the start of the run-up are considered, as only the bore propagation and start value of the run-up formulation are dependent on the set-up. The start location of the run-up is defined the water depth equal to 0.15* wave breaking depth.

Scour Processes

In order to simplify the scour process at the end of the terrace, a maximum slope formulation is used. This simplification was introduced by Duró et al.(2020). Since the scour processes at the end of the terrace length are quite complicated to model, while this simplification is sufficient to fulfill the model purpose.

By the use of the maximum slope formulation sharp angles are removed and the erosion at the end of the terrace is only based on the induced bed shear stresses (Subsection 3.3.1). At the moment the maximum allowable slope is set at 0.1. A deviation of this number has a large influence on the shape of the induced bed shear stresses (Figure 3.12, Subsection 3.3.1). However, the maximum deviation in total eroded terrace length for different maximum slope formulations after 800 waves is around the 10%. This is the same deviation as found

by Duró et al. (2020) comparing his simplified scour process with reality. For this reason a deviation close to 10% is expected to be found for a lake situation, but laboratory or field experiments are needed to confirm this assumption.

Sediment deposition
The choice is made to exclude the deposition processes from the model and assume that the eroded soil is transported away from the shore. This assumption results in a conservative approach in terms of erosion and shore stability.

This choice was also made in the model of Duró et al. (2020). The logic behind that assumption was that along a river bank the eroded sediment will be transported away with the currents of the primary ship waves.

In a coastal situation sediment deposition is taken into account, where the eroded sediments will be transported with the waves and settle during calmer conditions. In a lake, both effects concerning the sediment deposition and transportation can be expected, depending on the local conditions along the lake. At locations with a significant current velocity, or in storm conditions, it can be expected that the shore shows the same behaviour as the terrace along a river attacked by ship waves, where high current velocities transport all the eroded sediments away. In calmer conditions a high deposition can be expected. Which of the two processes is dominant is highly dependent on a combination of the settling velocity of the soil and the local velocities. For this reason the most conservative assumption is taken, but the settlement velocity could be added in a further development of the model.

Habitat of *Phragmites Australis*
The current model accounts for the presence of vegetation in a static manner, where the properties of the vegetation stays constant over time assuming a healthy population. The presence of vegetation is not restricted to the conditions in which vegetation can grow, which simplifies the model, but gives also restrictions concerning the wave climate and environmental conditions for which the model can be used.

In Subsection 2.4.1 the maximum wave height for *P. australis* is stated. Other factors contributing to a healthy population of *P. australis* are the presence of a water level fluctuation in order to bring oxygen to the roots and the presence of enough nutrients in order to grow (Sollie et al., 2006; Loeb et al., 2012). Duró et al. (2020) found that the most vegetation grows in areas with a low soil cohesion, where the vegetation can more easily root.

When these conditions are not met, a decrease in damping capacity can be expected, which is not accounted for by the model. When the model is used in this kind of conditions the damping capacity of the vegetation could be lowered by reducing the stem density, but for an accurate estimation further research is needed.

Root reinforcement
The area of soil reinforced by the presence of the roots is considered to exist fully below the vegetation, so only the soil directly below the vegetation is reinforced against erosion. In reality roots will spread below the surface, so the soil reinforcement in the middle of the vegetation patch will be higher than at the borders (Figure 5.5). Around the vegetation patch, the soil will be reinforced as well. Since the roots of the vegetation spread below the soil the roots will also grow below the non vegetated part.

The presence of roots is expected to make a difference in terms of the morphological changes, especially in front of the vegetation. It is therefore advised to include the root spread into the further development of the model.

In the current model the roots are modeled as an additional cohesion. This additional cohesion is a single value, while the strength of the roots changes in different climates concerning the soil properties. But also in different hydraulic conditions, such as the water depth (Vretare et al., 2001).
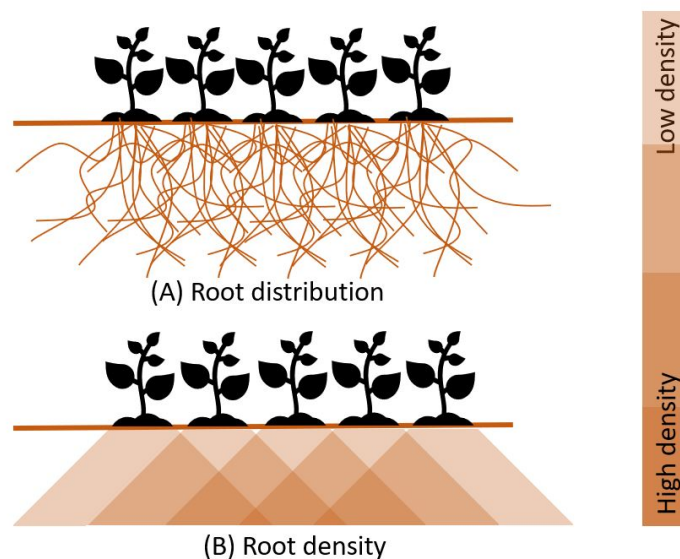

Figure 5.5: schematization of the root distribution. Plot (A) shows the root distribution below the soil surface, plot (B) illustrates the root density for the upper part of the soil surface.

Velocity reduction inside the vegetation
In the current model velocity is not directly included which results in a collection of the vegetation's capability to reduce the wave celerity before the run-up.

Vegetation reduces the total amount of wave energy. Besides the loss of wave energy, the wave celerity will change as well. The wave celerity will partly increase, as the available area is reduced due to the presence of the vegetation. At the same time, there may be sheltering and a velocity decrease due to the wake of upstream plants.

A higher accuracy for the run-up height and the induced shear stresses at the end of the vegetated field can be archived by including the changes in the wave celerity through the vegetation. The reason can be found in the fact that the induced bed shear stresses and total run-up height depends mainly on the wave celerity, which is responsible for the velocities inside the vegetation.

5.2. Sensitivity analysis

A sensitivity analysis is done in order to investigate the influence of the calibration parameters such as the start location of the run-up and the wave breaking parameter. In this way, the influence of the uncertainty coming from the calibration parameters can be established. Also the sensitivity of the estimated parameters such as the stem density, vegetation growing depth, shore slope, wave period, stem density and drag factor are investigated. A distinction is made between the maximum induced bed shear stress during bore propagation and the maximum induced bed shear stress over the total terrace length. This is done in order to get more insight in the location of the changes in maximum induced bed shear stress, and to see the influence of the formulation of the induced shear stresses by run-up.

The sensitivity of the parameters is determined as the relative change in maximum induced bed shear stresses by an increase and decrease of 10% from the established parameter in the model. It must be noted that a larger deviation in the maximum resulting shear stress

compared to a different parameter does not necessarily mean that that parameter results in a higher inaccuracies, as the accuracy of the parameter itself is not evaluated since this would involve field and/or lab experiments for most parameters.

Reference values
- Start run-up hbr* [-] = 0.15

- Wave breaking parameter [-] = 0.8

- Stem density N [stems/m^2] = 166

- Maximum vegetation growing depth [m] = 0.499

- Slope [-] = 0.03

- Wave period [s] = 2

- Drag coefficient [-] = 1.94

(A)

(B)
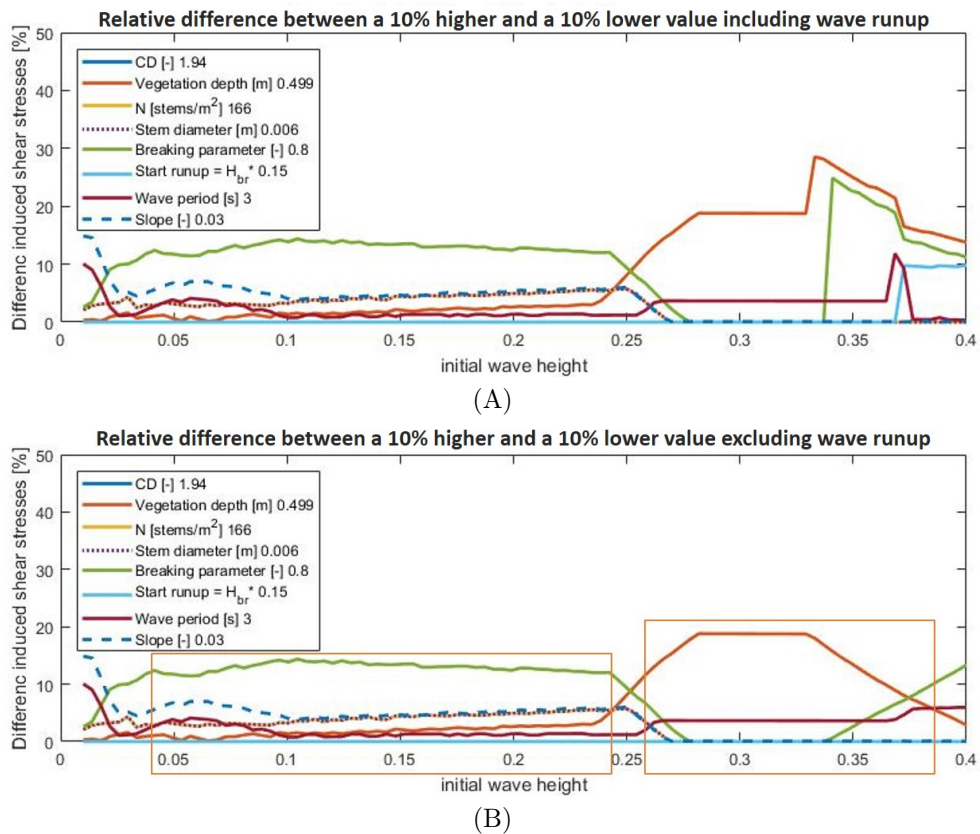
Figure 5.6: Sensitivity analysis of different model parameters as presented in Section 4.2. This figure shows the relative influence of a 10% higher and 10% lower value of the tested parameters on the induced bed shear stresses. The tested parameters drag coefficient (CD), stem diameter (D[m]) and stem density (N [stems/m^2]) have exactly the same results. The other lines are the vegetation growing depth, breaking parameter (γ[-]), Start location of the run-up [-], wave period (T[s]), Terrace Slope(m[-]). This is done for all the wave heights ranging from 0.01 to 0.4m (vertical axis) in order to include the changing behavior of different parameters for different wave heights. As the model calculation of the induced bed shear stresses exist of two phases, bore propagation and run-up, the results of the sensitivity analyses are also deviated in a graph including the run-up and excluding run-up. For plot (B) two different areas are marked, where a change in the breaking parameter is dominant in the first box and the vegetation depth in the second box, after which the breaking parameter increases again in dominance.

The following results are found for the parameters with the highest sensitivity:

Vegetation growing depth
A deviation of 20% in the vegetation growing depth of 0.5m gives one of the largest changes in the amount of induced shear stresses, especially for wave heights above the 0.24m (Figure 5.6). This increase in the magnitude of the sensitivity for the vegetation growing depth in the range of wave heights between the 0.25m and the 0.4m can be explained by the change of wave breaking location (Figure 5.7). When the start of the vegetation is just before the point were a wave should break, it removes the largest peak of induced bed shear stresses, so a small change in the start location for the vegetation can result in a large difference of maximum induced shear stresses. This means that every wave height has his own crucial vegetation growing depth, where a small increase of vegetation growing depth can lead to a large difference of induced bed shear stresses (Figure C.15, Appendix C.4.1).

(A) Vegetation after wave breaking (B) Vegetation before wave breaking
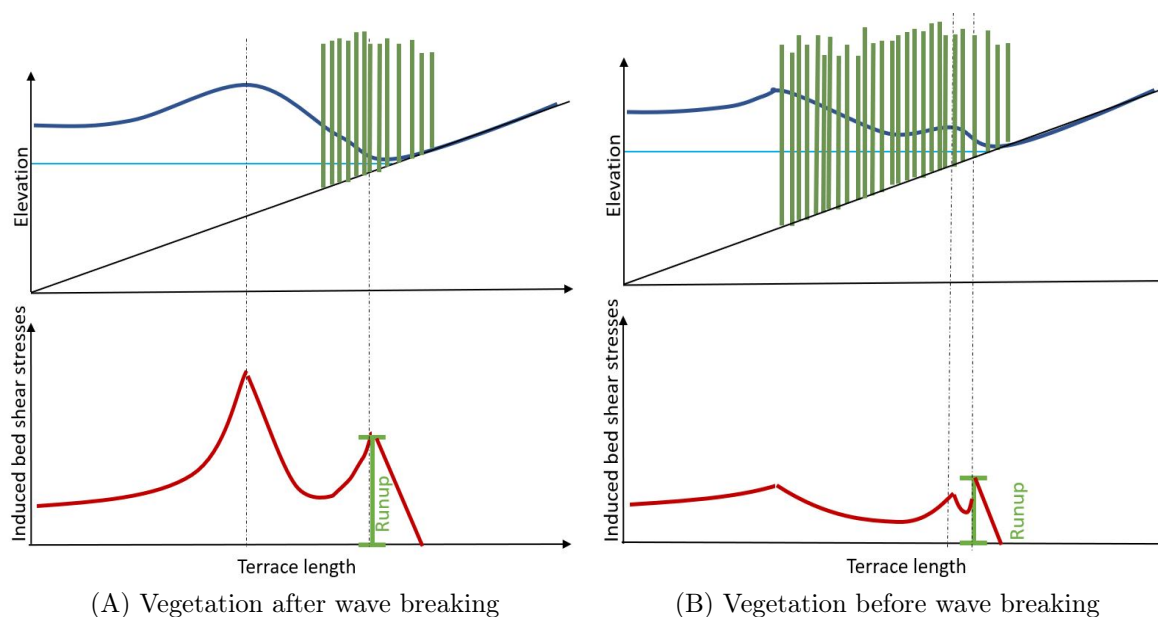
Figure 5.7: Illustration of the impact of vegetation after (A) or in front (B) of wave breaking. A small change in the maximum growing depth of the vegetation can have a large impact on the maximum induced bed shear stress. The reason for this high sensitivity can be found in the delay of wave breaking, which results in a decreased impact at the point of wave breaking.

Breaking parameter
From the tested calibration parameters, the breaking parameter is the most sensitive parameter (Figure 5.6). For wave heights below the 0.25m on a vegetated slope of 0.03 a deviation of 20% (10% above and below the tested value) of the breaking parameter leads to a total deviation of 12% of the maximum induced bed shear stress. For wave heights above 0.25m, the maximum induced shear stresses are found at the end of the bore propagation and not longer at the point of wave breaking (Figure C.19.B, Appendix C.4.1). This transition is responsible for a decrease of the influence of the breaking parameter (Figure 5.6, between the wave heights 0.27 and 0.34m). For the total induced shear stresses the same trend can be seen. After a wave height of 0.34m, an increase of influence can be seen as the process of run-up becomes dominant.

The two parameters with the largest sensitivity show both a strong relation with the breaking parameter. This relation can be found implicitly in the vegetation depth and explicitly by the influence of the breaking parameter self. There is a lot of uncertainty in the wave breaking parameter. Different theories give different values varying between the 0.78 and 0.88 for regular waves (Schiereck, 2001).

Since there is a high sensitivity of the system towards the breaking parameter, combined with its uncertainty, this results in point which is in need of a further consideration. With the introduction of partial wave breaking, as is found in the models of X-Beach and SWASH, the sensitivity of the breaking parameter is expected to be less, as the high increase in wave height through the shoaling processes is reduced. But it is unclear if the model still accounts for the maximum wave load when formulations for partially wave breaking are used. When the goal of the model would be to make a design for a stable shore accounting for a certain wave climate the use of partially wave breaking is advised. When the goal is to investigate the influence of different parameters on the shore stability under a single wave attack and/or to encounter for the morphology which depends mainly on the maximum wave a single wave breaking parameter would be preferred.

5.3. Design with vegetation for shore protection
In this section different aspects of the design with vegetation are discussed. In Subsection 5.3.1 the different ways in which vegetation protects the shore and how those aspects change over time are stated. In Subsection 5.3.2 it is discussed in which way those protective characteristics of vegetation can be used and which considerations must be made in order to determine the dimensions for a design. Also the considerations concerning maintenance are stated. At last, in Subsection 5.3.3, the previously stated points concerning reflection, maintenance and cross sectional land use are compared with other shore protecting structures. The ecological connection between the land and the water is also considered in the comparison.

5.3.1. The influence of vegetation
Vegetation protects the shore against erosion in two different ways. One mechanism is the vegetation's damping capacity, which effects increases when the vegetation width increases. The second aspect is the soil reinforcement through the roots, resulting in a higher critical bed shear stress. Combining the maximum wave height withstood by vegetation, with the lowest cohesion found by Duró et al. (2020) gives a good estimation of the relative importance of both aspects (Figure 3.14, Subsection 3.3.3). The wave damping capacity of *P. australis* decreases the induced shear stresses with almost 50% for a wave height of 0.4m propagating over a terrace with a slope of 0.1 and a vegetated area of 5m. The critical bed shear stresses increase with a factor 2, leading to a higher local stability of the shore.

For the design of a vegetated shore, both effects are important. An advantage of the soil reinforcement by the roots is the absence of seasonal influences, whereas the stems have a lower damping capacity in the winter months. A large advantage of the damping characteristic of vegetation is that not only the vegetated area, but also the area behind the vegetation is protected since the wave height is reduced.

5.3.2. Designing with vegetation
Cross shore location of vegetation
A successful design for shore protection with vegetation can be made combining the knowledge of the dominant wave climate and the erosion reducing characteristics of vegetation. The model results show that the dominant processes for erosion can be found at the point of wave breaking and at the start of the run-up (Chapter 4), as both locations give the highest wave height compared to the local water depth. This can be used for a strategic placement of vegetation in order to dampen the wave impact were it is needed the most (Figure 4.1, Section 4.1) and reinforce the soil through the roots on these locations. There are many situations in which a partially vegetated shore is sufficient to withstand the daily wave attack, so it can develop naturally until full strength, which is needed in a storm situation. This way a cost reduction can be reached considering placement costs, since not the entire shore needs to be vegetated. The placement of a partly vegetated shore results in a healthier shore as well, as higher biodiversity can be reached, as a large part of the vegetation has grown naturally (Uddin and Robinson, 2017).

Initial slope

One of the most important, but at the same time most limiting criteria for a vegetated shore is the slope. In order to give enough space for an ecological healthy shore a slope of 0.3 or milder is advised (Ministerie van Verkeer en Waterstaat, 1999a). In order to dampen the waves sufficiently enough to reduce or prevent erosion a milder slope might be needed, but this will mainly depend on the local hydrodynamic conditions and soil characteristics (Figure 4.2, Section 4.1). This consideration can not be investigated in detail with the current model, since there is limited accuracy concerning the induced bed shear stresses due to run-up.

Looking at the hydrodynamic and the ecological conditions a flatter slope is preferred. When placement cost and maintenance are considered, a steeper slope is usually preferred. Since these conditions are contradictory a balance must be found between the costs and the ecological conditions. In order to create a flatter slope on a natural way, brushwood structures can be installed. A brushwood structure is able to enhance sediment deposition behind the structure, which will create a flatter slope (Section 2.5).

Maintenance

When designing a vegetated shore protection the accessibility and frequency for maintenance should be considered as well. There is not one correct strategy to maintain a nature friendly shore. A frequent maintenance strategy is favorable for a diverse vegetation, as it prevents wooden species from dominating the shore, which lowers the wave attenuation by vegetation. When the vegetation has a protective role, yearly mowing is needed in order to keep the desired succession level. In order to reduce the amount of bed disturbance, maintenance is preferred from the land. To maintain from the land space needs to be available for mowing machines. An important consideration is the reach of the used machines. From the water side the reach is on average 2 meter (from an average depth of 1 meter), from the shore the average reach is 3 meter (van Vossen and Verhagen, 2009; van Breukelen et al.,2003).

From an ecological perspective there are three things to consider for the design of a maintenance plan (Pelsma et al., 2009):

- Maintaining the wanted succession level,

- Removing established nutrients to counteract an overload caused by decay,

- Creating a vegetation structure concerning the life cycle of the present/desired flora and fauna.

In a maintenance plan the needs from an ecological view need to be combined with the needs from a civil engineering view. Often contradictions arise, like a low maintenance frequency in order to disturb the soil as little as possible but a high maintenance in order to maintain the flow profile. So compromises have to be made (Pelsma et al., 2009).

5.3.3. Comparison in different structures

In the previous subsection we have taken a look towards the consideration concerning the slope, reflection and maintenance of a vegetation based shore protection. The research started with an elaboration on the benefits of a natural bridge between land and water (Section 1.1). But not in every situation a vegetated shore forms an optimal solution. This subsection discusses qualitatively the general benefits and disadvantages of the different solutions, summarised in Table 5.4. In practice their relative performance may be site-specific, and the effect of the different solutions should be modelled for a comparison in a particular site. The effect of hard structures could also be implemented in the present model using empirical expressions for wave reflection and transmission through the structures. This would constitute a practical tool for future designs, that includes the potential different alternatives.

Supportive structures
Rows of poles and brushwood structures are used to support the vegetation. These structures dampen waves, in order to allow vegetation to grow after sowing, or reduce the impact when waves are often higher than the maximum allowable wave height for a healthy population.

When a supportive structure is only needed for the first three years, the time needed to reach a fully grown population, maintenance after placement is not needed. As a result, the supportive structure can stand near the vegetation, as it will not be a problem when the vegetation grows around the structure. When a permanent structure is needed it must be considered that maintenance and or replacement of the structure can damage the grown population, so a more offshore location is preferred.

Hard solutions
Hard solutions often result in high reflections, with sheet pile walls as one of the most extreme examples. The sheet pile walls form a clear boundary between the land and the water in a reduced space. As the waves are fully reflected the wave forces will only interact with the soil in front of the structure, so the land can not erode away. In front of the structure scour can form a problem, because the wave forces are reflected, leading to a strong return current near the bed surface. As a sheet pile wall forms an abrupt transition the depth in front of the structure is often deep, so as long as the stability is not threatened the forming of a scour hole is not problem. And since it forms a direct transition the needed space for the shore is almost negligible. Also the maintenance is limited, since sheet pill walls can have a lifetime of 100 years (Holakoo et al., 2017).

When we look at the more natural and recreational aspects of the use of fully reflecting structures the solution is less ideal. The reflected waves keep disturbing the water and the bridge between land and the water is broken, which reduces the ecological value of the shore significantly (Section 1.1).

Another hard solution which has a high reflection are stone rip-rap structures. Like the sheet pile walls they have a high reflection, resulting in high current velocities near the structure. The pores of a rip-rap structure are responsible for some wave damping, reducing the reflection and return current. The pores also allow vegetation to grow through, but it is not nearly enough to speak about a bridge between land and water. A rip-rap exist of a slope, so it will take more space than a sheet pile wall, but it is a lot less space compared with a vegetated shore. Also the amount of maintenance is more when compared to a sheet pile wall, as a storm event can threaten the stability. However, the maintenance is significantly less when compared to a vegetated shore, where once a year/ once every three years maintenance is needed in order to keep the vegetation's characteristics (Water Land en Dijken, 2018).

Other hard solutions are the rows of pols and the brushwood structures. Since those structures are often combined with vegetation only the combined characteristics are taken into account, which is done in Subsection 5.3.2.

Table 5.4: Relative amount of the different shore protecting structures (vegetation, vegetation with a permanent supportive structure, rip-rap and sheet pile walls) concerning connection between water and land (bridge function, the amount of reflection in front of the structure, the amount of maintenance end the cross sectional with leading to a land use.

	Bridge function	Reflection	Maintenance	Space	Building costs
Vegetation	++	-	+	++	- -
Permanent supportive structure	++	+	+	+	-
Rip-rap	-	+	-	-	+
Sheet pile walls	- -	++	- -	- -	++

Location specific solutions
From the previous section it can be concluded that the different protection techniques have a different focus, resulting in solutions for different situations. One of the most important factors for the use of a vegetated shore is the available space. When space is limited and expansive, the best choice would be the use of a sheet pile wall. This is mostly the case in built-up areas. Since there is often no nature near the shore, the benefits of the bridge function would also be limited.

In a more natural situation space is already reserved for the natural solutions. In this case a vegetated shore protection is more favorable, as the bridge between land and water grows in importance and the costs for the used space are relatively low. Also the waterside can be used for the creation of the slope, when land is limited but there is enough space on the lake itself. If the waves are to aggressive supportive structures can be used.

Rip-rap structures form a solution in between. They can often be found close to the entrance of a harbour, were a sharp transition between water and land is preferred, without high amounts of wave reflection. For recreational harbours also the amenities plays an important part, but since the sailing depth is critical a vegetated shore is not preferred. Also the high velocities created by the wake of a ship can form a problem for a vegetated shore.

6

Conclusions and recommendations

6.1. Conclusions

In order to give a better insight in the different design choices concerning a vegetated shore this research has been conducted in order to answer the following main question:

How to estimate the contribution of reed-like vegetation, specifically *P. australis*, towards the shore protection along a lake against hydrodynamic loads using a process based model.
To answer this question, sub-questions are formulated. In this section an answer is provided for each sub-question based on the previous chapters.

Which effects of reed-like vegetation are important to consider based on the shore hydrodynamics and erosion processes?
Reed-like vegetation will influence the hydrodynamic conditions due to wave reflection, wave attenuation, and by affecting the wave-driven setup. It will also reinforce the soil, increasing its critical shear strength. As a process based model is used, the resulting hydraulic changes have to be implemented separately based on the vegetation characteristics.

Wave reflection
The importance of the wave reflection at the start of the vegetated field is validated with SWASH (Subsection 5.1.2). It is concluded that, with an increasing wave height and wave period, the relative reflection will increase as well. A maximum relative wave height increase of 18% is found, resulting in a relative increase of bed shear stresses of 44%. Wave reflection is often neglected in models for wave transformation through vegetation, but based on these results, this may lead to a non-negligible underestimation of the induced bed shear stresses in front of the vegetation. This can result in erosion in front of the vegetation undermining the stability of the vegetated area.

Wave attenuation
Wave attenuation in *P. australis* reduces the bed shear stresses up to 90%, with a terrace length of 50m and an experimental density of 1521 stems/m^2 (Figure 3.10). This is derived with the equation of Dalrymple et al. (1984) (Equations 2.27, 2.28 and 2.29) included in the model. This led to considerable differences between the shear stress with and without the effect of wave attenuation by vegetation. For *P. australis* differences up to 6 Pa are found, which decreases the impact on the shore with 50% (Figure 3.14, Subsection 3.3.3).

Set-up
The presence of the vegetation decreases the radiation stresses towards the shoreline, and an increase in the wave-driven set-up. Higher water levels enable waves to propagate further towards the shore, as the water depth increases.

An estimation of the influence of the setup without vegetation is made with SWASH and the modified model of Duró et al. (2020). The setup, modeled with SWASH, was included in the model of Duró et al. (2020) in order to evaluate the difference in shear stresses between a situation with and without setup. From this comparison it is concluded that the effect of setup on the shear stresses is negligible, as the differences in induced bed shear stresses is lower than 5% and only induced 1m further onshore (Appendix C.1.3). For situations with vegetation only lower setup values are found, from which is concluded that the setup through vegetation is negligible as well (Subsection 6.2.2).

Soil reinforcement
The presence of the roots reinforces the soil. The additional cohesion was estimated based on root parameters specific for *P. australis* using the formula of de Baets et al. (2008) (Section 2.30). The additional cohesion results in an increase of bed shear strength of 7 Pa, which is equal to the lowest found bed shear strength in the field measurements along the Maas, conducted by Duró et al.(2020). Resulting in a final bed shear stress of 14 Pa.

It is concluded that the load reduction induced by the wave attenuation through vegetation, the resistance against erosion induced by the soil reinforcement of the roots and the force increase induced by the wave reflection in front of the vegetation need to be considered based on the shore hydrodynamics and erosion processes. The influence of the set-up on the shear stresses was negligible for the present conditions, but should be reconsidered when another vegetation type is used. The processes of wave attenuation through vegetation and the soil reinforcement of the roots are included in the model, but wave reflection is not included due to time constrictions. The effect of wave reflection should be incorporated in future developments. The reflection is especially important to consider as it causes scour and an increase of the water depth before the vegetation, which means that neglecting it is not a conservative assumption.

How can the model of Duró et al. (2020) be used to estimate the induced bed shear stresses at a reed-like vegetated shore in a lake situation?
The original model of Duró et al. (2020) was developed to calculate the final morphological state of the river banks along the Maas under attack of ship waves. The model is adapted to reproduce the hydrodynamic shore processes along a vegetated lake. The change in bed shear stresses resulting from the vegetation is already successfully implemented. The main differences concerning a transition towards a lake situation are the change in shore profile and the change in loads. An elaboration on the change in shore profile and the change in impact forces is made after which a conclusion is given.

Shore profile
The shore profile shows the largest differences relative to the model of Duró et al. (2020). Along the Maas terrace lengths up to 30m with an elevation of 1m can be found, resulting in a slope of 0.03. Along a lake a slope of 0.3 is more common, resulting in a different type of wave impact and run-up. The impact of this change can be seen clearly in the formulations for the start of the run-up and the run-up itself. The induced bed shear stresses correspond well with the results of SWASH for slopes around the 0.03, but deviate strongly for slopes of 0.3. The main reason is found in the change of wave breaking, expressed in the Iribarren number. The effect of a steeper slope should be incorporated in future developments in order to calculate the induced bed shear stresses along common lake shores correctly and use the morphological module of the model. The current model restrictions followed by this effect concerning the Water depth, wave height and bed slope are stated in Subsection 5.1.1. In the model recommendations (Section 6.2) the possibilities to encounter this problem are stated.

Loads
Wind waves can be calculated with the same principles as the secondary ship waves, so the wave propagation processes are present in the original model. The largest differences found

between the shore attack based on ship waves and the shore attack based on wind waves is found in the presence of the primary ship wave, which is not present and/or similar to one of the processes found by wind wave attack. The primary waves were the dominant processes in the original model, so the wave breaking and run-up processes resulting from the secondary waves were not validated, since there influence was negligible, resulting in unexpected results which needed to be solved (Section 3.2). The assumption of wave breaking on a single point is the most remarkable assumption, since none of the other relevant models solving the shore processes use it in this way. The assumption is relevant for its original use, since the morphology depends on the impact of the largest wave only. Additional monitoring data is needed in order to validate this assumption.

The model can reproduce the effect of vegetation on mild slopes. Lakes often have steeper slopes, which requires implementing formulations for the different type of wave impact and run-up, suitable for those situations. This effect should be incorporated in further model developments. The process of wave propagation was already implemented in the original model in order to describe the behavior of the secondary waves. Since the influence of the secondary waves was not dominant an additional validation for the wave propagation was done and successful.

Which parameters, concerning the hydrodynamics, morphodynamics and vegetation characteristics, have a high influences in a reed-like shore protection?

In order to make an estimation which parameters are important for a designs with a vegetated shore a sensitivity analyses is conducted. For this analysis different input parameters which can be influenced or measured are taken into account, such as the vegetation growing depth, stem diameter, stem density, incoming wave height and the terrace slope. For this analysis the value of the main input parameters of the model was modified.

The model showed that the highest sensitivity depends on the hydrodynamic conditions. The sensitivity of the vegetation growing depth increases when the start location of the vegetation is near the location were the waves break, while the sensitivity of the stem density, vegetation drag factor and stem diameter stay constant, and become insignificant when the vegetation growing depth becomes dominant. So it can be concluded that those changes in sensitivity depends mainly on the fact if the waves break in front or inside the vegetation, as this influences the impact of the vegetation in the wave attenuation. In Section 5.2 the important processes are elaborated into more depth.

Overall conclusion

In general it can be seen that the dominant processes for erosion can be found at the point of wave breaking and at the start of the run-up, as both give the highest wave height compared to the local water depth. When vegetation is present at a location were waves do not yet break the maximum induced shear stress from wave breaking will be lowered. With sufficient vegetation wave breaking can be delayed until it is almost negligible. This illustrates that even a partial vegetated shore protection can be significant, if used efficient.

6.2. Model Recommendations

In Subsection 6.2.1 an elaboration is made on the difficulties arising with the use of a process based model, leading to limitations in the current model. Those limitations can mostly be reduced with the use of calibration coefficients when sufficient validation data is available, which is described as well. In Subsection 6.2.2, different processes which are not implemented of the model in need of further investigation in order to reach its full potential are stated, like the improvement of important calibration coefficients, wave reflection and the root distribution below the soil. In Subsection 6.2.3, possible additional processes are listed which could be added to the model in the future as modules in order to extend the models possibilities regarding design processes. At last, in Subsection 6.2.4 an elaboration is made in which situation it is profitable to continue with a process based model and when it is

better to expand an existing numerical model in order to calculate the morphology along a vegetated lake.

6.2.1. Process based model

The process based model of Duró et al. (2020) was modified to be able to give more insight in the different processes helping design choices concerning a vegetated shore along a lake. The choice to use a process based model knows many benefits, as described in Subsection 2.6.4. However, a process based model also has limitations, as the used formulas are often derived, calibrated and/or validated for a restricted range of conditions. The problem of a limited range can be solved with the use of different calibration coefficients for the different conditions. In order to derive the calibration coefficients validation data is needed concerning the velocities and morphological changes. After the validation of the system, a sensitivity analyses must be conducted in order to measure the accuracy for small variations, as is illustrated in Section 4.2. But once the model is fully developed and validated, it may constitute an useful tool for designs.

In this subsection an elaboration is made about the limitations, the needed calibration coefficients to reduce the model limitations and the needed validation data in order to calibrate and validate the current model.

Model limitations

The problem arising with the use of formulas which are derived for different situations can be seen in Subsection 3.2.3, were it is found that steeper slopes result in an unrealistic high amount of induced bed shear stress. This especially forms a problem when morphology processes are involved, since the initial shore profile will change towards steeper shores, reaching the boundaries for which the model is validated. For this problem there are two possible solutions.

The first solution is recommended, in which different empirical relations for the different stages of the morphology are implemented. All of these relations need a separate validation. This way the model can be used to account for the different stages without losing the benefits of a process based model. This is a time consuming process and will always contain an uncertainty between the validated morphology stages.

Another solution could be found in the use of a numerical part in the model. It can be expected that a higher accuracy can be reached with the implementation of the numerical shallow water equations, which has been done in X-Beach. This will remove the benefits of the simplicity of a process based approach as stated at the start of Section 6.2, but will increase the accuracy of the model. The computation time will also increase.

Calibration coefficients

For this research the most calibration coefficients are taken from the model of Duró et al. (2020). It can be questioned in which amount the calibration factors are still the same for a lake setting looking at the parameters related towards the slope, such as the start location of the run-up and the total run-up height.

Calibration coefficients in formulas are used to describe the relation between different parameters. When the calibration coefficients are validated on a large data set, they are assumed to be constants. They can also be used as a variable calibration factor, so that a single, empirical formula can be adjusted to new situations.

As the initial conditions have changed from the model of Duró et al. (2020) a further investigation and validation of most of the calibration factors is needed in order to remove the

limitations with the largest impact. It is recommended to extend the investigation into the start location of the run-up and the maximum slope formulation. But also to investigate into the wave breaking parameter, the change of the vegetation characteristics when they are damaged, the erodibility coefficient and the energy conservation responsible for the total run-up height. The different calibration parameters used in the model are listed and discussed in Appendix B.3.

Validation data

Further validation of several processes is needed in order to accurately predict the effect of vegetation on a lake shore under changing conditions. There are formulations where the effect of a changing slope could be incorporated, such as the run-up formulation by Bergsma et al. (2019), but this should be further investigated and validated. In the current model these formulations are not used. Also the availability of a long period of monitoring data of lake specific location could help to validate the different used equations and the needed changes for the different slopes which can be encountered. In order to use monitor data it is preferred that all the main physical processes affected by the presence of vegetation are monitored/measured, since the final morphology depends on a combination of many factors such as the wave attenuation, wave velocity and run-up velocities. When only the morphology is known it can be concluded whether the model is correct or not, but it can not be used to investigate the different processes and indicate which of the processes must be investigated in more depth.

6.2.2. Processes which are not implemented

In order to simplify the processes involved for the vegetated shore erosion multiple processes are not implemented (Subsection 5.1.2). In most cases the influence of the absence of these processes is small, but this does not account for the reflection in front of the vegetation and the distribution of the roots. The rest of the neglected processes can be important for a specific situation, but are overall considered to have a limited effect on the induced bed shear stresses. It is therefore recommended to implement at least the following two factors.

The influence of the **reflection** increases with an increasing wave height. It is estimated that the reflection from *P. australis* with an incoming wave height of 0.3m can result in an increase of 44% of the bed shear stresses in front of the vegetation. This can easily result in a new, critical point were erosion would take place, so is important to consider when a design with vegetation would be made. Another measure is represented by the **roots distribution** in front of the vegetation, which will influence on the final morphology due to the soil reinforcement.

6.2.3. Processes that can be added

In order to extend the model, processes can be added. In this subsection possible extensions are stated concerning the vegetation, lake situation and the cost estimation.

Time variation of wave attenuation by vegetation

At this stage, the model accounts for the presence of vegetation in a static manner, where the properties of the vegetation stay constant over time. In reality vegetation grows and dies, depending among other things on the hydraulic conditions and the annual growth cycle. As the hydraulic conditions are modeled a dependency of the vegetation state based on the hydraulic loads can be added.

One example can be found for a wave attack with wave heights above the maximum allowable wave height for the considered species. In the current model the attenuation would be calculated based on a fully developed vegetation. When the hydraulic conditions exceed

the limiting condition for a certain species, a part of the vegetation will break, so less wave attenuation takes place compared with the model results.

Another process is the growing capacity of vegetation. For newly sown vegetation, the bed shear stresses play a critical part in the growing rate. When a certain amount of wave energy is linked to an specific period of time/duration, the wave attenuation over time through the growth of the vegetation could be modeled. This can be used to determine the lifetime of supporting structures since it can be determined in which extend the vegetation has to grow to give sufficient protection.

Lake situation
In order to use the model when a limited amount of wave data is available a quick estimation of the wave height and period for a lake situation can be made with the **Sverdrup-Munk-Bretschneider equations** (Schiereck, 2001). These formulas can added to the model to calculate the current input value of the wave height and wave period. In order to use this formulation a dominant wind direction and force is needed combined with the knowledge of the lakes geometry. As it is a rough estimation it will always results in a higher inaccuracy compared with measurement data, but if there is no data available it can be an useful addition.

Another process which is still missing, but not crucial for the model use would be the processes of **shore accretion**. In order to include this process more information is needed about the settlement velocity of the sediment, the influence of the lake currents on the settlement velocity and the average time between storm attacks.

Cost estimation
In the current model the feasibility of a vegetated shore is based on the hydrodynamic and the shore conditions. In order to tell something on the total feasibility, the cost should be included as well. In order to include the cost, an estimation is needed for both the placement cost and the maintenance costs. For the placement cost two elements are important, besides the creation of the shore profile, are the costs related to the land use and the cost in order to plant or sow the vegetation. One of the main elements determining the land use concerns the final equilibrium slope, so a direct link towards the model can be made.

6.2.4. Overall recommendation
The present work investigated whether the conceptual model could be used and/or expanded in order to calculate the morphology along a vegetated lake. The recommendation whether to continue with the current model, is case specific. At this stage the model has shown to be able to calculate the wave attenuation through vegetation and the related amount of induced bed shear stresses correctly, but at the end of the terrace length, difficulties arise when the wave breaking and run-up processes starts to dominate. The model shows that the location of wave breaking, the start location of the run-up and the run-up velocity are particularly important to model the morphodynamic evolution of the profile under waves. Those parameters should be accurately evaluated based on field or laboratory data, in order to precisely model future vegetated shore protections. An alternative is to extend existing numerical models (like SWASH and XBeach) with the relevant morphodynamic and hydrodynamic processes. A downside of the improvement of an existing model can be found in the flexibility of adding new processes in the source code, which is quite complex and often not accessible as user.

It can be concluded that both approaches have their advantages. The final goal of the model will determine which approach would be best. For a higher accuracy it is better to continue with an existing model. But in order to fulfill the need of a more flexible model, a further extension of the model of Duró et al. (2020) would be a better choice.

<div align="right">

A

</div>
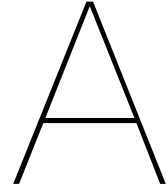
Hydrodynamics of Vegetation

A number of empirical expressions have been derived to model the effect of vegetation on different hydrodynamic loads (Chapter 2). This is done by an analytical description of different processes which describe the interaction between waves and vegetation. Multiple studies focus on the description of those physical processes. Often, those processes are represented by a single drag coefficient. In this appendix, the processes contributing to the alternation of the flow field through a canopy are explained. Also, an overview of the different formulations found in the literature is given.

A.1. Drag forces on a single stem

A.1.1. Forces

The vegetation is subject to a drag force, which exists of the velocity differences between the vegetation and the surrounding flow. This mean drag force (F_D), consists of two components. The first component is the drag force contributed by the pressure differences between the upstream and downstream side of the vegetation (F_p, illustrated in Figure A.1), the second component is the drag arising from the surface friction (F_f). In Figure A.2 the contribution of friction drag to the total mean drag has been shown for Reynolds numbers common found in practice. It can be seen that the contribution of friction drag is minimal (2 to 3 %) and therefore it can be neglected in most cases (Sumer and Fredsoe, 1997).

$$\overline{F_D} = \overline{F_p} + \overline{F_f} \tag{A.1}$$

$$\overline{F_p} = \int_0^{2\pi} \overline{p} cos(\theta) r_o d\theta \tag{A.2}$$

$$\overline{F_f} = \int_0^{2\pi} \overline{\tau_0} sin(\theta) r_o d\theta \tag{A.3}$$

where: $\overline{p}$ = Time average pressure

$\overline{\tau_0}$ = Time average Wall shear stress

$\overline{F_d}$ = Mean drag

$\overline{F_p}$ = Form drag

$\overline{F_f}$ = Friction drag

r_0 = Radius of the stem

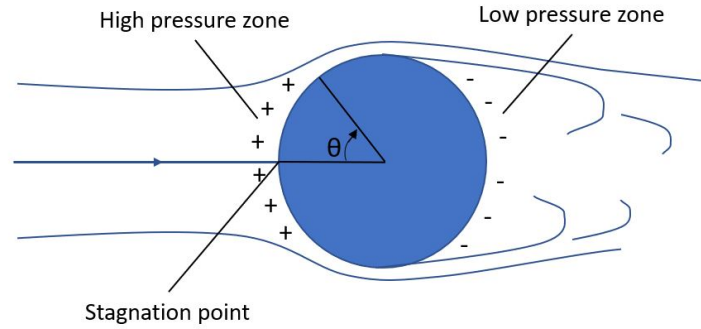θ = Place along circular surface measured from the stagnation point

Figure A.1: Formation of the form drag through the presence of a high and a low pressure zone.
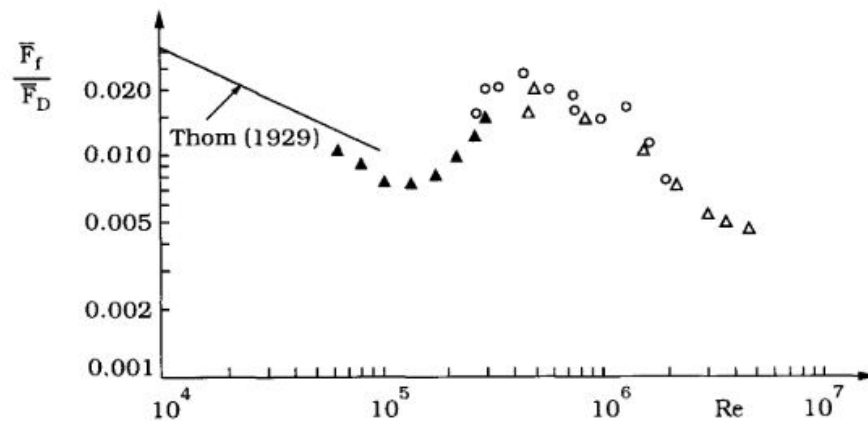

Figure A.2: Contribution of surface drag to the mean drag for different Reynolds numbers (Sumer and Fredsoe, 1997).

A.1.2. Flow characteristics around a cylinder

The flow characteristics around a single stem, simplified as a smooth cylinder, depends on the Reynolds number. The Reynolds number describes if the flow is turbulent or laminar. The Reynolds number is defined as the ratio between the internal forces and the viscous forces (Equation A.4).

$$Re = \frac{Inertia\,forces}{Viscous\,forces} = \frac{Du}{v} \tag{A.4}$$

where: Re = Reynolds number
D = Stem diameter
u = Water celerity
v = Viscosity

When the Reynolds number changes, the flow behind the cylinder changes as well. It can be seen that the flow characteristics behind the stem are strongly correlated with the Reynolds number (Figure A.4). This is the result of the different levels of turbulence, which results in different reactions of the wake and the boundary layer, as shown in Figure A.3. The distance of the wake is comparable with the cylinder diameter, the thickness of the boundary layer of the wake δ is normally very small compared with the cylinder diameter D (Equation A.5)(Sumer and Fredsoe, 1997).

$$\frac{\delta}{D} = O\left(\frac{1}{\sqrt{Re}}\right) \tag{A.5}$$

where: Re = Reynolds number
D = Stem diameter
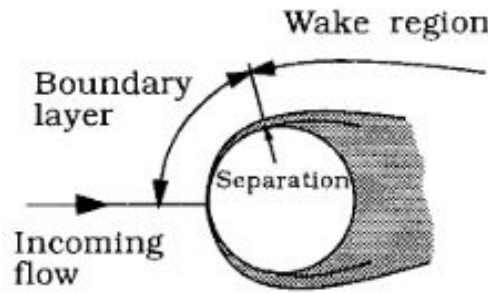δ = Wake boundary layer

Figure A.3: Definitions of the flow areas around a single cylinder (Sumer and Fredsoe, 1997)

When the Reynolds number increases, the turbulent regime increases as well. When the Reynolds number reaches the 40 the wake becomes unstable and vortexes are shed alternately on either side of the cylinder. Up to a Reynolds number of $3x10^5$, the boundary layer will stay laminar. At Re = $1.5 * 10^6$, a transition in the boundary layer from laminar (at the stagnation point) to turbulent takes place. With higher Reynolds numbers, the boundary layer becomes fully turbulent (Illustrated in Figure A.4) (Sumer and Fredsoe, 1997).

The change in turbulence characteristics can be explained by looking at the boundary layer of the cylinder. This boundary layer is the result of the velocity difference between the surface of the cylinder and the flow around the cylinder, a shear layer will be formed (Figure A.5.A). In this shear layer, vortexes will arise causing the shear layer to "roll up" into a vortex directed around the cylinder. When the vortex of the upside of the cylinder (Vortex A) increases in size, it will attract Vortex B, which will separate A fro the stem so vortex C can grow. This process is called vortex shedding (Sumer and Fredsoe, 1997).

(A) Processes in the shear layer

(B) Schematization of vortex shedding
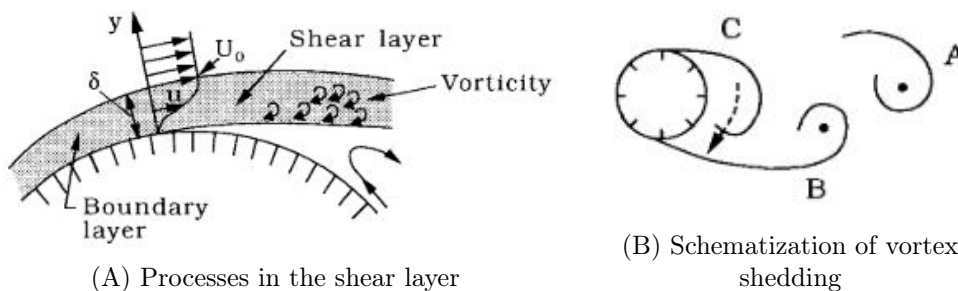
Figure A.5: Process of vortex shedding. Near the surface a boundary layer arises. When the boundary layer separates from the surface the side near the surface has a lower velocity, resulting in the formation of vortexes directed inwards. (Sumer and Fredsoe, 1997)

The wake characteristics depend on many factors. The main characteristics depend on the Reynolds number, which exists of the stem diameter, velocity and viscosity. But other factors
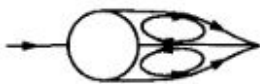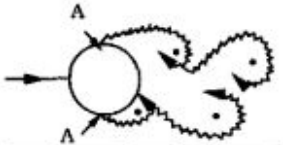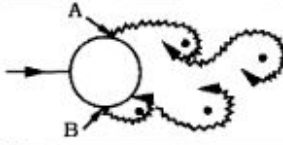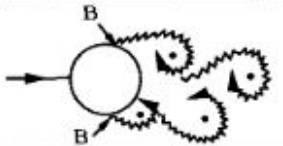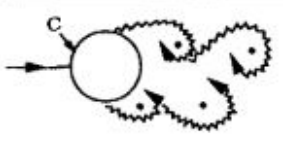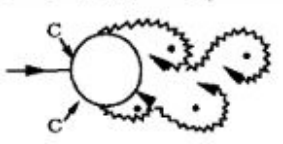
a)	No separation. Creeping flow	$Re < 5$
b)	A fixed pair of symmetric vortices	$5 < Re < 40$
c)	Laminar vortex street	$40 < Re < 200$
d)	Transition to turbulence in the wake	$200 < Re < 300$
e)	Wake completely turbulent. A:Laminar boundary layer separation	$300 < Re < 3 \times 10^5$ Subcritical
f)	A:Laminar boundary layer separation B:Turbulent boundary layer separation;but boundary layer laminar	$3 \times 10^5 < Re < 3.5 \times 10^5$ Critical (Lower transition)
g)	B: Turbulent boundary layer separation;the boundary layer partly laminar partly turbulent	$3.5 \times 10^5 < Re < 1.5 \times 10^6$ Supercritical
h)	C: Boundary layer completely turbulent at one side	$1.5 \times 10^6 < Re < 4 \times 10^6$ Upper transition
i)	C: Boundary layer completely turbulent at two sides	$4 \times 10^6 < Re$ Transcritical

Figure A.4: Flow seperation for different turbulance regimes (Sumer and Fredsoe, 1997)

influence the wake characteristics as well, such as the surface roughness, the cross-sectional shape, the incoming turbulence and the shear in the incoming flow (Sumer and Fredsoe, 1997).

A.1.3. Mean drag

The mean drag on a smooth cylinder is described by combining Equation A.1, A.2 and A.3, resulting in the following formulation (Sumer and Fredsoe, 1997):

$$\overline{F_D} = \int_0^{2\pi} (\overline{p}cos(\theta) + \overline{\tau}sin(\theta))r_0 d\theta \tag{A.6}$$

$$\frac{\overline{F_D}}{\frac{1}{2}\rho_w D u^2} = \int_0^{2\pi} \left[\left(\frac{\overline{p} - p_0}{\rho_w u^2}\right)cos(\theta) + \left(\frac{\overline{\tau_0}}{\rho_w u^2}\right)sin(\theta)\right]d\theta \tag{A.7}$$

where: F_D = Induced drag force
$\overline{p}$ = Time average pressure
$\overline{\tau}$ = Time average shear stress
θ = Location along stem surface
r_0 = Cylinder radius
ρ_w = Water density
D = Stem diameter
u = Velocity
p_0 = Hydrostatic pressure
$\overline{\tau_0}$ = Wall shear stress
θ = Location along stem surface

As both the pressure term and the wall shear stress are a function of the Reynolds number Equation A.7, can also be expressed as a single drag coefficient $\overline{C_D}$, as is shown in Equation A.8 (Sumer and Fredsoe, 1997).

$$\frac{\overline{F_D}}{\frac{1}{2}\rho_w D u^2} = \overline{C_D} \tag{A.8}$$

where: F_D = Induced drag force
ρ_w = Water density
D = Stem diameter
u = Velocity
$\overline{C_D}$ = Time averaged drag factor
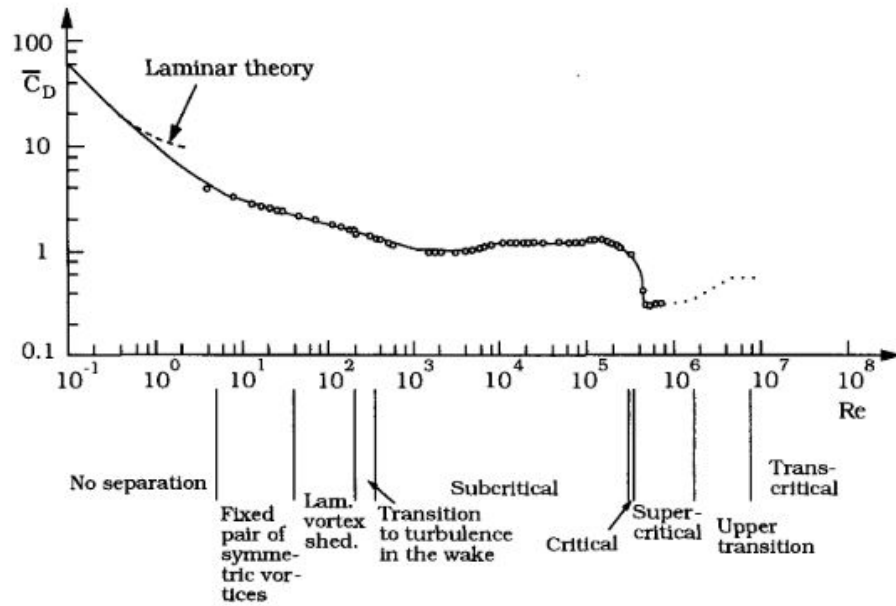
Figure A.6: Drag coefficient as a function of the Reynolds number for a smooth cylinder (Sumer and Fredsoe, 1997).

A.1.4. Surface roughness

When the surface roughness of the cylinders increases, the contribution of the friction force will stay equally small (2 to 3 %), so it can be neglected in most cases. The new drag coefficient will be determined by a combination of the Reynolds number and the surface roughness, $\frac{k_s}{D}$, with k_s the Nikuradse equivalent sand roughness. Looking to Figure A.7 the following observations can be made(Sumer and Fredsoe, 1997):

- The C_D value for the lower Re range of a rough surface are equal to the C_D values of a smooth surface.

- The curve shifts towards the lower Re values, so the wake becomes turbulent faster.

- The drag decrease is less extreme (drop of the drag coefficient).
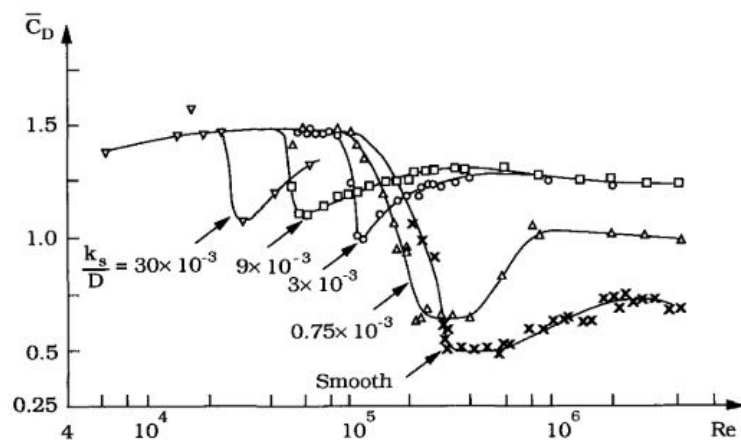
Figure A.7: Drag coefficient changes with changing roughness of a cylinder for different Reynolds numbers (Sumer and Fredsoe, 1997)

A.1.5. Pressure differences through vortex shedding

Under most circumstances, the stems are subjected to a periodic change of the pressure distribution through the effect of vortex shedding. This means that, even when a laminar straight flow approaches, the vegetation experiments a vertical force. The frequency of the drag forces created through the vortexes is twice as high as the frequency of the fortex shedding. It can also happen that some periods are missed. The magnitude of the vortex induced pressures can be described with their statistical properties, for example with the use of the root mean square value. The oscillating part of the drag force and the oscillating lift force can be described as followed (Sumer and Fredsoe, 1997):

$$F_D' = \frac{1}{2}\rho_w C_D' D u^2 \tag{A.9}$$

$$F_L' = \frac{1}{2}\rho C_L' D u^2 \tag{A.10}$$

where:
F_D = Induced drag force
F_L = Induced lift force
g = Gravity constant
C_D = Drag coefficient
C_L = Lift coefficient
D = Stem diameter
u = Velocity
ρ_w = Water density
$\overline{C_D}$ = Time averaged drag factor
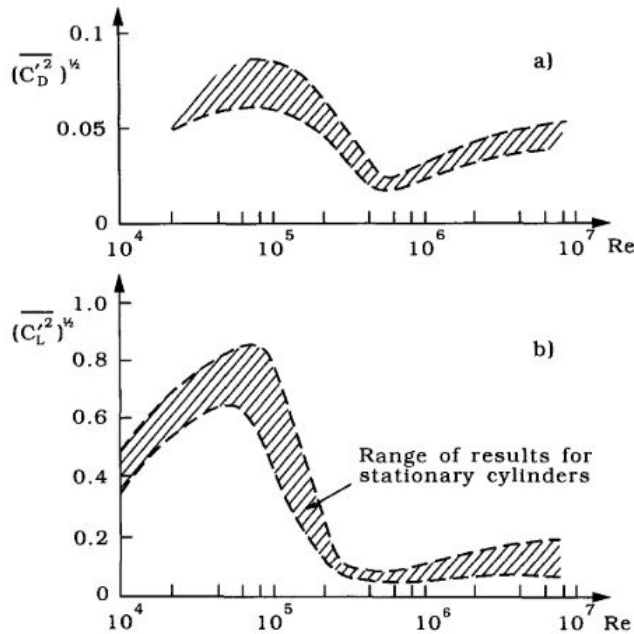
Figure A.8: R.M.S values of drag C_D and lift C_L oscillations for different Reynolds numbers (Sumer and Fredsoe, 1997)

The frequency of vortex shedding is calculated with the use of the Strouhal number (St). The Strouhal number depends on the Reynolds number and is expressed in π groups (Elger and Lebret, 2015). The corresponding Strouhal number can be found in Figure A.9.
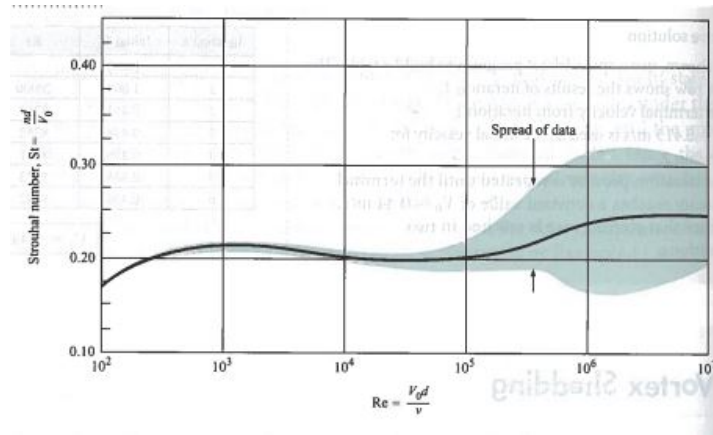
Figure A.9: Strouhal number for different Reindalds numbers (Elger and Lebret, 2015)

$$St = \frac{nD}{V_0} \tag{A.11}$$

where: n = frequency of shedding of vortexes
D = cylinder diameter
V_0 = free-stream velocity
St = Strouhal number

A.2. Interaction between Vegetation and currents

In this section an overview will be given for the different processes that are found in the literature that are contributing to the canopy drag force for currents.

One of the largest uncertainties in determining the influence of the vegetation on the energy dissipation is the determination of the bulk drag coefficient (C_D). In the research of Chen et al. (2018), an overview is given of different studies that are conducted in order to determine the drag coefficient for waves. In these different studies, both the calibration method, as the direct measurement method are applied (Table A.2 and Figure A.14). The study of Chen et al. (2018) underlines the uncertainty concerning the representation of the canopy drag coefficient. The calculated drag coefficients depends on Re (Reynolds number) or KC (Keulegan Carpenter number). The Keulegan Carpenter number can only be used for waves.

$$KC = U_m T_p / D \tag{A.12}$$

$$Re = U_m D / \nu \tag{A.13}$$

where: U_m = Maximal measured horizontal velocity on half the water depth
T_p = Peak wave period
D = Diameter of the circular cylinder (for real vegetation, mean diameter of the stems)
ν = Viscosity
Re = Reynolds number
KC = Keulen-Carpenter number

A.2.1. Stem density

Not only the stem characteristics influence the amount of wave damping, but also the interaction between the stems are important. Important processes to consider for the final canopy drag are Blockage and Sheltering. This is illustrated with the finding of Lima et al. (2006), who concluded that the canopy drag was on average four times higher than the summation of the individual drag forces. From different studies it can be concluded that in a medium to high canopy density, the stem interaction has a large influence on the canopy drag coefficient.

Blockage effect

When the blockage effect is referenced , the effect of an enhanced drag force originated by a flow flowing along a body confined by lateral walls is meant. The blocking of the flow happens in several ways: the reduction of the cross sectional area results in an increase in flow velocity around the body and the widening of the wake is hindered by the vertical walls. It can be seen that the wake characteristics will be influenced a lot through the surrounding vegetation. The vortex shedding frequency in the wake will be increased due the blockage effect (Etminan et al., 2019).

Sheltering effect

When a body is located in the wake region of another body, we are speaking of sheltering. The body located in the wake region experiences a lower velocity than the body in the full stream, what results in a lower drag force. With an increased density, the effect of sheltering will increase as well. The effect of sheltering does not only depend on the stem density, but also the stem arrangement. The sheltering effect takes only place when the upstream velocity is lower than the average velocity in the canopy (Etminan et al., 2019).

Nepf (1999) studied the altered drag coefficient of a stem in the wake of a single other stem, which result is summarised in Figure A.10. The sheltering effect that results in a suppressed drag coefficient increases when the distance between the two cylinders increases (both in the direction of the streaming, as in the direction perpendicular to the streaming). There are two wake properties that are responsible for this behavior (Nepf, 1999):

- The lowered velocity in the wake of cylinder A

- The increased turbulence before cylinder B. Through the increased turbulence upstream of B, the point of separation downstream of B will be delayed, what results in a lower pressure difference over the cylinder, so a lower drag.

In an uni directed flow with a high canopy density, the effect of sheltering is insignificant in comparison with the blockage effect. Only in sparse canopies ($\lambda < 0.04$), the sheltering effect is noticeable (Etminan et al., 2019). The effect of sheltering becomes important in an oscillatory flow, especially when the cylindrical spacing of the vegetation is smaller than the excursion of the flow amplitude (i.e. $KC\sqrt{\lambda} \geq 1.25 \, or \, KS * d/S \geq 1$).
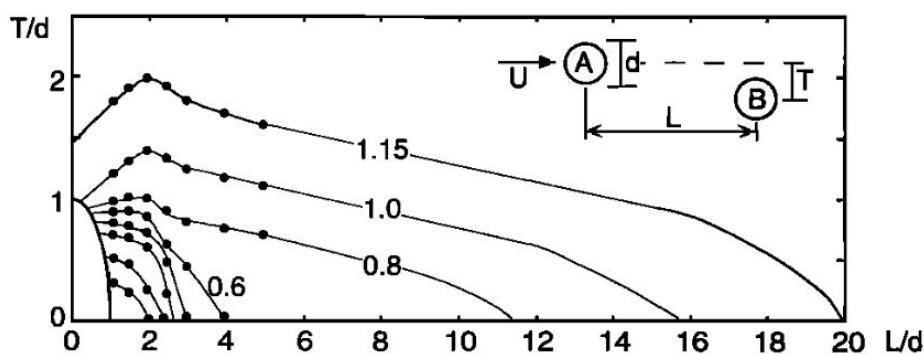
Figure A.10: Sheltering effect according Nepf(1999) for different configurations of stem A and B.
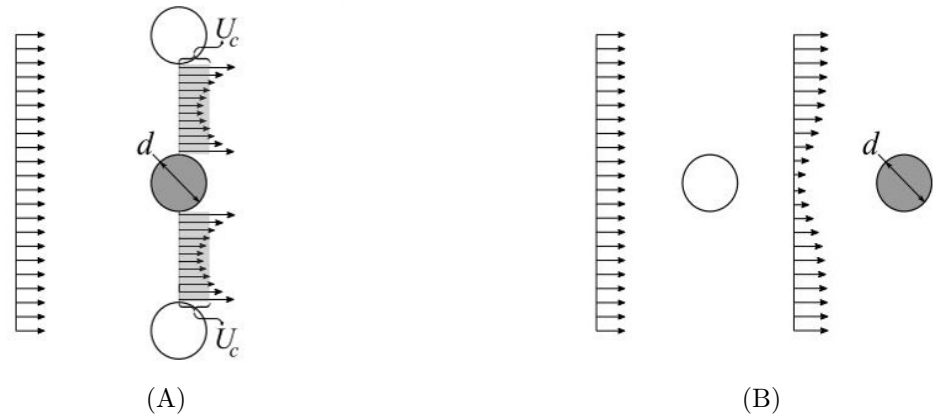
Figure A.11: Illustration of the effect of Blockage (A) and Sheltering (B) (Etminan et al., 2019)

Delayed separation

As shown above, the point of separation has a large influence on the height of the created drag force. This happens especially as the drag form dominates, mainly at the moderate and high Reynolds numbers (Re > 100). The mean separation angle from the canopy can exceed the separation angle of a single stem by two processes. One, the kinetic energy added to the boundary layer by the upstream turbulence may delay the separation. Two, the higher velocity's in the restricted canopy flow width keeps the flow around the stems (Etminan et al., 2017).

A.2.2. Canopy drag coefficient in currents

As stated before, the canopy drag coefficient depends on the drag coefficient for a single stem, the vegetation density and arrangement. In Figure A.12 the pressure coefficient is given for different densities (A) and different Reynolds numbers (B). It can be seen that an increase in canopy density leads in most cases to an increase of the drag force over the cylinders (higher differences in the pressure coefficient). At high densities (λ = 0.2 - 0.25), the pressure coefficient decreases. In this case, the wake pressure of the upstream cylinders is strengthened by the high pressure stagnation region of the cylinder directly downstream. Also interesting to see is that, with a sparse density (λ = 0.016), the pressure coefficient is even smaller than the pressure coefficient of a single stem. This is due the sheltering effect. (Etminan et al., 2017).
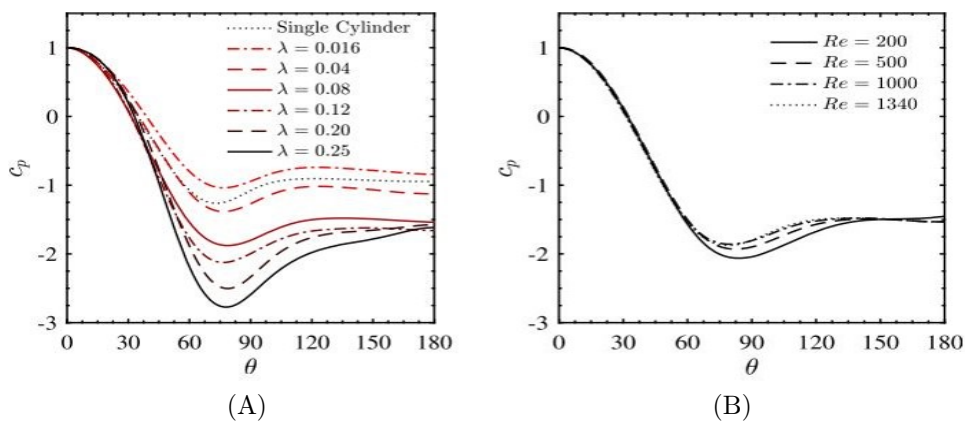
Figure A.12: Relation between the Pressure coefficent and different canopy density's at Re = 1340 (A) and different Reynolds numbers at λ = 0.08 (B) (Etminan et al., 2017).
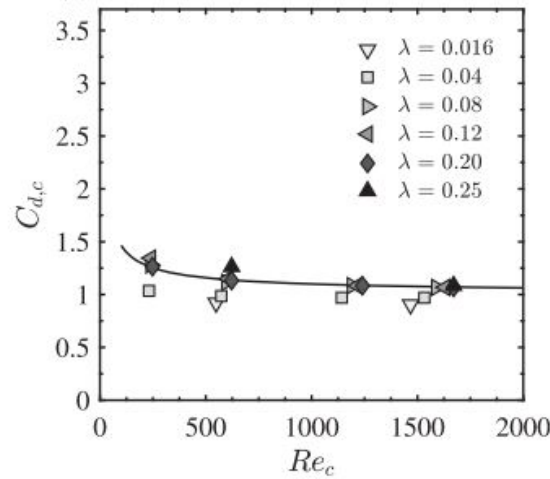
Figure A.13: Validation of drag coefficiant based on the constricted cross sectional flows (Etminan et al., 2017).

As many different processes influences the canopy drag coefficient, it is difficult to derive an equation that will encounter all the processes described in Section A.1 and A.2. Often a formula has been calibrated in order to describe the canopy drag, but also analytical approaches have been used. Two of the most recent derived drag coefficients are from Etminan et al. (2019) and Sonnenwald et al. (2019).

According Etminan et al. (2019), the blockage factor is dominant in high densities. In order to derive a canopy drag coefficient (Equation A.14), Etminan et al. (2017) calculated the corresponding Reynolds number. The corresponding Reynolds number is based on the constricted cross section flow velocity (Equation A.15). A validation has been given in Figure A.13 where data from a model has been used.

$$C_{d,c} = 1 + 10Re_c^{-2/3} \tag{A.14}$$

$$U_c = \frac{1-\lambda}{1-\sqrt{\frac{2\lambda}{\pi}}} U_p \tag{A.15}$$

where: $C_{D,c}$ = Drag coefficient based on the constricted cross-section velocity
Re_c = Reynolds number based on the constricted cross-section velocity
U_c = Constricted cross-section velocity
λ = Canopy density or solid fraction
U_p = Pore velocity

Sonnenwald et al. (2019) derived an equation which represents the canopy drag based on a calibration of data from previous researches. Using a least square fit, the following formula has been derived:

$$C_D = 2 \left(\frac{6475D + 32}{R_d} + 17D + 3.2\phi + 0.50 \right) \tag{A.16}$$

where: C_D = Drag coefficient
D = Cylinder diameter
Re_D = Cylinder Reynolds number
ϕ = Solid volume fraction

An overview of previous derived canopy drag coefficients in currents is given in Table A.1.

Table A.1: Overview of conducted researches concerning velocity through an emerged vegetation field.

Derived formula's for C_D			
Reference	Validation region	Drag coefficient	Deriving method
Armani et al. (2005)*	Re= 5000-20000	1.5 with foliage 1 without foliage	Willow
Ghisalberti and Nepf (2006)*	Re = 80-400	O (1) for Re>200 1 - 10 for Re <200	Rigid cylinder array
Wilson et al. (2008)*	U = 25-60 cm/s	Pine with foliage, 0.5-1.1 Pine w/o foliage, 0.5-1.3 ($\neq f(U)$) Ivy with foliage, 0.5-0.8 Ivy w/o foliage, 0.5-3.3 ($\neq f(U)$)	Pine and ivy stems
Nepf (1999)		$\frac{\sqrt{k}}{U_{yz}} = \alpha_1 [\overline{C_D} ad]^{1/3}$	
M. Ben Meftah, F. De Serio (2012)	Re = 234 - 607	$C_d = \frac{1}{\pi} \left(\frac{s_y^4}{dl^2 s_x} \right)$	straight rigid iron cylinders
Etminan et al. (2017)	Re = 0 - 2000	$C_{d,c} = 1 + 10Re_c^{-2/3}$ see eq A.15	staggered array of cylinders
Cheng (2012)**		$C_D = (1-\phi)(11\left(\frac{R_d}{1+80\phi}\right)^{-0.75}$ $+0.9\left[1 - exp\left(-\frac{1000(1+80\phi)}{R_d}\right)\right]$ $+1.2\left[1 - exp\left(-\left(\frac{R_d}{4500(1+80\phi)}\right)^{0.7}\right)\right])$	pseudofluid model
Ghisalberti and Nepf (2004)**		$C_d = \frac{C_{D,White}}{1.16}(1.16 - 9.31(ad)^2 - 59.8(ad)^3)$	Wake shading numerical model
Tanino and Nepf (2004)**		$C_D = 2(0.46 + 3.8\phi)$	Rigid cylinder
Tinoco and Cowen (2013)**	$R_d > 1000$	$C_D = 2(0.58 + 649\phi)$	Rigid cylinder
White (1991)**		$C_D = 1 + 10.0R_d^{-2/3}$	Rigid cylinder
Sonnenwald et al. (2018)		$2\left(\frac{6475d+32}{R_d} + 17d + 3.2\phi + 0.50\right)$	data rigid cylinders

* cited in Nepf (2011), ** cited in Sonnenwald et al. (2018).

A.2.3. Canopy drag coefficient in waves

In the study of Chen et al. (2018), a formula has been derived for C_D based on KC (Table A.2) where the C_D has been derived for the waves and current interaction with vegetation. As KC is specifically for wave period, while Re depends only on the viscosity a higher accuracy for C_D for oscillatory flows can be expected with the use of KC. But, looking at the accuracy for the C_D relation formulated by Hu et al. (2014) (Table A.2) the opposite seems to be true. A reason could be the use of different vegetation mimics, where Hu et al. (2014) uses rigid wooden cylinders a different result can be expected compared with studies that used flexible plastic strips (Chen et al., 2018). According Bradley and Houser (2009). The use of a rigid stem results in a reasonable estimation of the drag coefficient, especially in a more turbulent environment (Re > 400). According Bradley and Houser (2009) the Reynolds number has a higher accuracy in describing the wave energy decay through a canopy in a low energy environment. For the wave frequency depended dissipation, which is driven by blade motion, the Keuglan-Carpenter (KC) gives a better result.

Other difficulties in determining a single formula for the C_D factor are the influences of turbulence, surface friction of the vegetation mimics and the presence of the flume walls. As long as those parameters have an influence on the measured values, inaccuracies will be present, resulting in different drag formulas (Chen et al., 2018).
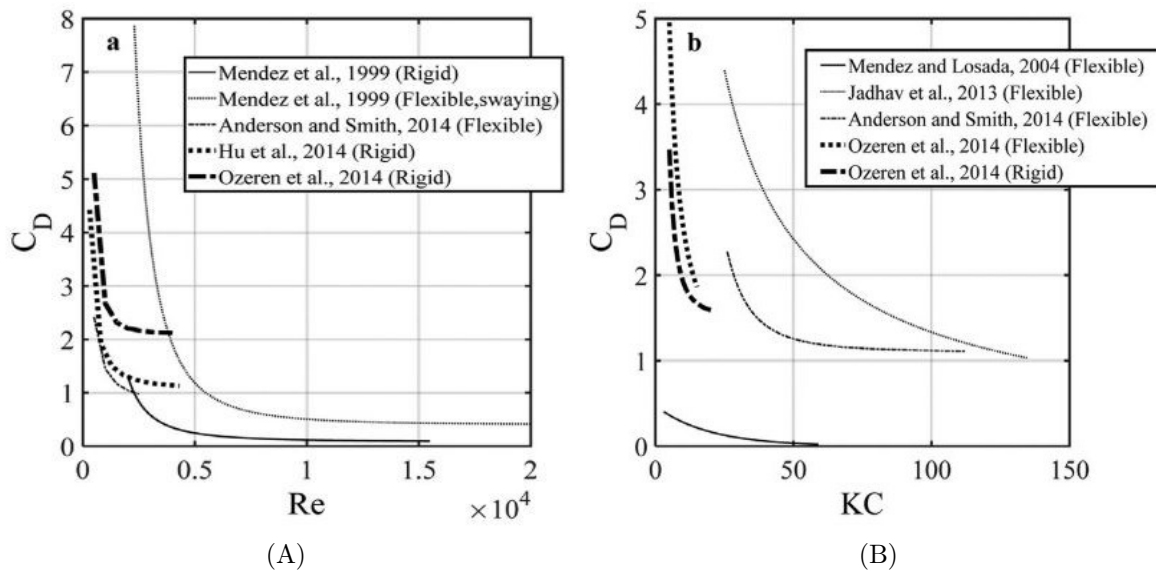
Figure A.14: Visualisation of C_D relations according Table A.2 (Chen et al., 2018).

Table A.2: A review of C_D relations in vegetation-wave interaction and their deriving methods from Chen et al. (2018).

Derived formula's for C_D				
Reference	Mimic Type	Flow condition	C_D relation	Deriving method
Kobayashi et al. (1993)	Flexible plastic strips	Waves	$C_D = 0.08 + (2200/Re)^{2.4}$ $2200 < Re < 18000$	Calibration method
Méndez et al. (1999)	Flexible plastic strips	Waves	$C_D = 0.08 + (2200/Re)^{2.2}$ $2200 < Re < 15500$ (no swaying) $C_d = 0.40 + (4600/Re)^{2.9}$ $2300 < Re < 20000$ (swaying)	Calibration method
Mendez and Losada (2004)	Flexible real strips	Waves	$C_D = 0.47\exp(-0.052KC)$ $R^2 = 0.76$ $\qquad$ $3 < KC < 59$	Calibration method
Brandley and Houser (2009))	Flexible real strips	Waves	$C_D = 253.9KC^{-3.0}$ $R^2 = 0.95$ $\qquad$ $0 < KC < 6$ Using relative velocity of seagrass blades	Calibration method
Ranjit . Jadhav et al. (2013)	Flexible real strips	Waves	$C_D = 70KC^{-0.86}$ $R^2 = 0.95$ $\qquad$ $25 < KC < 135$	Calibration method
Anderson and Smith (2014)	Flexible plastic strips	Waves	$C_D = 1.10 + (27.4/KC)^{3.08}$ $R^2 = 0.88$ $\quad$ $26 < KC < 112$ $C_D = 0.76 + (744.2/KC)^{1.25}$ $R^2 = 0.94$ $\qquad$ $533 < KC < 2296$	Calibration method
Ozeren et al.(2014)	Rigid wooden cylinders	Waves	$C_D = 1.5 + (6.785/KC)^{2.22}$ $R^2 = 0.21$ $\qquad$ $N_v = 156m^-2$ $h_v = 0.63m$ $C_D = 2.1 + (793/Re)^{2.39}$	Calibration method
	Flexible plastic strips		$C_D = 0.683 + (12.07/Re)^{2.25}$ $N_v = 350m^-2$ $\qquad$ $hv = 0.48m$	
Infantes et al. (2011)	flexible real vegetation	Waves	$lgC_D = -0.6653 * lgRe + 1.1886$ $R^2 = 0.77$	Direct measurement method
Hu et al. (2014)	Ridgid wooden cylinders	Waves + Current	$C_D = 1.04 + (730/Re)^{1.37}$ $R2 = 0.66$ $\qquad$ $300 < Re < 4700$	Direct measurement method
Losada et al. (2016)	Flexible real vegetation	Waves + Current	$C_D = 0.08 + (50,000/Re)^{2.2})$ $R^2 = 0.60$(regular waves) $C_D = 0.25 + (75,000/Re)^9)$ (regular waves + currents) $C_D = 0.50 + (50,000/Re)^9)$ (regular waves - currents)	Calibration method
Chen et al.(2018)	Ridgid wooden cylinders	Waves	$C_D = 6.94 * KC^{-0.72} + 0.87$ $R^2 = 0.79$	Direct measurement method
		Waves + Current	$C_D = 12.89 * KC^{-1.25} + 1.17$ $R^2 = 0.66$	Calibration method

<div style="text-align: right; font-size: 4em;">B</div>

Model Equations

This appendix describes the used equations in the modified model of Duró et al. (2020). In Section B.1 the formulas for wave attenuation through structures and vegetation are given. In Section B.2 the used model equations are given. Section B.3 explains the different calibration parameters and coefficients used in the model.

B.1. Wave dissipation formulas

Wave dissipation through structures and vegetation happens in multiple ways. In Subsection B.1.1 the wave transformation through a structure is described for a generally case. In Subsection B.1.2 the used formula for energy dissipation through vegetation is derived.

B.1.1. Energy dissipation by waves

The wave energy is given by Equation B.1 with ρ_w the water density, g the gravitational constant and H the wave height (Bosboom and Stive, 2012).

$$E = \frac{1}{8}\rho_w g H^2 \tag{B.1}$$

When a wave reaches an obstacle, such as brushwood structure, dike or vegetation, the incoming wave energy can be reflected, dissipated or be transmitted (Thornton and Calhoun, 1972).

$$E_i = E_r + E_{diss} + E_t \tag{B.2}$$

Since the variation in water density and the gravity constant are small, ρ_w and g can be assumed as constants. Equation B.2 can be written into a form where the energy losses are represented as wave height. Dividing Equation B.3 by the incoming wave height the different processes of wave attenuation are expressed in a single equation.

$$H_i^2 = H_r^2 + H_{diss}^2 + H_t^2 \tag{B.3}$$

$$1 = (\frac{H_r}{H_i})^2 + (\frac{H_{diss}}{H_i})^2 + (\frac{H_t}{H_i})^2 \tag{B.4}$$

$$1 = C_r^2 + C_{diss}^2 + C_t^2 \tag{B.5}$$

With C_r the reflection coefficient, C_{diss} the dissipation coefficient and C_t the transmission coefficient (Thornton and Calhoun, 1972).

B.1.2. Analytical model for wave energy dissipation in vegetation

Dalrymple et al. (1984) studied the wave dissipation through an array of vertical cylinders, representing a vegetated field. He derived an analytical formula in which the wave dissipation is the result of the horizontal drag force. For this equation the assumption has been made that all the energy of the mean flow is converted to turbulent energy (Stam, 2018). The horizontal force per unit volume can be given as (Mendez and Losada, 2004):

$$F_x = \frac{1}{2}\rho_w C_d b_v u \mid u \mid N \tag{B.6}$$

where: F_x = Horizontal force per unit volume
u = Horizontal velocity (due to the wave motion)
C_d = Drag coefficient)
N = Number of elements per unit area
b_v = Plant area per unit height
ρ_w = Water density

Looking at the energy dissipation over the total length of the cylinder (in emerged conditions) the energy dissipation can be derived as shown below. For this derivation it is assumed that the linear wave theory is valid and that the waves travel perpendicularly to a straight shore.

$$-\frac{dEc_g}{dx} = E_{diss} = \overline{\int_0^d F_d * u dz} = \overline{\int_0^d \frac{1}{2}\rho C_d D u \mid u \mid N * u dz} \tag{B.7}$$

Following the linear wave theory the horizontal motion of waves can be described as

$$u = \omega a \frac{cosh(k(z+d))}{sinh(kd)}cos(\omega t - kx) \tag{B.8}$$

With the wave frequency given by the dispersion relation:

$$\omega^2 = gktanh(kd) \tag{B.9}$$

Neglecting the inertia forces in the vegetation and using the dispersion relation for waves Dalrymple et al. (1984) expressed the energy dissipation by waves as followed (Mendez and Losada, 2004):

$$E_{diss} = \frac{2}{3\pi}\rho C_D bN \left(\frac{kg}{2\sigma}\right)^3 \frac{sinh^3(k\alpha h) + 3sinh(k\alpha h)}{3kcosh^3(kh)}H^3 \tag{B.10}$$

In the case of a horizontal bed Equation B.10 can be written as follows:

$$\frac{dH^2}{dx} = -A_0 H^3 \tag{B.11}$$

$$A_0 = \frac{8}{9\pi}C_D b_v Nk \frac{sinh^3(k\alpha h) + 3sinh(k\alpha h)}{(sinh(2kh) + 2kh)sinh(kh)} \tag{B.12}$$

$$H = \frac{H_0}{1 + \beta x} = K_v H_0 \tag{B.13}$$

$$\beta = \frac{A_0 H_0}{2} = \frac{4}{9\pi}C_D b_v NH_0 k \left(\frac{kg}{2\sigma}\right)^3 \frac{sinh^3(k\alpha h) + 3sinh(k\alpha h)}{(sinh(2kh) + 2kh)sinh(kh)} \tag{B.14}$$

where: ρ_w = Water density

b_v = Plant area per unit height of each vegetation stand normal to u

N = Stem density

k = wave number

g = Gravity constant

σ = Angular wave frequency

α = Relative vegetation height

H = Wave height m^2

H_0 = Wave height in previous grid

A downside of the formula of Dalrymple et al. (1984) is that the reflection induced by the vegetation is neglected and the assumption that the horizontal velocity is smaller than the orbital velocity, in which case vegetation can be represented by a rigid stem (Bradley and Houser, 2009)

B.2. Numerical implementation

This section describes the used formulas in the modified model of Duró et al.(2020).

B.2.1. Grid Set-up

The computational domain starts with a foreshore in order to stabilise the wave parameters resulting from the spin-up. At the end of the foreshore, a single slope reaches until a distance equal to 5 times the initial wave height above the still water level. In this way, enough space is available to compute the wave run-up. The total length of the bed profile is divided into grid cells of 0.02m for the computation of the hydraulic changes, while the morphology update has been calculated every 2m. The start of the terrace length is defined at the start of the slope.

When a single wave height has passed, an update of the bed profile is made based on the difference between the critical bed shear stresses and the induced bed shear stresses. This new bed profile will be used for the next computation of wave heights and induced shear stresses. This will continue until the bed profile does not change anymore.

B.2.2. Wave height propagation

The bed profile and still water level are known, the wave height is estimated for every location and at the end of the energy balance the calculated wave height replaces the estimated wave height so a more exact calculation can be made.

Calculation of parameters

$$L_m = \frac{gT^2}{2\pi} tanh \left(\frac{2\pi}{L_m} h_m \right) \tag{B.15}$$

When the differences between the estimated and calculated L is less than 0.00001 the calculations will continue.

$$n_m = \frac{1}{2} \left(1 + \frac{2\pi}{L_m} * \frac{2h_m}{sinh \left(2h_m \frac{2\pi}{L_m} \right)} \right) \tag{B.16}$$

$$C_{g,m} = n_m * \frac{L_m}{T} \tag{B.17}$$

$$\theta_m = \frac{180}{\pi} * asin(\frac{c_m}{c_{m-1}}) * sin(\frac{\pi * \theta_{m-1}}{180}) \tag{B.18}$$

$$k_m = \frac{2\pi}{L_m} \tag{B.19}$$

Calculation of the drag coefficient

- I3 = location m of the start of the vegetation

- I4 = location m of the end of the vegetation

$$u_{c1} = \frac{H_{I3}}{2}\omega_{I3}\frac{cosh(k_{I3}\alpha_{I3}h_{I3})}{sinh(k_{I3}h_{I3})} \tag{B.20}$$

$$KC = \frac{u_{c1}T}{D} \tag{B.21}$$

$$Q = \frac{KC}{\alpha^{0.76}} \tag{B.22}$$

$$CD = \frac{exp(-0.0138Q)}{Q^{0.3}}(7 < Q < 172) \tag{B.23}$$

Calculation of energy dissipation by vegetation

$$\beta_m = \frac{4}{9\pi}C_D b_v N H_{m-1} k_m \left(\frac{k_m g}{2\sigma_m}\right)^3 \frac{sinh^3(k_m\alpha h_m) + 3sinh(k_m\alpha_m h_m)}{(sinh(2k_m h_m) + 2k_m h_m)sinh(k_m h_m)} \tag{B.24}$$

$$H_m = \frac{H_{m-1}}{1 + \beta_m * \delta x} \tag{B.25}$$

$$E_{diss,m} = \frac{2}{3\pi}\rho C_D bN \left(\frac{k_m g}{2\sigma}\right)^3 \frac{sinh^3(k_m\alpha_m h_m) + 3sinh(k_m\alpha h_m)}{3k_m cosh^3(k_m h_m)} H_m^3 \tag{B.26}$$

Calculation dissipated energy, bore formation
Only after wave breaking ($H_{m-1} < H_{br,m-1}$) the energy dissipation from bore formation will be considered.

$$H_{br,m-1} = \frac{0.88}{k_{m-1}}tanh\left(\frac{\gamma k_{m-1}h_{m-1}}{0.88}\right) \tag{B.27}$$

$$D_{b,m} = \frac{1}{4}\rho g\frac{1}{T}\frac{H_m^3}{h_m} \tag{B.28}$$

Calculation dissipated energy, Bottom friction

$$U_m = \frac{\pi * H_m}{T * sinh(\frac{2\pi}{L_m * h_m})} \tag{B.29}$$

$$RE_m = \frac{U_m * h_m}{10^{-6}} \tag{B.30}$$

$$f_{b,m} = -4log\left(\frac{k_m}{14.8h_m} + \frac{2.51}{Re_m 2\sqrt{f_{b,m}}}\right)^{-2} \tag{B.31}$$

When the differences between the guessed and calculated f_b is less than 0.00001 the calculations will continue. f_b has a maximum value or 0.03.

$$D_{friction,m} = \frac{2}{3\pi}\rho f_{b,m}\left(\frac{\pi H_m}{T_m sinh(k_m h_m)}\right)^3 \tag{B.32}$$

Calculation of the energy flux

$$E_{flux,m} = \frac{(B_0 \rho g H_{m-1}^2 c_{m-1} cos(\frac{\pi}{180*\theta_{m-1}})) - (E_{diss,m} + D_{bore,m-1} + D_{friction,m})\Delta x)}{cos(\frac{\pi}{180*\theta_m})} \tag{B.33}$$

$$H_m = \sqrt{\frac{1}{B_0}\frac{E_{flux,m}}{\rho g c_m}} \tag{B.34}$$

When the differences between the wave height at the start of the energy balance differs less than 1E-5 m from the calculated wave height the calculations for the morphological update will made.

B.2.3. Induced Shear stresses
Induced bed shear stresses by wave propagation and wave breaking

$$\tau_b = \frac{1}{2}f_b \rho U^2 \tag{B.35}$$

Induced bed shear stresses by wave run-up
The run-up starts at the point that the water depth equals 0.15* the water depth at the point of wave breaking.

$$Fr_{start} = \frac{c_{g,start}}{g*H_{start}} \tag{B.36}$$

$$R_v = \frac{(Fr_{start} + 0.889)\sqrt{gH_{start}}}{2g} \tag{B.37}$$

$$\frac{\tau_{b,max}}{(\rho C_{start}^2)/2} = 0.01\left(1 - \frac{x_R}{R_h}\right) \tag{B.38}$$

B.2.4. Morphological update
After every iteration (representing a single wave) the induced bed shear stresses will be calculated and the terrace slope will be updated with the use of Equation B.43. The model stops at the moment that their are no longer morphological changes.

Soil strength

$$t_{cr} = a_{soil} * Cohe + b_{soil} \tag{B.39}$$

with a_{soil} and b_{soil} constants 0.89 and -0.1 according Kimiaghalam et al. (2016)

Induced soil strength by vegetation

$$T_{root,P} = a_{root,P} * D_{root,P} - b_{root,P} \tag{B.40}$$

$$Cohe_{root,P} = 1.04 * \frac{\sum T_{root,P,i} n_{root,P,i} a_{root,P,i}}{A} \tag{B.41}$$

with $a_{root,P} = 34.29$, $b_{root,P} = 0.78$ and $n_{root,P} = 20$ (de Baets et al., 2008)

$$t_{cr}[I3 : I4] = t_{cr}[I3 : I4] + a_{soil} * Cohe_{root} \tag{B.42}$$

Amount of erosion

$$\Delta Z_b = \epsilon(\tau_b - \tau_{cr}) \tag{B.43}$$

Only slopes between the 0.00 (S_{min}) and 0.1 (S_{max}) will be used in order to prevent negative slopes or scarps (which will be unrealistic through the smoothing in practice) (Duró et al., 2020). Slopes outside this range will be filtered with a slope check.

B.3. Calibration parameters and coefficients

In this section the calibration parameters and coefficients present in the model are listed and discussed.

Breaking parameter γ

When regular waves are used, a small deviation of the breaking parameter can lead to a large deviation in the maximum amount of induced bed shear stresses (Figure 4.4 and C.19 Section 5.2), which is especially crucial as the breaking parameter itself knows a high uncertainty (Schiereck, 2001). One way to remove this uncertainty is to implement partial wave breaking, which has been used in other models such as SWASH and X-beach (Zijlema et al., 2011; Roelvink et al., 2015). For the modified model of Duró et al. (2020) the choice has been made to work without partially wave breaking in order to account for the maximum impact coming from the maximum wave, so with the high uncertainty of the breaking parameter included. However, a new consideration could be made in order to remove this uncertainty without undermining the models purpose.

Reduction energy dissipation by bore propagation

After wave breaking, the energy dissipation is calculated with Equation B.44. In the model of Duró et al.(2020), a calibration factor is used to increase the amount of dissipated energy with a factor between the 1 and the 1.5. For this study this factor has not been used.

$$D_b = \frac{1}{4}\rho_w g \frac{1}{T}\frac{H^3}{h} * B_{cal} \tag{B.44}$$

where: D_b = Energy dissipation by bore propagation
   ρ_w = Water density
   g = gravity constant
   T = Wave period
   H = Wave height
   h = Water depth
   B_{cal} = Calibration coefficient

Nikuradse roughness length

The Nikuradse roughness length is used in order to calculate the bed friction coefficient f_b. The Nikurase roughness length stands for the equivalent sand roughness and equals several times the characteristic grain diameter, but can exist of higher values with an in-regular bed (Schiereck, 2001). As both the original and the modified model of Duró et al. (2020) are based on a cohesive soil, the same value (0.02) is used. As the influence of the bed friction is small (Appendix C.1.2) the influence has been assumed negligible.

Vegetation characteristics *P. australis*

Most formulas used to describe the influence of vegetation know a lot of different calibration parameters, as they are often derived by fitting a trend line through data. This is also the case by the derivation of the drag coefficient by Wu et al. (2011) and the armoring capacity of the roots derived by de Baets et al. (de Baets et al.) (Subsection 2.4.2). In order to estimate the influence of those approximations the standard error of the original data is needed, often expressed in R. The used formula for the calculation of the drag factor has a R^2 (standard error) of 0.84, which is an average standard error for the derivation of the drag factor (Table A.2). This combined with the relative low deviation of maximum induced shear stress with a changing parameter of CD, it can be assumed that the influence of the uncertainty is small. For the roots a standard error (R^2) of 0.92 has been found by de Baets et al. (2008). The soil reinforcement of the roots is high enough that even a large deviation does not result in erosion.

Start run-up

The used start location of the run-up is set on the location with a water depth of 0.15 times the water deptH at the point of wave breaking. This value results from observations along the Maas done by Duró et al. (2020). In previous work (Putrevu and Svendsen, 1991) a value of 0.12 has been observed. As it concerns an observed value without a theoretical background for its dependency, it can not be assumed that this value can be used in a situation outside the validated boundaries. The expected variation is also unknown. In the tested situation for the sensitivity analyses, the influence of a 10% deviation of 0.15 did not show any difference in the maximum amount of induced bed shear stress for waves lower than 0.37m (Figure 4.4). However, looking at results derived for steeper slopes (Figure 4.2), the exact boundary from wave propagation to run-up becomes critical. The effect of a changing transition point has been illustrated in Figure B.1. In order to use the modified model of Duró et al. (2020) the transition point between bore propagating and run-up should be invested in more detail.
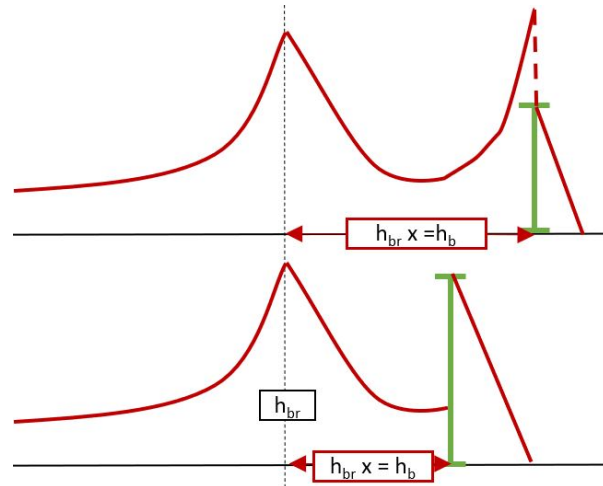
Figure B.1: Changing transition point. A) lower value for x. B) higher value for x. A change of the transition point fromwave propagation to run-up can lead to a large change in the maximum amount of induced bed shear stresses. At a certainpoint after wave breaking the shoaling effect starts to dominate over the dissipation processes, resulting in fast increasein induced shear stresses. At some stage this formulation gives an unrealistic result, this is were the run-up should start.The sooner the run-up starts, the higher the wave celerity is, resulting in a higher bed shear stress through run-up

Energy conversion run-up [α]

In order to calculate the total horizontal run-up distance, the vertical run-up height (R_h) has been calculated with the use of energy conservation. The horizontal kinetic energy from wave propagation is conversed to potential energy, resulting in a run-up height (Equation 3.8). Through the conversion of energy, energy will be lost. This has been expressed in α. Bergsma et al. (2019) has found an average α value of 0.889 which has been used in the model of Duró et al. (2020). In order to account for varying conditions the α factor should be added as a variable. Bergsma et al. (2019)) has derived an equation which accounts for varying conditions (Equation 3.9), which should first be tested and validated before it can be used. As the run-up height is responsible for the horizontal distance the run-up will travel, and not the maximum amount of induced shear stresses, a change in α will not influence the maximum amount of shear stress and has therefore not been investigated further. However, it is important when the morphology will be considered. Thus, further investigation into the run-up height is needed when morphology is considered.

$$R_v = \frac{(c_b + \alpha\sqrt{gH_b})^2}{2g} \tag{B.45}$$

$$\alpha = \sqrt{\frac{2R_h}{H_b}} - Fr_b \tag{B.46}$$

where: R_v = Vertical run-up height
            c_b = Water celerity at start run-up
            α = Factor accounting for imperfect energy conversion
            g = Gravity constant
            H_b = Wave height at start run-up
            Fr_b = Froude number at start run-up

Calculation critical shear stress from soil cohesion

The calculation of the critical shear stress is based on the research of Kimiaghalam et al.(2016) (Equation B.47). His research is based on soil samples from relatively undisturbed river banks. As the soil samples are taken from close to the surface with varying properties, a good representation of an average river bank can be expected. For the modified model of Duró et al. (2020), a lake situation is considered. As both situations exist of a cohesive soil a similar response is expected but further investigation is needed.

$$\tau_c = 0.89 * Cohesion - 0.1 \tag{B.47}$$

Erodibility coefficient ϵ

When the bed shear stresses (τ_b) exceeds the critical bed shear stress (τ_c) the bed will erode. The Erodibility coefficient ϵ determines the amount of erosion based on the difference between τ_b and τ_c (Equation B.48). The estimation of ϵ is found with mixed techniques of experimental and mathematical modeling (Boukhemacha et al., 2013). The Erodibility coefficient is strongly correlated with the critical bed shear stress (τ_c), it is even possible to find multiple combination for τ_c and ϵ resulting in the same amount of erosion. Another difficulty can be found in the fact that those values have also a dependency on the applied hydraulic charge (Boukhemacha et al., 2013). In the model of Duró et al. (2020) ϵ has been taken as a calibration coefficient with a value of 0.01, which is good for a first guess but has to be investigated in depth to use at a specific location.

$$\frac{\delta Z_b}{\delta t} = \epsilon(\tau_b - \tau_c) \tag{B.48}$$

where: τ_c = Critical bed shear stress
            τ_b = Induced bed shear stress
            Z_b = Bed level

Maximum slope formulation

In order to represent the upper bank retreat without involving the processes, a maximum slope formulation has been implemented in the model of Duró et al. (2020) (Subsection 3.3.1). In the model of Duró et al. (2020) a different value for the maximum slope formulation [$smax$] leads to a maximal difference in terrace length of 10 %. A variation of smax in the modified model of Duró et al. (2020) shows the same sensitivity when 800 identical waves propagate over the terrace (Figure 3.12). In order to estimate the real influence of this simplification a comparison needs to be made with lab or field data, but it can be expected that the same range would be found.

C
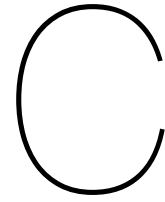
Tested aspects

In order to improve the model, different aspects have been investigated. Not all the investigated aspects resulted in an implementation in the model. In this appendix different tested aspect are showed in order to show the results of different hypothesises.

C.1. Wave height before breaking between different models

In Subsection 3.1.4 it has been shown that the model could reproduce the wave height through the vegetation quite well. However, a large different in wave attenuation can be seen in the part before wave breaking (Figure C.1). The wave height development in the model happens as expected when looking at the effects of shoaling and wave breaking based on $\gamma = H_b/h$. In this section different formulations were evaluated to investigate the differences in wave transformation. Also an estimation of the magnitude of those differences has been made. The following hypotheses have been tested:

1. Difference between a wave spectrum and non wave-spectrum

2. Implementation of energy dissipation formula's used in X-Beach and SWASH

3. Formulation of wave breaking
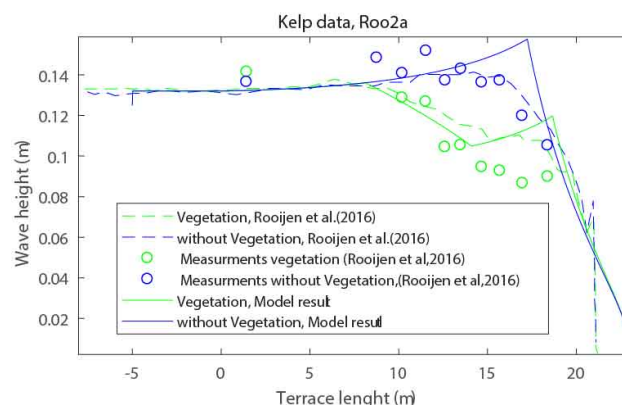
4. Adding wave setup

Figure C.1: Comparison in wave height development. A compairison is made between the model results of X-beach van Rooijen et al. (2016) (dashed line), the expanded model of Duró et al. (2020)(solid line) and the field observations of Wu et al. (2011)(dots). The situation with vegetation is shown in green, without vegetation in blue.

C.1.1. Use of a wave spectrum

The used data set and plot made with the use of X-Beach have an input wave height based on a Jonswap spectrum with a γ = 7.0. When a spectrum is used, the wave input exist of a distribution of wave heights with a mean wave height of the given wave height input. In that case the larger waves will break in deeper water than the smaller waves, what could explain the regular wave breaking in the measurements of Wu et al. (2011). When a single wave is modeled the wave breaking occurs at a single point, so a sharp transition at the point of wave breaking can be expected.

In order to compare the results based on a Johnswap spectrum and a single wave condition SWASH has been used in order to model the wave height development over a slope. The result of the X-Beach model with the use of a Johnswap spectrum, the model results of SWASH and the current model have been plotted in Figure C.2. The expected sharp transition by regular waves between wave propagation and wave breaking is indeed visible in the SWASH results, but the wave height before breaking shows still some dissipation while an increase in wave height was expected looking at greens law.
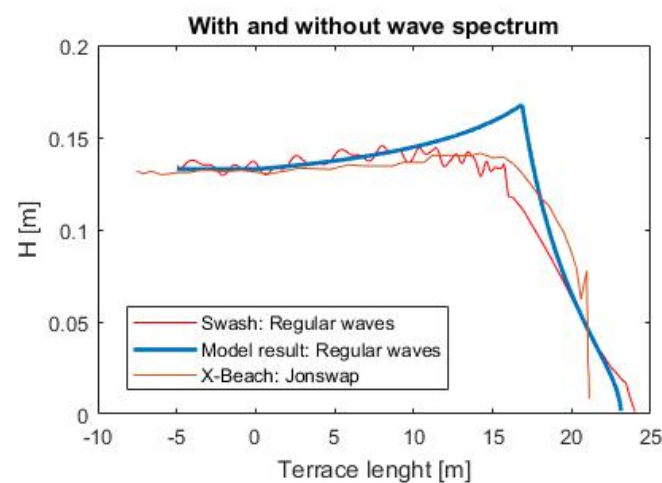
Figure C.2: Compairison in model results concering the wave height development over a slope between SWASH, X-beach and the presented model

Another difference between the results of the presented model and SWASH results is the presence of the oscillations in the wave height calculations. This can be explained by the schematization used for the two models. SWASH has been based on a numerical model which uses both boundary conditions for its calculations. This way, the model takes also the processes onshore in account for the offshore conditions. In this case the system accounts for the reflection inside the model. This can be concluded for the fact that the period of the oscillation shown in SWASH equals the wave period (4m).

C.1.2. Effect of bottom friction
As the wave height increases too much due the effect of shoaling, there is a probability that a dissipation parameter is missing. For this reason, a look has been taken into the different formulations for energy dissipation in both X-Beach and SWASH. In the original model the effect of energy dissipation through bottom friction has been neglected, as small values were expected.

X-beach formulations
In X-Beach three different wave dissipation processes have been included: dissipation through wave breaking, bottom friction and vegetation. As the largest issue can be found before wave breaking the focus lies on the energy dissipation through bottom friction. In X-beach the energy dissipation by bottom friction has been described using Equation C.1 (Roelvink et al., 2015).

$$D_f = \frac{2}{3\pi}\rho_w f_w (u_{orb})^3 \tag{C.1}$$

with

$$u_{orb} = \frac{\pi H_{rms}}{T_{m01} sinh(kh)} \tag{C.2}$$

where: D_f = Energy dissipation through bottom friction
ρ_w = Water density
f_w = friction coefficient
u_{orb} = Orbital wave velocity
H_{rms} = Root mean square wave height
T_{m01} = Mean absolute wave period
k = Wave number
h = Water depth

In order to identify the effect of the implemented bottom friction, a comparison is made between the model results without bottom friction and the model results including the formulation for bottom friction. As a reference level, the SWASH results has been plotted as well.

Looking at Figure C.3 a small differences is visible between the situation without bottom friction (C.3 (A) and (B)) and the situation with bottom friction (C.3 (C) and (D)). The main discrepancy can be found at the breaking point, which will be delayed if there is accounted for bottom friction (C.3 (C) and (D)).

In order to see what happens as the bottom friction increases plots C.3 (E) and (F) have been made. It can be seen clearly that, when the overall energy dissipation increases, it results in a worse fit at the first part of wave propagation (before a terrace length of 10m) and after wave breaking. The fit through the vegetation becomes worse when the energy dissipation through friction increases. It can be assumed that the overestimation of the wave height can not been found in the neglecting of energy dissipation due bottom friction.

(A)

(B)

(C)

(D)

(E)

(F)

(G)
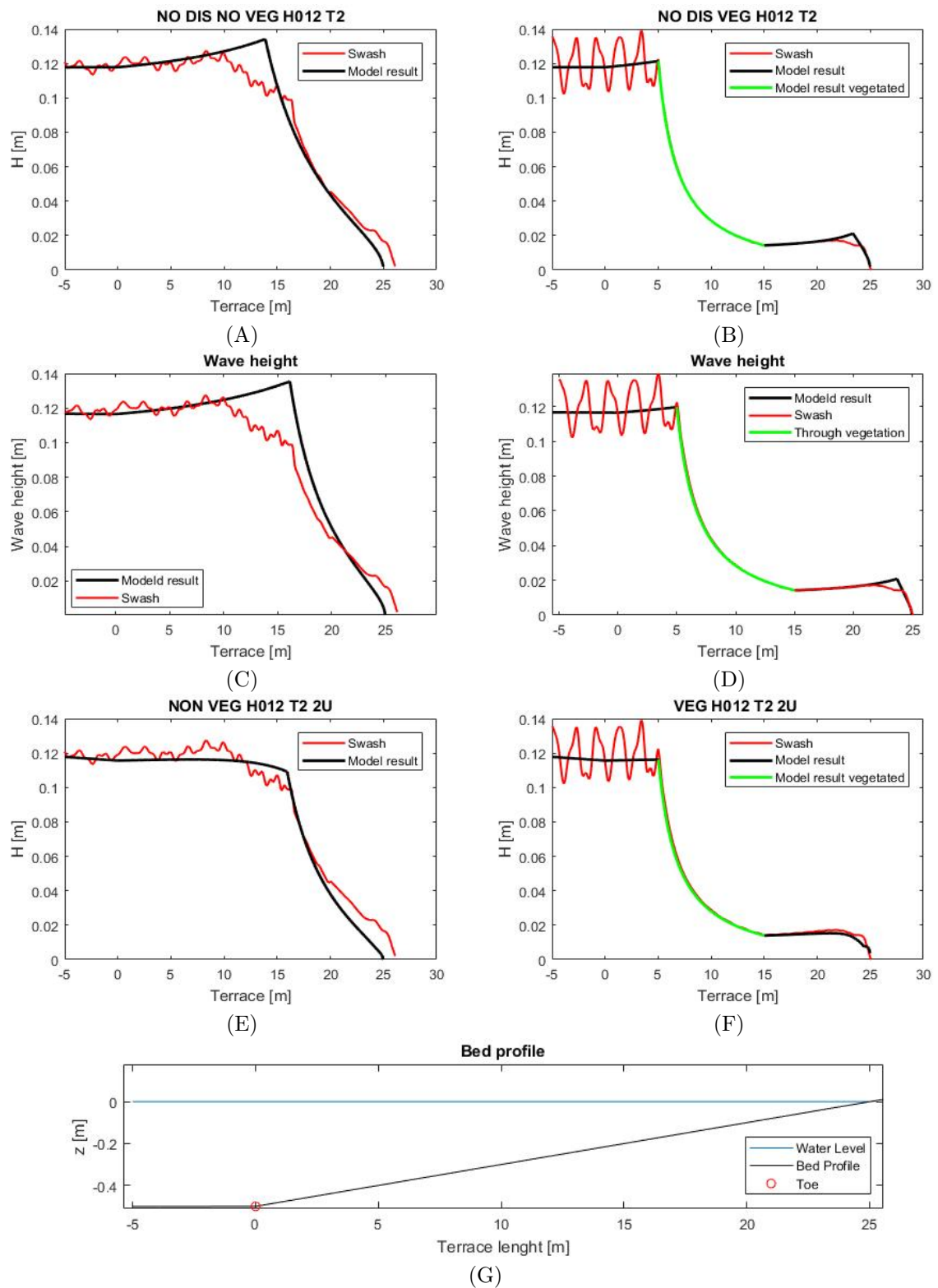
Figure C.3: Influences of including dissipation due to bottom friction. Plot (A) and (B)) No dissipation due to bottom friction. Plot (C) and (D)) with dissipation. Plot (E) and (F)) doubled velocity resulting in an extreme amount of dissipation due bottom friction. Plot G shows the used bottom profile

SWASH formulations

In SWASH the bottom friction has been implemented with the use of Manning's formula. In order to estimate the influence of Manning's constant two plots have been made, one with a Manning's constant of 0.012 (which is a common parameter for the roughness of river beds) and 0.0001, for which the friction is negligible. The differences between wave height is visible, but almost negligible. This has been shown in Figure C.4.
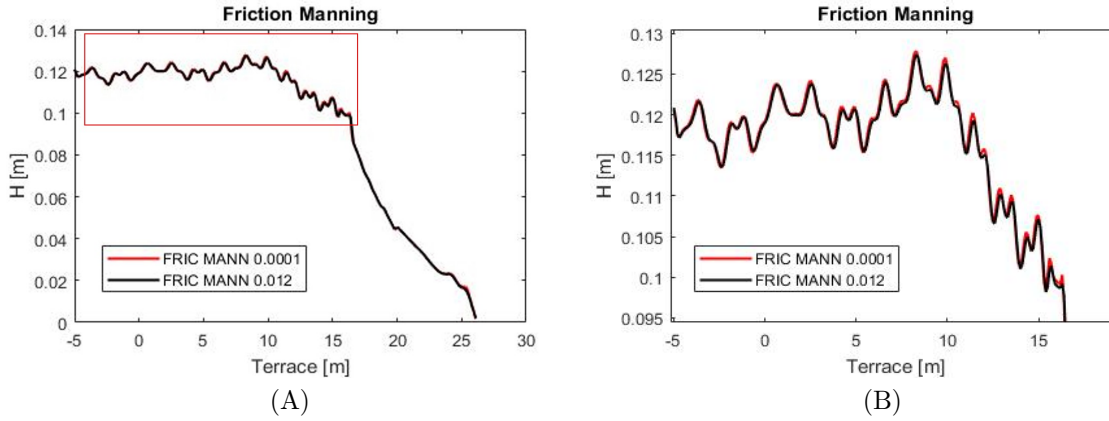
Figure C.4: Influence of Mannings Friction. Plot (A) Shows the differences in SWASH results for a Mannings friction coefficient of 1E-4 and 1.2E-2. Plot (B) is a magnified version of Plot (A).

C.1.3. Wave-driven setup

The wave setup can be calculated with the use of Equation C.3 (Dean and Bender, 2005) but before implementation an estimation of the influence has been made. This estimation has been done by increasing the still water line manually until the same setup has been archived as found in SWASH.

$$\frac{\delta \eta}{\delta x} = \frac{1}{\rho_w g(h + \eta)} \frac{\rho \nu \beta H^2 C}{8h^2} \left(\frac{3}{2} - 1 \right) \tag{C.3}$$

$$\beta \equiv \sqrt{\frac{\sigma}{2\nu}} \tag{C.4}$$

where: η = Set-up

ρ_w = Water density

g = Gravity constant

h = Water depth

ν = Viscosity

H = Wave height

σ = Wave angular frequency

To get a feeling for the influence of the setup resulting of the breaking waves the water level after wave breaking has been increased. The amount of expected setup has been compared with the results from SWASH and the expected setup given by the formulation of Bosboom and Stive (2012)

$$\eta_{max} = \frac{5}{16} \gamma_b H_{br} \tag{C.5}$$

$$\text{where:} \quad \eta_{max} = \text{Maximum Set-up}$$
$$\gamma_b = \text{Wave breaking index}$$
$$H_{br} = \text{Wave breaking height}$$

In Figure C.5 it can be seen that the the addition of wave setup has almost a negligible influence on the wave height and induced shear stresses. In the last meter, a small difference can be found, as the wave height starts to increase a little at the end. It can be seen that the run-up starts a little later what results in the same amount of shear stresses, but only a meter later. Therefore a more exact formulation has not been made.

(A)   (B)

(C)   (D)

(E)   (F)

Figure C.5: Effect of implementing set-up over the cross section of the shore. Plot A, C and E are without set-up. Plot B, D and F are with set-up. Plot A and B show the induced set-up, C and D show the wave height development with and without the setup and E and F show the induced bed shear stresses with and without setup. In Figure F the difference in induced bed shear stresses is indicated with arrows.
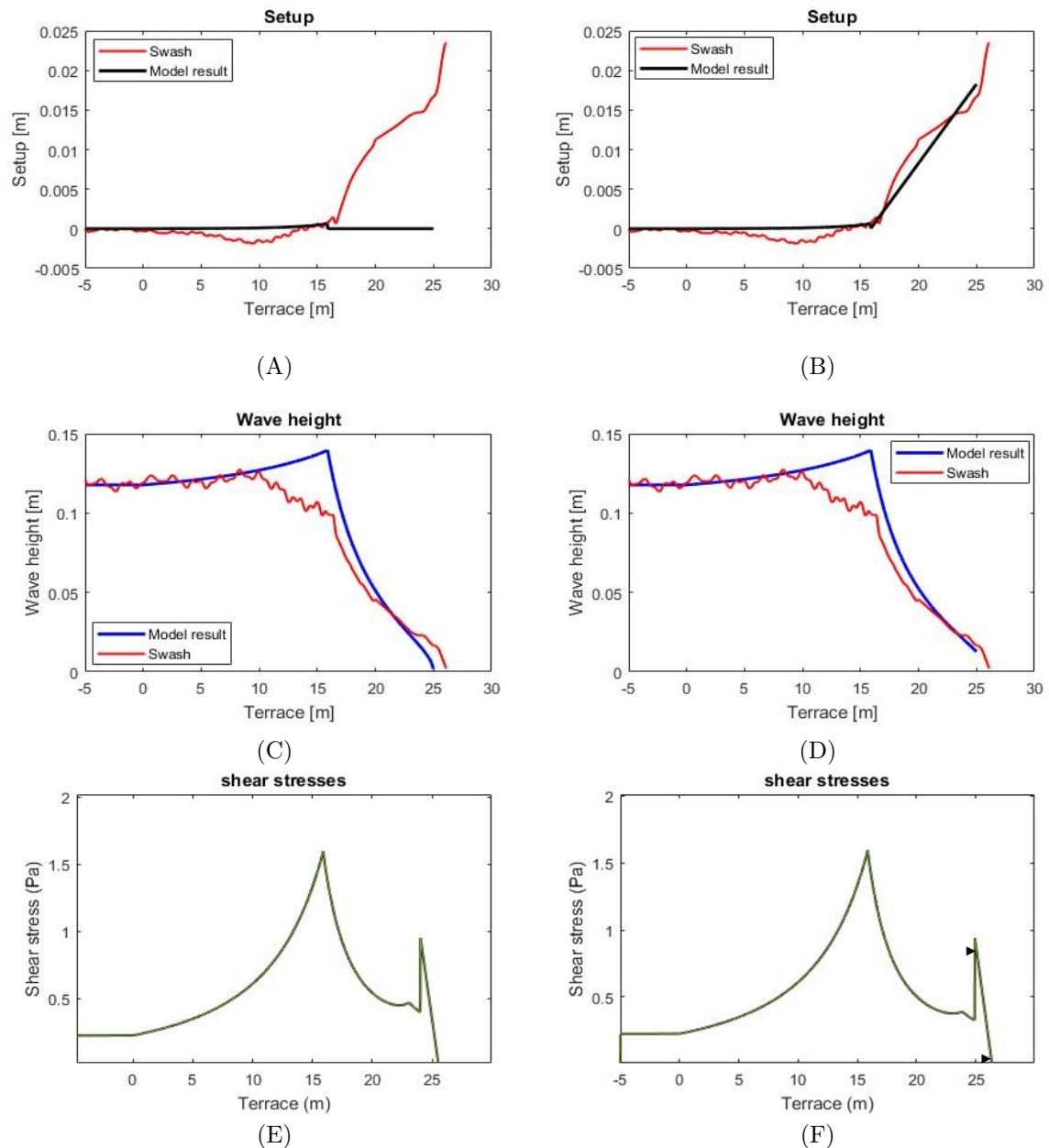
C.1.4. Formulation of wave breaking

As the overestimation of the wave height lies before the point of wave breaking, there is also the possibility that the reason can be found in the formulation for wave breaking. Until this point wave breaking has been formulated as followed:

$$\frac{H}{h} = \gamma_b \tag{C.6}$$

where: h = Water depth
γ_b = Wave breaking index
H = Wave height

SWASH

SWASH accounts for depth-limited wave-breaking with a shock-capturing conservation scheme (Zijlema et al., 2008). Besides this scheme it is possible to control the wave breaking with the use of a factor α, the threshold parameter where wave breaking starts and the parameter β, after which wave breaking stops. Those formulations are mainly implemented when the amount of vertical layers is small,what results in an incorrect calculation of the phase velocity at the breaking front.

The α parameter represents a maximum local surface steepness relative to the shallow water celerity. An advised value for α is 0.6. The β parameter represents the persistence of wave breaking and has an default value of 0.3. It must be noted that those formulations are additional formulations for wave breaking and are not needed if the velocity at the breaking front is computed with enough accuracy (SWASH team, 2011).

$$\frac{\delta \zeta}{\delta t} > \alpha \sqrt{gh} \tag{C.7}$$

$$\frac{\delta \zeta}{\delta t} > \beta \sqrt{gh} \tag{C.8}$$

where: δ = Surface elevation
g = Wave breaking index
h = Wave height
α = Maximum local surface parameter
β = Persistence against wave breaking

In the plots C.6 and C.7 it can be seen that a change of β has almost no influence, but at the moment α lowers the overestimated part becomes bigger, what could suggest that breaking occurs through steepness, what is not included in the model of Duró et al. (2020). As the wave steepness is not directly included in the model presented in this theses a look has been taken at different formulations of wave breaking presented in X-Beach
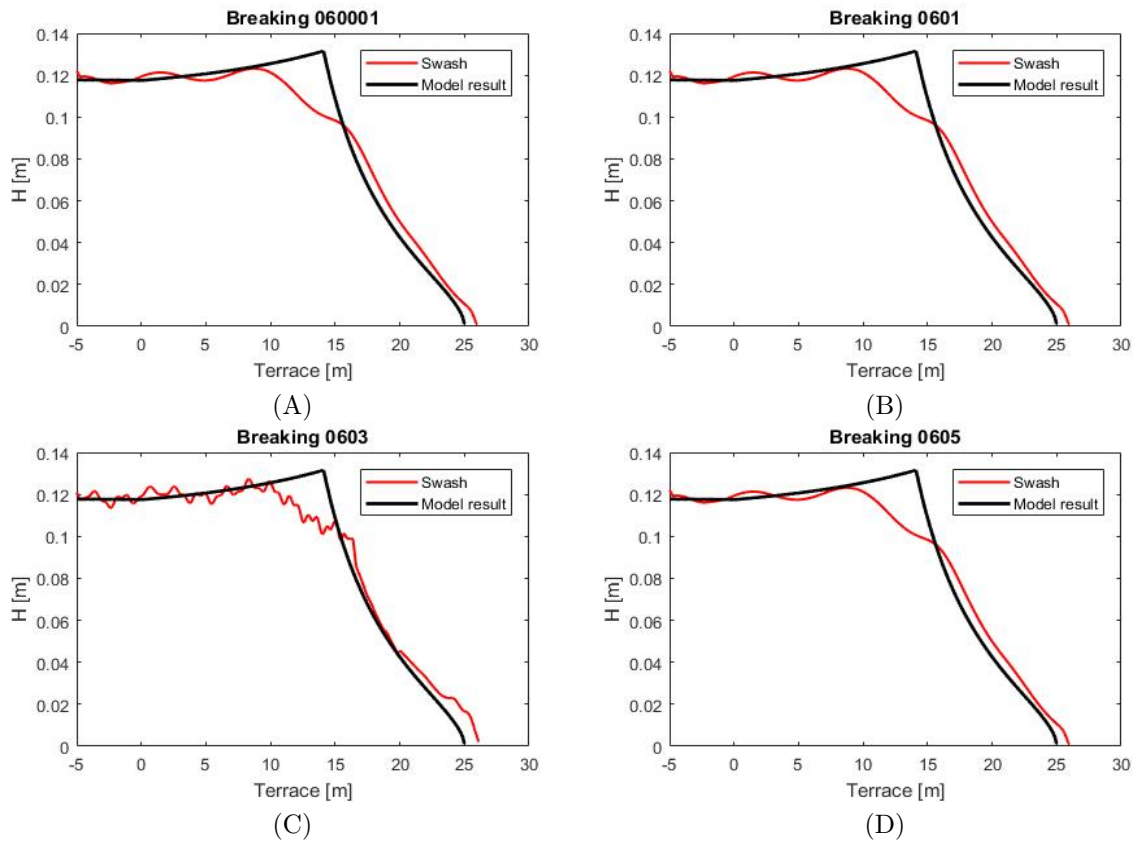
Figure C.6: Influence of a changing wave breaking parameter β in SWASH with: $\alpha = 0.6$. β: (A) = 0.001, (B) = 0.1, (C) = 0.3 and (D)= 0.5
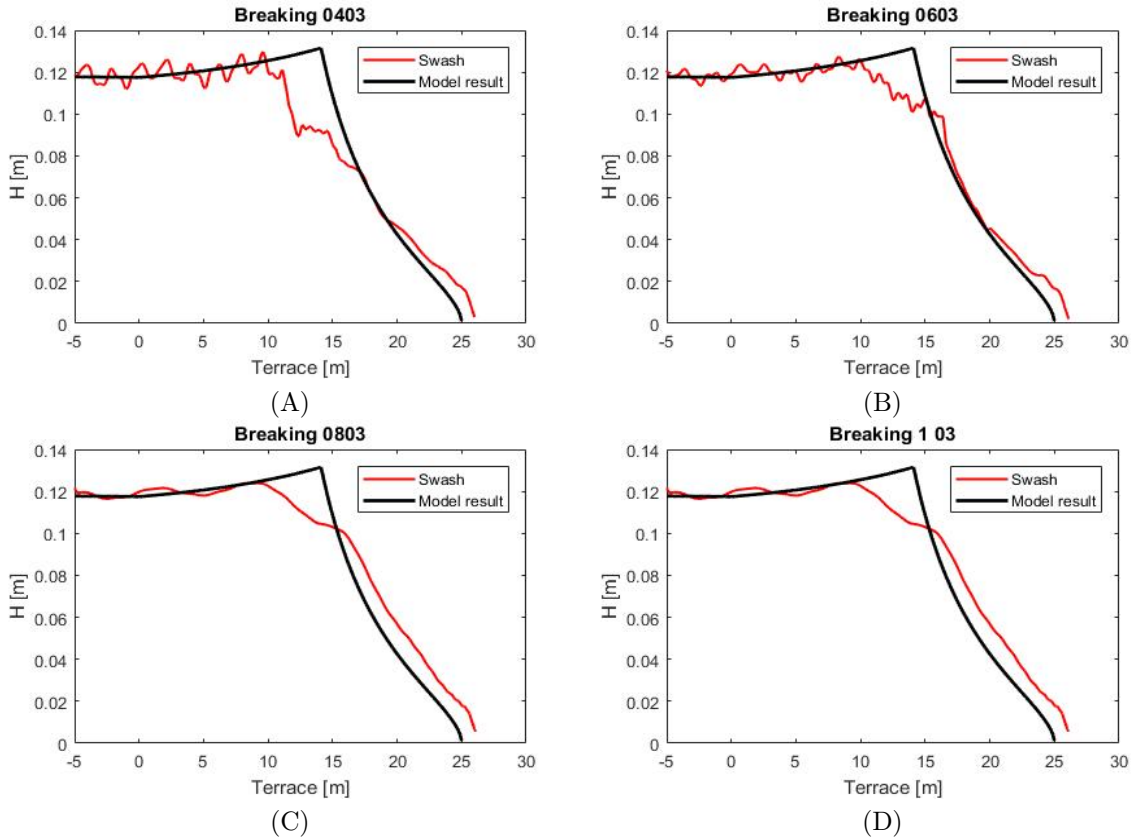
Figure C.7: Influence of a changing wave breaking parameter α in SWASH. $\beta = 0.3$, α: (A) $= 0.4$, (B) $= 0.6$, (C)$=0.8$ and (D) $=1$.

The part of wave equations that includes the conservation of mass and momentum of the nonlinear shallow water equation and the vertical acceleration can not be changed (Zijlema and Stelling, 2008), wave breaking is always accounted (SWASH team, 2011). In order to model the wave breaking correctly in swash the amount of vertical layers should be higher than 10, or else the horizontal velocities are underestimated near the wave crest, so the wave height will be underestimated (SWASH team, 2011). The factors of α and β can be used to compensate for the lack of vertical layers. For this comparison the amount of vertical layers equals 1 in order to show this influence.

X-Beach

X-Beach knows multiple formulations for wave breaking. For stationary waves the formulation of Baldock et al. (1998) and Janssen and Battjes (2007) can be used. As the overestimation only occurs before wave breaking, the point of wave breaking (Equation C.11) has been used in the script. This did not seem to change the overall results.

$$\overline{D_w} = \frac{1}{4}\alpha Q_b \rho_w g f_{rep}(H_B^2 + H_{rms}^2) \tag{C.9}$$

$$Q_b = exp\left[-\left(\frac{H_b^2}{H_{rms}^2}\right)\right] \tag{C.10}$$

$$H_b r = \frac{0.88}{k}tanh\left(\frac{\gamma_b kh}{0.88}\right) \tag{C.11}$$

where: D_w = Energy dissipation during wave propagation
α = Wave dissipation coefficient
ρ_w = Water density
g = Gravity constant
f_{rep} = Representative intrinsic frequency
$H_B r$ = Wave breaking height
H_{rms} = Root mean square wave height
k = Wave number
γ_b = Wave breaking index
h = Water depth

Even as formulation C.9 is formulated for stationary waves it still includes the parameters encountering for a distributed wave height. The parameters accounting for partially wave breaking, which is often related towards the use of a wave spectrum, are H_{rms} and the parameter Q_B.

C.2. Comparison of Shear stresses with SWASH results

Engelstad et al. (2019) has successfully applied SWASH to investigate the importance of different bed load transport processes. Liao (2015) showed that SWASH could reproduce the vertical flow structure correctly. For this reason it is expected that, if the magnitude of the induced shear stresses calculated in SWASH corresponds with the magnitude of the shear stresses in the presented model, the resulting morphology is correct.

C.2.1. Calculated bed shear stresses in SWASH

SWASH resolves the nonlinear shallow water equations with the conservation of mass and momentum. The formulations account also for the non-hydrostatic pressure (Zijlema et al., 2011) . In the cross shore mode the main equations are (Engelstad et al., 2019):

$$\frac{\partial u}{\partial t} + \frac{\partial u^2}{\partial x} + \frac{\partial wu}{\partial z} = -\frac{1}{\rho}\frac{\partial(p_h + p_{nh})}{\partial x} + \frac{\partial \tau_{xz}}{\partial z} + \frac{\partial \tau_{xx}}{\partial x} \tag{C.12}$$

$$\frac{\partial w}{\partial t} + \frac{\partial uw}{\partial x} + \frac{\partial w^2}{\partial z} = -\frac{1}{\rho}\frac{\partial(p_{nh})}{\partial z} + \frac{\partial \tau_{zz}}{\partial z} + \frac{\partial \tau_{zx}}{\partial x} \tag{C.13}$$

$$\frac{\partial u}{\partial x} + \frac{\partial w}{\partial z} = 0 \tag{C.14}$$

where: t = Time
x, y = Locations at still water level
z = Vertical location
ζ = Surface elevation
d = Still water depth
h = Water depth
u = Velocity
ρ_w = Water density
p_h, p_{nh} = Hydrostatic and non-hydrostatic pressure
τ = Turbulent stresses

The surface boundary has been described by (Engelstad et al., 2019):

$$\frac{\partial \zeta}{\partial t} + \frac{\partial}{\partial x} \int_{-h}^{\zeta} u\,dz = 0 \tag{C.15}$$

And the bottom boundary has been defined with the use of the bottom friction (Engelstad et al., 2019):

$$\tau_b = c_f \frac{U|U|}{h} \tag{C.16}$$

with

$$c_f = \frac{n^2 g}{h^{1/3}} \tag{C.17}$$

where: τ_b = Induced bed shear stress
         U = Depth averaged velocity
         h = Water depth
         n = Menning's roughness coefficient
         g = Gravity constant

The bed shear stresses calculated by SWASH can't be used directly (SWASH team, 2011), but the shear velocity u_* can be shown which can be used to calculate the bed shear stresses (Schiereck, 2001)(Equation C.18):

$$u_* = \sqrt{\tau_b / \rho_w} \tag{C.18}$$

C.2.2. Comparison model Duro et al. (2020) and SWASH

As u_* represents the shear stress, it is not a velocity which can be measured, even as it has the dimensions of velocity (m/s) (Schiereck, 2001). For this reason it cannot be compared directly with the orbital wave velocity near the bed that is calculated in the model with Equation B.29. The final calculated bed shear stresses through u_* show a different result as the bed shear stresses calculated with U_{orb} as well. Kabir and Torfs (1992) shows that the friction velocity u_* has a high sensitivity towards the used roughness height k and the height at which the bed velocity is taken. A change of 2mm can change the friction velocity obtained from a velocity profile with 25 up to 30 %. For this reason only the magnitude and not the absolute value is of interest. The dependency of the roughness height of the bed can be illustrated with the following formula (Schiereck, 2001):

$$u_* = \bar{\bar{u}}\sqrt{g}/C \tag{C.19}$$

$$C \approx 18 log \frac{12R}{k_r} \tag{C.20}$$

where: τ_b = Induced bed shear stress
         u_* = Shear velocity
         $\bar{\bar{u}}$ = Time and depth average velocity
         g = Gravity constant
         R = Hydraulic Radius
         k_r = Roughness equivalent of the bottom

As the calculation of the bed shear stresses in a situation without vegetation has already been calibrated and validated in the original model by Duró et al. (2020), we are mainly interested in the changes of magnitude between bed shear stresses over the terrace length. For that reason the magnitude of the calculated bed shear stresses at the start of the terrace have been matched with the bed shear stresses calculated by SWASH, by multiplying the SWASH results with 5/2. If the value of u_* would be used to calculate the bed shear stresses in the model of Duró et al. (2020) a new calibration must be done concerning the sensitivity of the system through erosion (ϵ) in Equation B.43 (Section B.3).

C.3. Run-up velocity

In the run-up formulation used by Duró et al. (2020) the dissipated wave energy has not been included in the final run-up formulation, what results in a continuous run-up height and run-up shear stresses, independent of the terrace slope and length after wave breaking (Subsection 3.2.3). For this reason, a look has been taken towards the calculations of an over topping discharge from sea dikes with a very shallow foreshore (Altomare et al., 2016). The over topping discharge can be calculated for an imaginary very shallow dike. This way, a run-up velocity can be derived by dividing the discharge at the start of the run-up by the the water depth at this point. This has been schematized in Figure C.8.
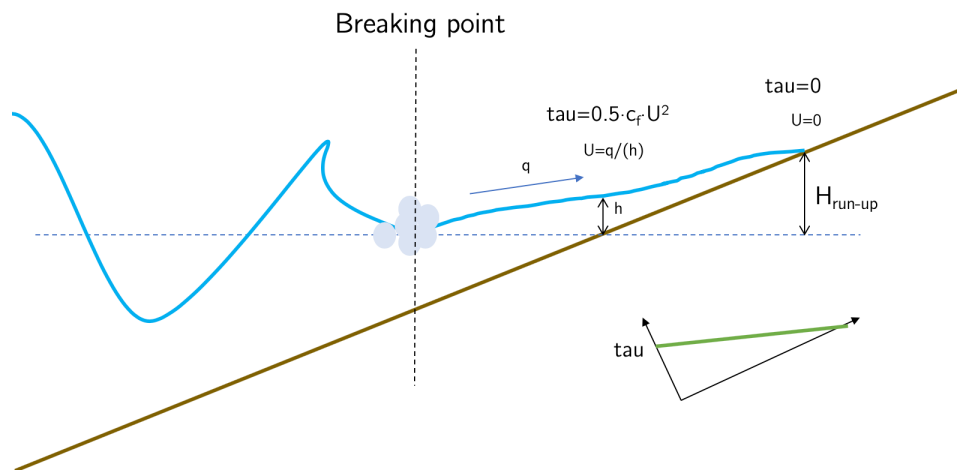
Figure C.8: Schematization of the run-up induced by wave breaking based on the over topping discharge q.

In order to calculate the over-toppings discharge the following formula of Schiereck(2001) is used:

$$Q = \frac{q}{\sqrt{gH^3}} * \sqrt{\frac{Hs/L_o}{tan(\alpha)}} \tag{C.21}$$

$$Q = a * exp(-b\frac{R}{\gamma}) \tag{C.22}$$

$$R = \frac{h_c}{H_s \xi} \tag{C.23}$$

where: q = Over topping discharge

g = Gravity constant

H_s = Significant wave height

a, b = Constants for plunging or surging waves

R = Dimensionless free board

Q = Dimensionless over topping

h_c = Free board

ξ = Iribarren number

α = Slope

Average slope calculation:

$$\alpha = \frac{(1.5H_{m0} + Ru_{2\%})}{L_{slope}} \tag{C.24}$$

α = Average slope

H_{m0} = Spectral significant wave height

$Ru_{2\%}$ = Minimum run-up height highest 2% of the waves

L_{slope} = Horizontal length of the slope

with L_{slope} from the water depth $1.5H_{m0}$ until the run-up height of $Ru_{2\%}$ which can be calculated as followed:

$$Ru_{2\%} = \left(4.0 - \frac{1.5}{\sqrt{\xi_{m-1.0}}}\right)\gamma_b H_{m0} \tag{C.25}$$

where: $\xi_{m-1.0}$ = Iribarren number based on $T_{m-1.0} and \alpha_{average}$

γ_b = Wave breaking index

By testing the influence of this formula, it was found that there was a height dependency for the height of the "very shallow dike". A height difference of 1mm leads to a difference in over topping discharge of 50%. Since this is unrealistic it has been assumed that the formula for the over topping discharge has a minimum value for the dike height. Further investigation is not done.

Random error

Some of the plots show an almost random increase in wave velocity and wave height at a single point. Connecting the correct points and the overestimated values in a normalized H h graph gives a straight line, indicating a kind of a trend (Figure C.10). Since it only occurs for some of the initial wave heights a direct connection was not expected.

By generating fast multiple plots at the same time the conditions resulting in an error could be found (Figure C.10). After the conditions and the location was known the origin of the error could be found with Matlabs breakpoint option.

In order to solve equations needing an input value of the result a loop is written which continues until the difference between the initial and the guest value are negligible (Figure C.9 upper plot). By the definition of the error the difference has been used, while the absolute difference should be used. This resulted in an error for the calculation of the wave period (T), as the first guess was to height, the second to low and so on. It can be expected that only once in the 10000 situations the wave height did not need a second iteration, so only in that situation it would result in an error. Else the loop would continue for a variation in H value, which update the T value as well. This has been changed in the model for the final results.

```matlab
%Calculation of parameters
    err2     = 1; count2 = 0;
    while err2 > 0.00001
% Dispersion relation to obtain wave length
        count2 = count2 + 1;
        L_temp = g.*Tsec1.^2 ./(2*pi) .*tanh(2*pi*(hsec(i))./Lsec(i));
        err2     = Lsec(i) - L_temp;
        Lsec(i)= L_temp;
        if count2 > 10000;   fprintf('Lsec not converging');   break;    end

    end
%----------------------------------------------------------------------------------------------------------------------------------

%Calculation of parameters
    err2     = 1; count2 = 0;
    while err2 > 0.00001
% Dispersion relation to obtain wave length
        count2 = count2 + 1;
        L_temp = g.*Tsec1.^2 ./(2*pi) .*tanh(2*pi*(hsec(i))./Lsec(i));
        err2     = abs(Lsec(i) - L_temp);
        Lsec(i)= L_temp;
        if count2 > 10000;   fprintf('Lsec not converging');   break;    end

    end
```

Figure C.9: Error origin with in the top plot the original formulation and in the lower plot the changed formulation
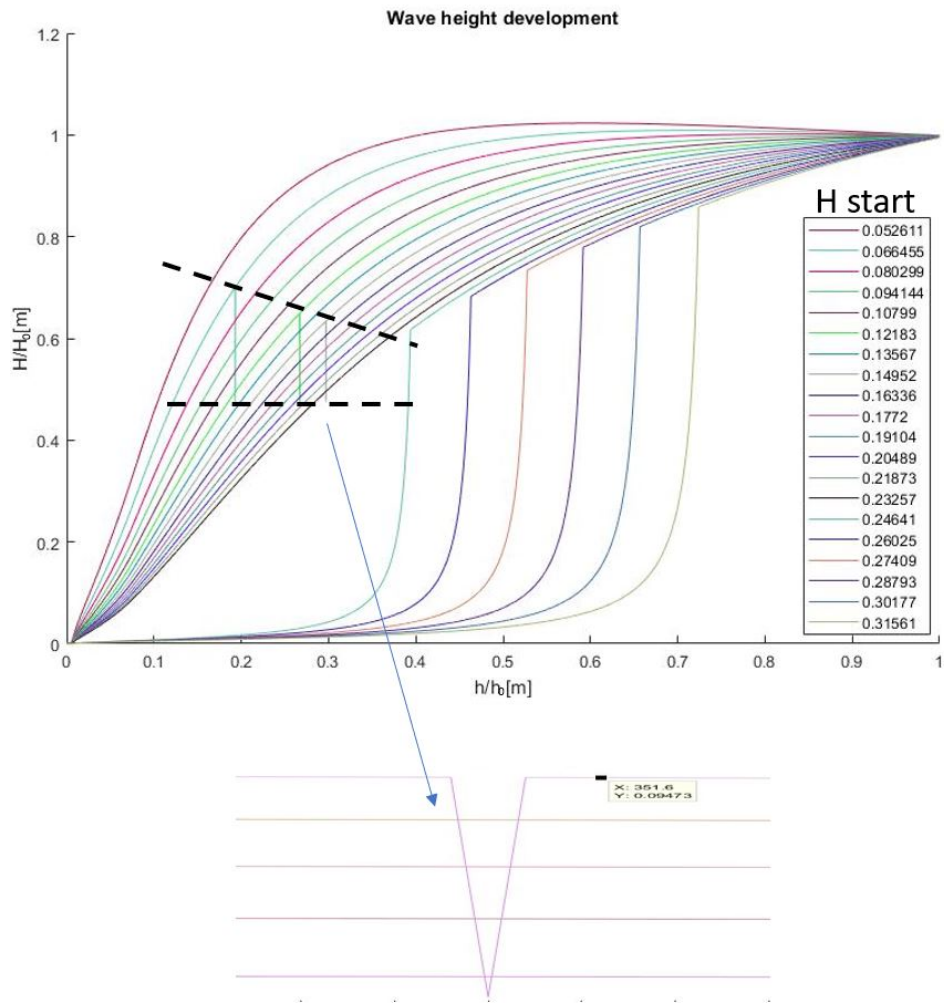
Figure C.10: Trent and result of the model error

C.4. graphs, examples and tables

Figure C.11: Used parameters for Figure 3.3

plot	A1	A2	H(2)	T(2)	m
MODA2_3_H027_T0_5	0,3419	3,0798	0,3	0,5	0,0333
MODA2_3_H027_T1	0,3419	3,0887	0,30087	1	0,0333
MODA2_3_H027_T1_5	0,3419	3,0874	0,30074	1,5	0,0333
MODA2_3_H027_T2	0,3419	3,0882	0,30082	2	0,0333
MODA2_3_H027_T3	0,3419	3,0801	0,30003	3	0,0333
MODA2_3_H027_T4	0,3419	2,9893	0,29893	4	0,0333
MODA2_3_H027_T6	0,3419	3,0891	0,30091	6	0,0333
MODA2_3_H027_T8	0,3419	3,0564	0,29772	8	0,0333
MODA2_3_H027_T10	0,3419	3,0844	0,30045	10	0,0333
MODA2_3_H027_T30	0,3419	3,1012	0,30209	30	0,0333
MODA2_3_H007_T10	1,3681	3,0021	0,073143	10,0984	0,0333
MODA2_3_H01_T10	0,9273	3,0118	0,10826	10,0984	0,0333
MODA2_3_H04_T10	0,2512	3,0136	0,39996	10,0985	0,0333
MODA2_3_m01	0,0942	2,9691	0,31525	8,1236	0,01
MODA2_3_m05	0,189	3,012	0,78109	8,1235	0,049
MODA2_3_m001	0,0212	2,9763	0,1401	8,1236	0,001

With A1 a summarised vegetation parameter, A2 a summarised parameter and hydraulic condition parameter, H the wave height in m after spin-up time , T the wave period in s after spin-up time and m the slope.

Figure C.12: Used parameters for Figure 3.6.

plot	CD	H0(2)	Tp(2)	h
CD21	0,21	0,096463	3,8004	0,4
CD21C	0,21	0,096463	3,8004	0,4
CD08	0,08	0,17553	2,5294	0,5
CD08C	0,08	0,16458	2,5294	0,5
CD28	0,28	0,11405	1,5803	0,6
CD28C	0,28	0,11405	1,5803	0,6
CD18	0,18	0,13742	2,2138	0,6
CD18C	0,18	0,13742	2,2138	0,6
CD18B	0,18	0,16743	1,8889	0,7
CD18BC	0,18	0,16644	1,8889	0,7
CD09	0,09	0,19004	2,529	1
CD09C	0,09	0,19005	2,529	1
CD21M	0,21	0,084	3,79	0,4
CD08M	0,08	0,15	2,53	0,5
CD028M	0,28	0,114	1,58	0,6
CD18M	0,18	0,131	2,21	0,6
CD18BM	0,18	0,161	1,89	0,7
CD09M	0,09	0,187	2,53	1

C= Constant Alpha, M = Mendez and Losada(2004), non = Variable alpha
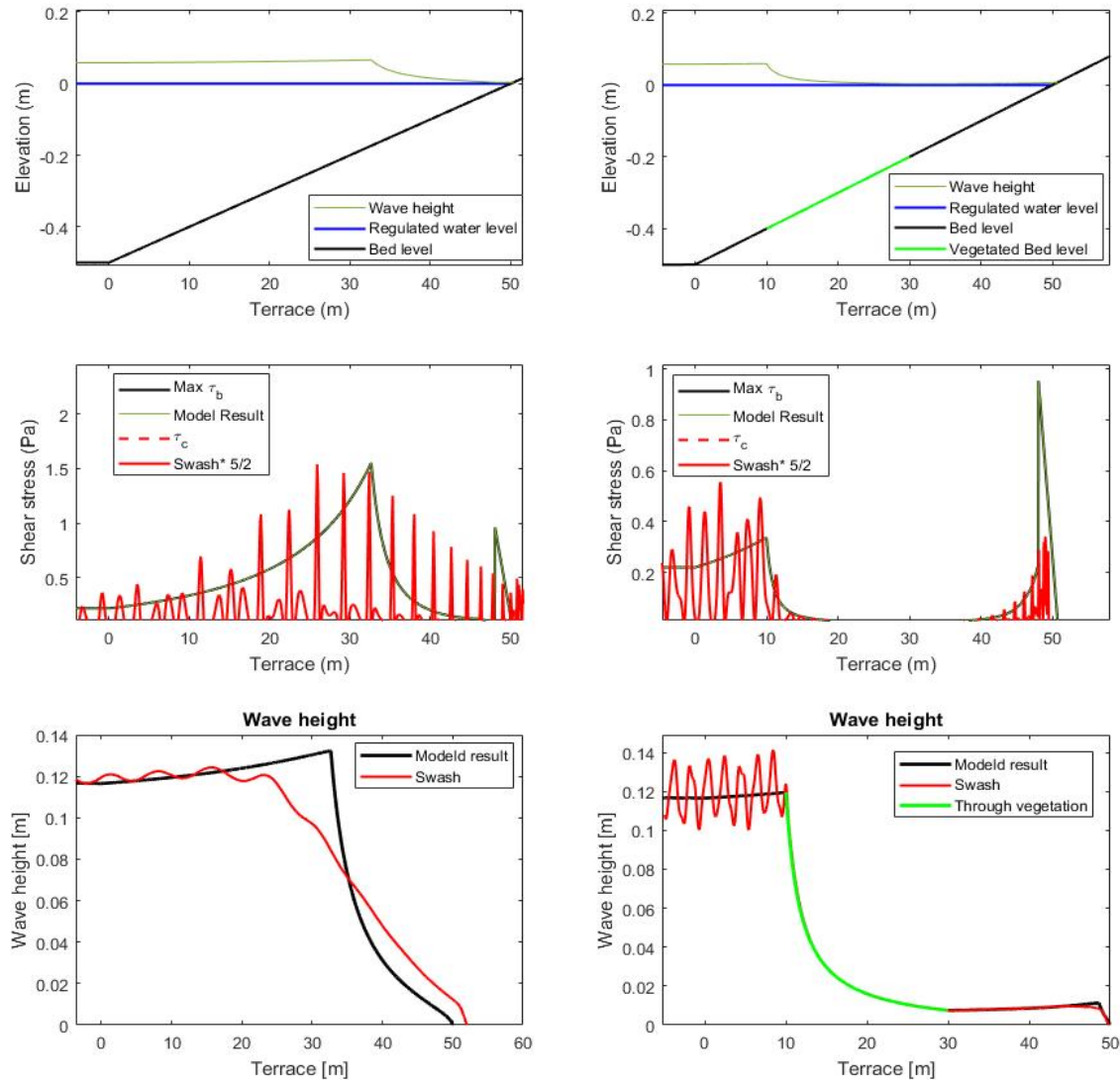
Figure C.13: Induced bed shear stresses for H=0.1m, T = 2s and m= 0.01
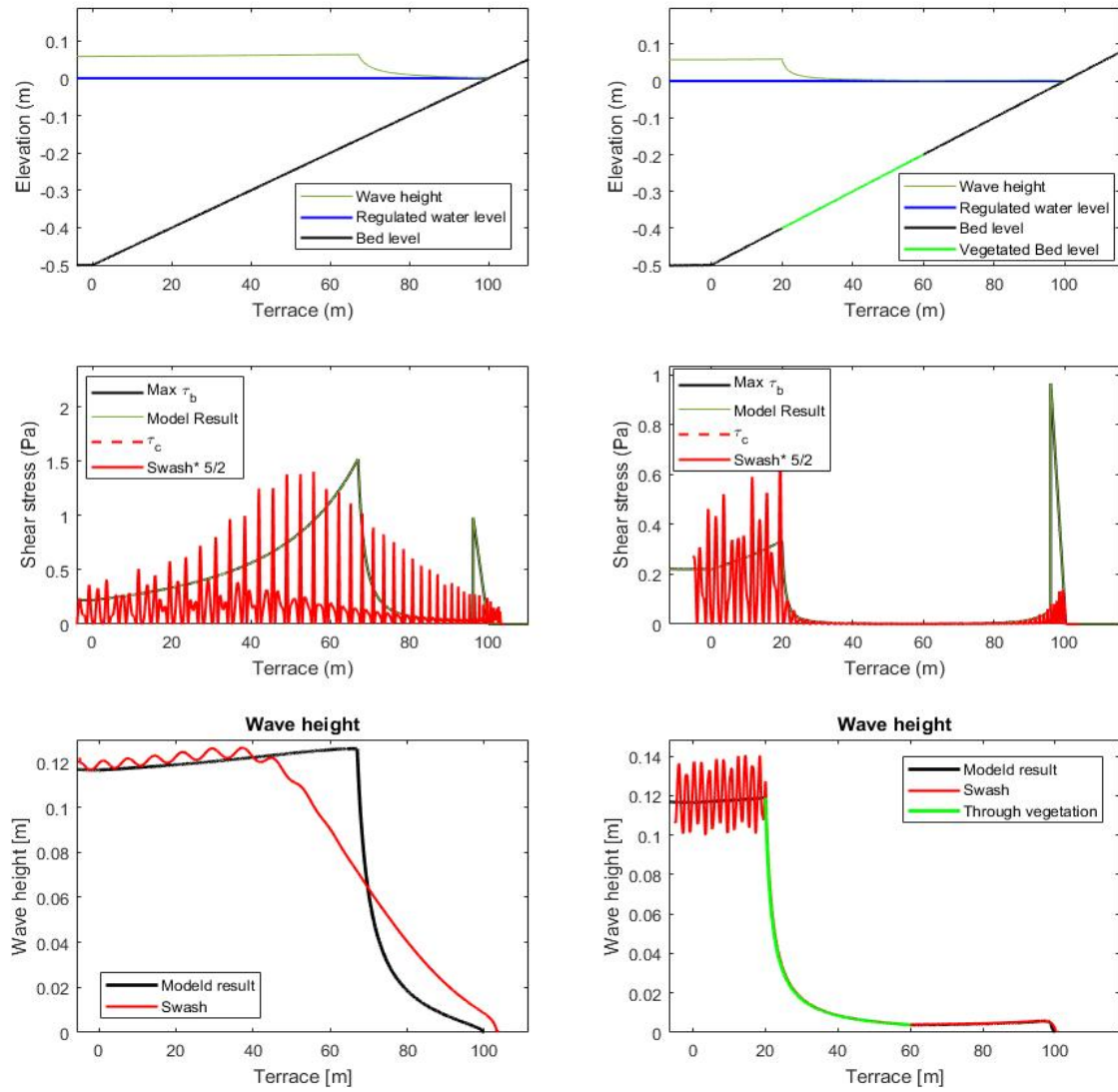
Figure C.14: Induced bed shear stresses with H = 0.1m, T = 2s and m=0.005

C.4.1. Sensitivity analyses

(A)

(B)

(C)

(D)
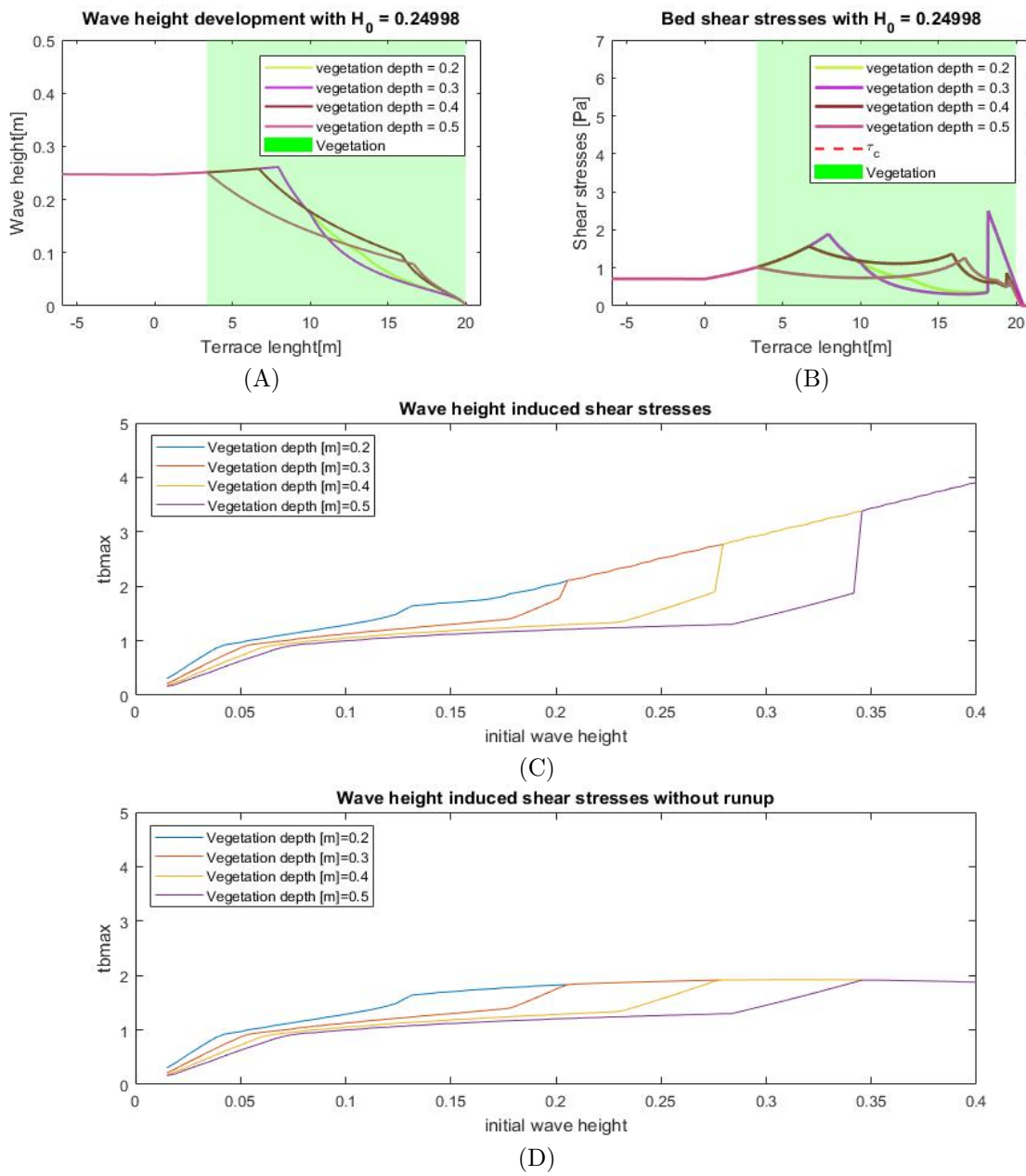
Figure C.15: Influences of different maximum growing depths for P. australis, $m = 0.03$ and $T = 2$s. In this figure four different maximum growing depths are tested. The influences of the different maximum growing depths is illustrated by the wave height development over the terrace length (A) with the corresponding induced bed shear stresses (B). In the final two plots (C and D) only the maximum induced bed shear stresses for the different maximum growing depth is shown based on different incoming wave heights. This is done for the bed shear stresses including wave run-up (C) and excluding wave run-up (D), in order to get more insight on the dominating processes.

(A)

(B)

(C)

(D)

Figure C.16: Influences of different vegetation densities for P. australis, $m = 0.03$ and $T = 2$s. In this figure four different vegetation densities are tested. The influences of the different vegetation densities is illustrated by the wave height development over the terrace length (A) with the corresponding induced bed shear stresses (B). In the final two plots (C and D) only the maximum induced bed shear stresses for the different maximum growing depth is shown based on different incoming wave heights. This is done for the bed shear stresses including wave run-up (C) and excluding wave run-up (D), in order to get more insight on the dominating processes.

(A)

(B)

(C)

(D)

Figure C.17: Influences of different mean stem diameters for P. australis, $m = 0.03$ and $T = 2$s. In this figure four different stem diameters are tested. The influences of the different stem diameters is illustrated by the wave height development over the terrace length (A) with the corresponding induced bed shear stresses (B). In the final two plots (C and D) only the maximum induced bed shear stresses for the different maximum growing depth is shown based on different incoming wave heights. This is done for the bed shear stresses including wave run-up (C) and excluding wave run-up (D), in order to get more insight on the dominating processes.

(A)

(B)

(C)

(D)
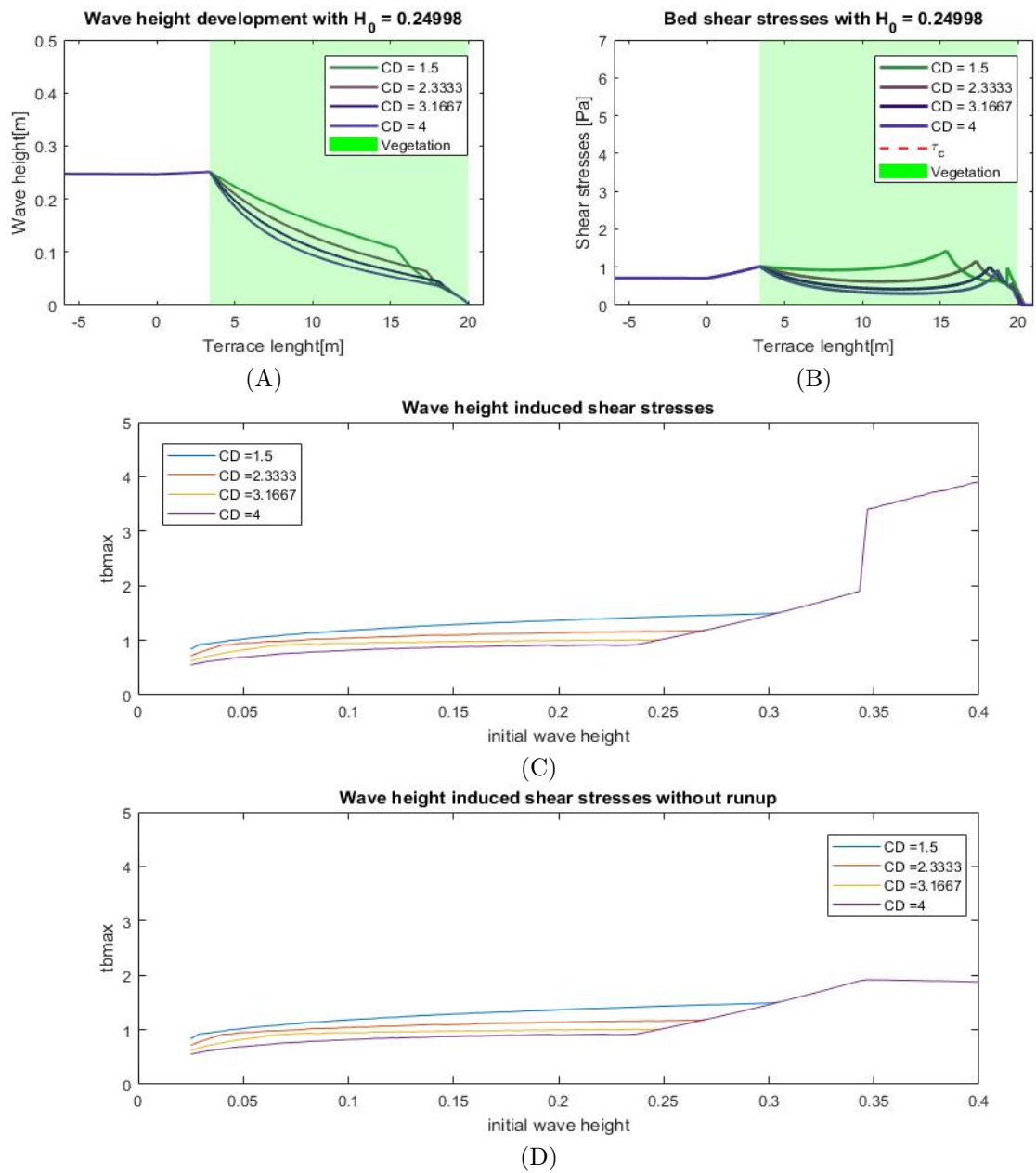
Figure C.18: Influences of different drag factors for P. australis, $m = 0.03$ and $T = 2$s. In this figure four different drag factors are tested. The influences of the different drag factors is illustrated by the wave height development over the terrace length (A) with the corresponding induced bed shear stresses (B). In the final two plots (C and D) only the maximum induced bed shear stresses for the different drag factors are shown based on different incoming wave heights. This is done for the bed shear stresses including wave run-up (C) and excluding wave run-up (D), in order to get more insight on the dominating processes.
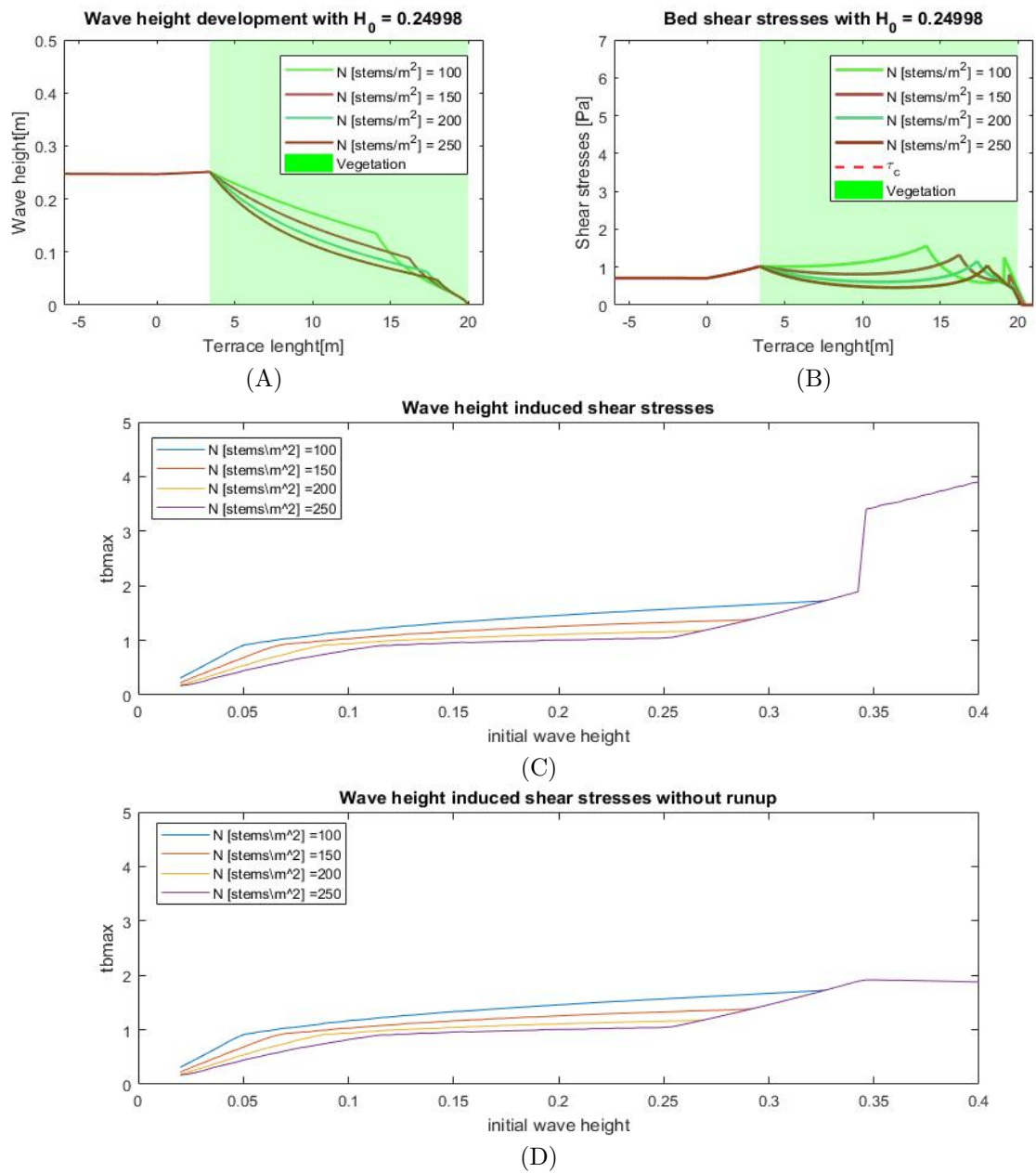
(A)

(B)

(C)

(D)
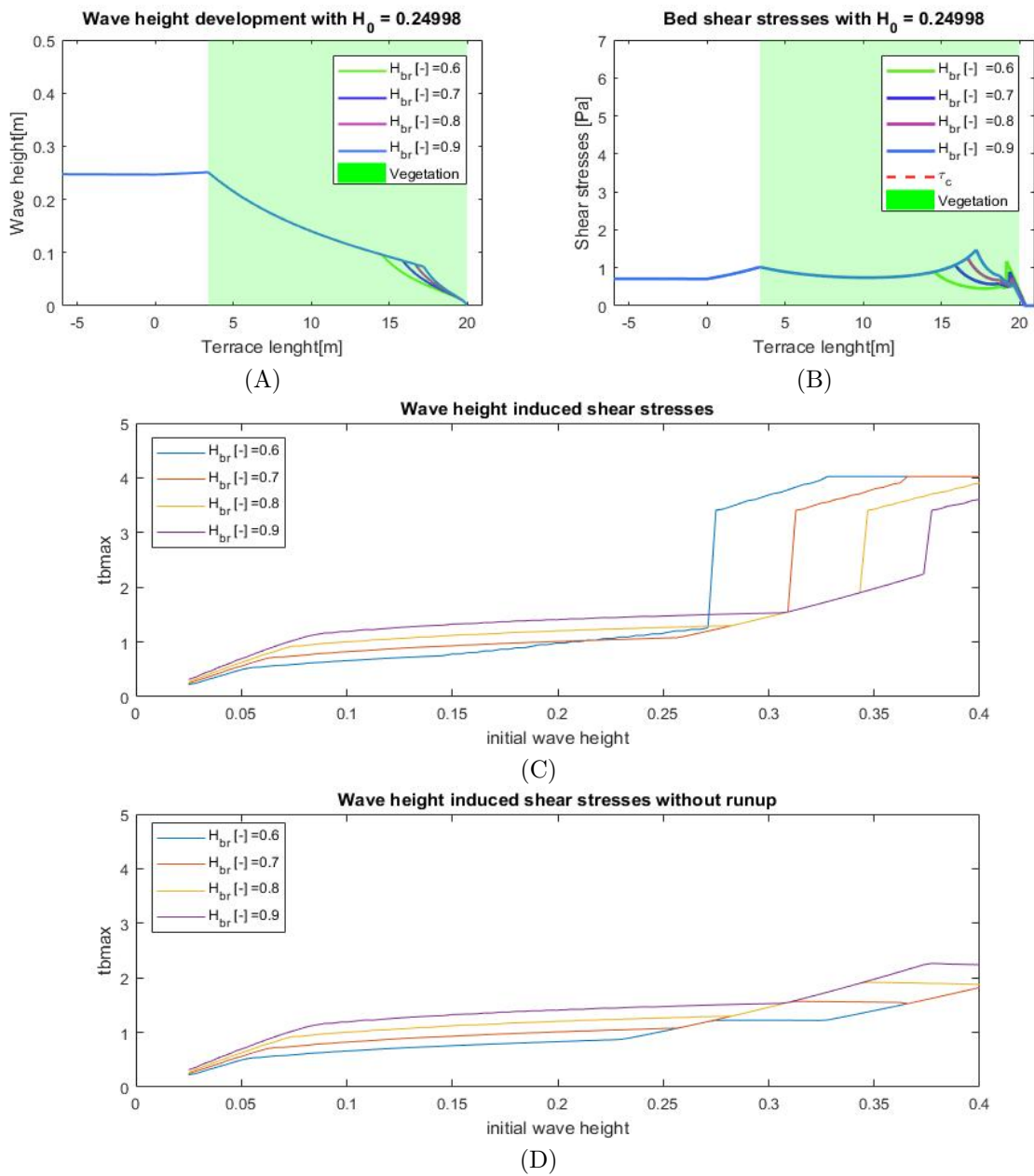
Figure C.19: Influences of different breaking parameters for P. australis, $m = 0.03$ and $T = 2$s. In this figure four different breaking parameters are tested. The influences of the different drag factors is illustrated by the wave height development over the terrace length (A) with the corresponding induced bed shear stresses (B). In the final two plots (C and D) only the maximum induced bed shear stresses for the different breaking parameters are shown based on different incoming wave heights. This is done for the bed shear stresses including wave run-up (C) and excluding wave run-up (D), in order to get more insight on the dominating processes.
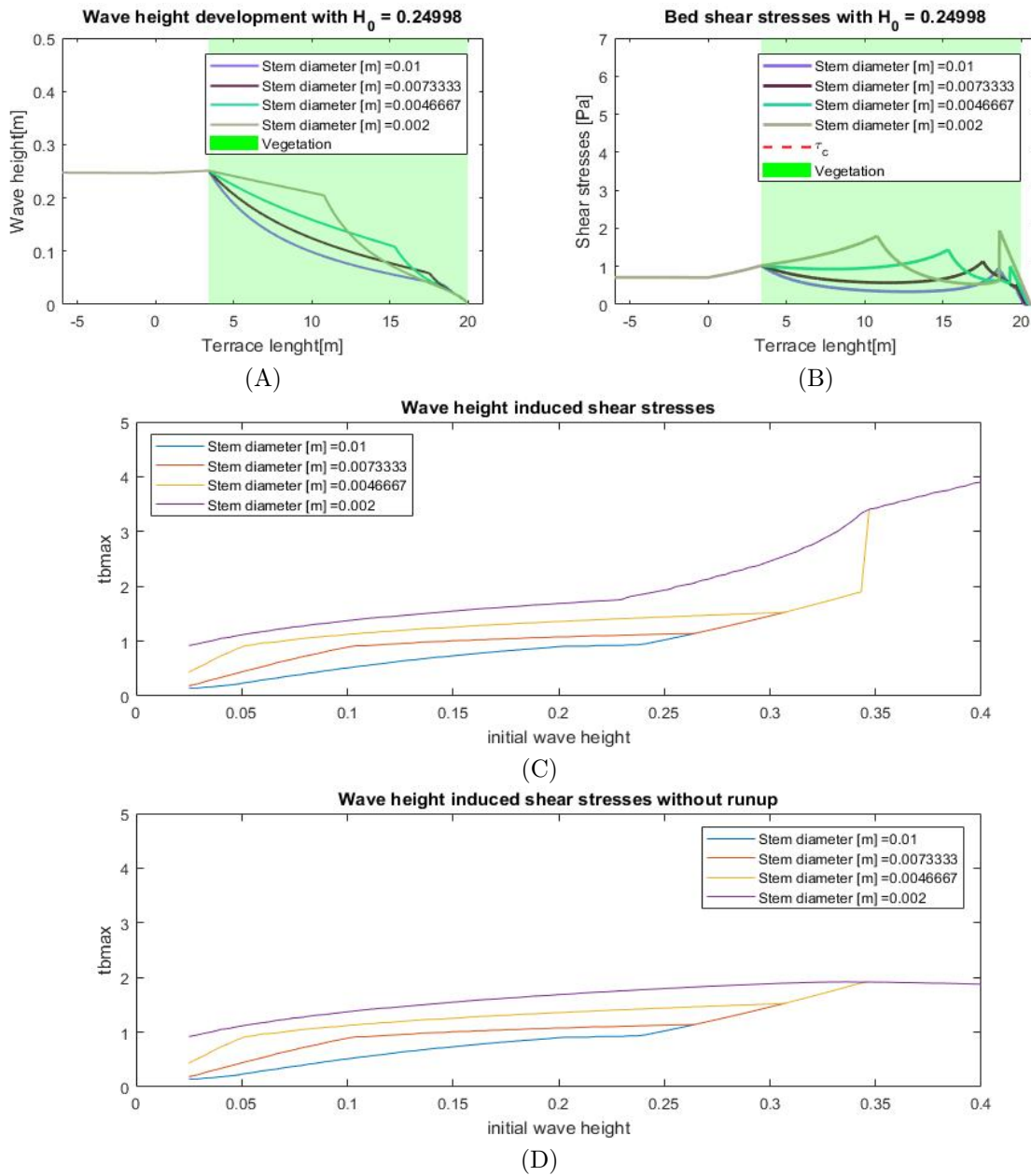
(A)

(B)

(C)

(D)
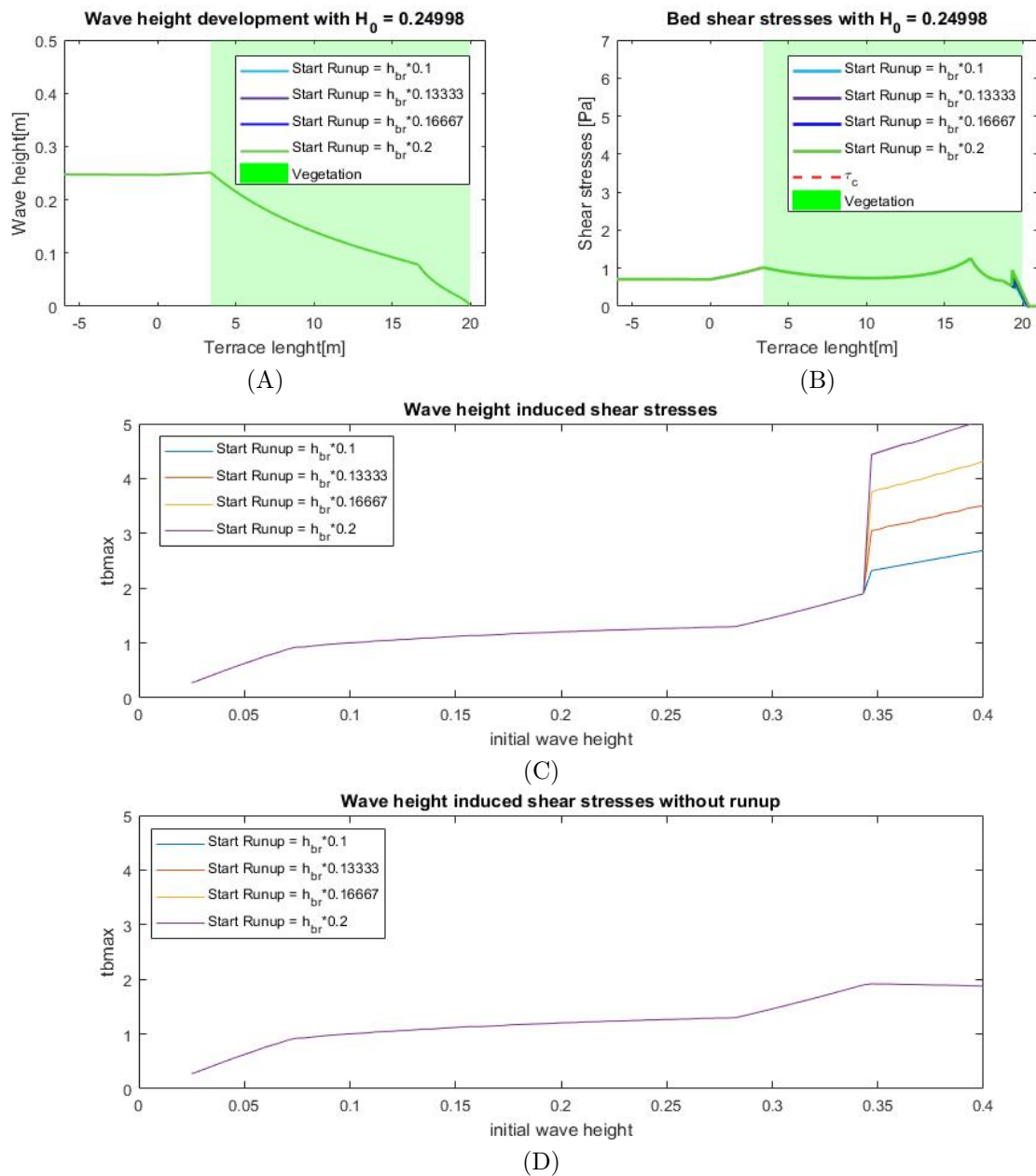
Figure C.20: Influences of different run-up start locations for P. australis, $m = 0.03$ and $T = 2$s. In this figure four different breaking parameters are tested. The influences of the different run-up start locations is illustrated by the wave height development over the terrace length (A) with the corresponding induced bed shear stresses (B). In the final two plots (C and D) only the maximum induced bed shear stresses for the different run-up start locations are shown based on different incoming wave heights. This is done for the bed shear stresses including wave run-up (C) and excluding wave run-up (D), in order to get more insight on the dominating processes.

```
$*************HEADING*****************************************
$
PROJ 'H01m002'
$
$*************MODEL INPUT*************************************
$
MODE NONST ONED
SET LEVEL   0.000
$
CGRID   0.0   0.0   0.0  31.1   0.0   311     0
$
INPGRID BOTTOM   0.0   0.0   0.0   311     0  0.10  0.00
READINP BOTTOM -1. 'l49veget002.bot' 1 0 FREE
$
INPGRID NPLANT   0.0   0.0   0.0   311     0  0.10  0.00
READINP NPLANT   1. 'l49veget002.den' 1 0 FREE
$
INIT zero
$
BOU SIDE W CCW BTYPE WEAK CON REG 0.12 2.
$
FRIC MANN 0.012
BREAK                           $alpha = 0.6, beta = 0.3
VEGEtation 1. 0.012 1521 1.          $height, diam, N, drag
$
NONHYDROSTATIC
DISCRET UPW MOM Vertical SMArts
TIMEI 0.1 0.5
$
$************* OUTPUT ****************************************
$
QUANT HSIG   dur 15 min
QUANT SETUP dur 15 min
$
BLOCK 'COMPGRID' NOHEAD 'H01m002' HSIG SETUP UFRIC
$
TEST 1 0
COMPUTE 000000.000  0.01 SEC 002000.000
STOP
```

Figure C.21: Example of the used SWASH input files for a wave height of 0.12m, wave period of 2s.

Nomenclature

α	Factor accounting for imperfect energy conversion	-
α	Relative vegetation height	-
$\bar{\bar{u}}$	Velocity, average over time and depth	m/s
β	Angle of attack	rad
Δ	Erosion sensitivity parameter	m/s
δ	Boundary layer	m
δ	Surface elevation	m
ϵ	Erodibility coefficient	-
η	Set-up	m
γ_b	Wave breaking index	m
γ_b	parameter of the Thornton and Guza (1983) model	-
λ	canopy density or solid fraction (= $\pi/2s^2$ for a cylinder array)	-
ν	viscosity	m^2/s
ϕ	Solid volume Fraction of canopy	-
ϕ_0	Internal friction angle of the soil	degree
ρ_w	Water density	kg/m^3
σ	Soil strength	N/m^2
σ	Wave angular frequency	rad/s
τ_0	Wall shear stress	m
τ_b	Induced bed shear stress	N/m^2
τ_c	Critical bed shear stress	N/m^2
τ_w	Shear stress induced by waves	N/m^2
θ	Place along circular surface measured from the stagnation point	rad
ξ	Irebarren number	-
ζ	Blockage factor based on a ships geometry	-
ζ	Ship blocking factor	-
A	Specimen area	m^2
a	Wave amplitude	m
$A1$	Value representing the vegetation characteristics	-
$A2$	Value representing the vegetation and hydraulic characteristics	-

a_b	Horizontal amplitude of the wave on the bed surface	m
A_m	Velocity amplification ratio	-
A_R	Cross sectional area of the root	m^2)
B	Width of vegetation	m
b_v	Plant area per unit height of each vegetation stand normal to u	m
C	White-Colebrook parameter	-
C_0	Soil cohesion	kPa
c_b	Bore celerity at run-up start	m/s
c_b	Wave celerity at start run-up	m/s
C_D	Drag coefficient	-
c_f	Bottom roughness	-
c_g	Wave group celerity	m/s
C_L	Lift coefficient	-
C_r	Cohesion added by the roots	kPa
c_w	Wave celerity	m/s
D	Stem diameter	m
d	Still water depth	m
D_b	Energy dissipation by bore propagation	J
D_f	Energy dissipation through bottom friction	J
d_v	Plant height	m
E	Amount of erosion	-
E	Energy	J
E_i	Incoming energy	J
E_r	Reflected energy	J
E_t	Transmitted energy	J
E_{diss}	Dissipated energy	J
F	Fetch length	m
f_b	Bed friction coefficient	—
F_D	Induced drag force	N/m^2
F_D	Induced drag force	N/m^2
F_f	Friction drag	M/m^2
F_L	Induced lift force	N/m^2
F_p	Form drag	N/m^2
F_x	Force in x direction	N/m^2

F_x	Force in x direction	N/m^3
Fr	Froude number	-
Fr_b	Froude number at start run-up	-
g	Gravitational constant	m/s
H	Wave height	m
h	Water depth	m
H_0	Original wave height	m
H_b	Wave height begin run-up	m
h_b	Water depth begin run-up	m
H_diss	Dissipated wave height	m
H_i	Incoming wave height	m
H_p	Wave height primary wave	m
H_r	Reflected wave height	m
H_s	Significant wave height	m
H_t	Transmitted wave height	m
H_{br}	Wave breaking height	m
h_{br}	Water depth at wave breaking point	m
H_{max}	Maximum wave height	m
k	Turbulent kinetic energy	m^2/s^2
k	wave number	m^{-1}
k_r	roughness equivalent of the bottom	-
k_s	Nikuradse equivalent sand roughness	-
K_t	Transmitted coefficient	-
KC	Keulegan Carpente	-
L	Wave length	m
l	Integral length turbulence, l = D for D<S, l = ΔS for D > S	m
L_0	Offshore wave length	m
m	Slope	m/m (vertical/horizontal)
N	Number of stems per square meter	m^{-1}
n	Frequency of shedding of vortexes	Hz
n	Manning's roughness coefficient	-
n	frequency of vortex shedding	Hz
p	Pressure	N/m^2
p	structure porosity	-

p_{wave}	Pressure induced by waves	N/m^2
r_0	radius of a stem	m
R_c	Structure free board	m
R_h	Horizontal run-up	m
R_u	Vertical wave run-up	m
Re	Reynolds number	-
S	Hart to hart distance between stems	m
s	Dimensionless cylinder spacing (=S/d)	-
s	Ship to shore distance	m
S_{xx}	Radiation stress of the z momentum in the x direction	N/m)
S_{xx}	Radiation stresses	N/m
St	Strouhal number	-
T	Wave period	s
t	Time	s
T_p	Peak wave period	s
T_p	Primary wave period	s
T_s	Significant wave period	s
T_{m01}	Mean absolute wave period	s
T_R	Root tensile strength	N/m^2
U	Depth average velocity	m/s
u	Cross shore velocity	m/s
u_*	Bed shear velocity	m/s
u_0	Free stream velocity	m/s
u_b	Bulk velocity (= Q/Wh)	m/s
u_b	Velocity near the bed	m/s
u_c	Constricted cross-section velocity	m/s
u_m	Mean velocity	m/s
u_p	Pore velocity (= $U_b/(1-\lambda)$)	m/s
u_s	Separation velocity kU_p	m/s
u_w	Wind velocity	m/s
u_x	Velocity in x direction	m/s
u_{c1}	characteristic velocity acting on the plant	m/s
u_{orb}	Velocity through the orbital wave motion	m/s
W	Channel width	m
w	Velocity along the shore	m/s
x_h	Horizontal distance	m
Z_b	Bed level	m

Bibliography

Altomare, C., Suzuki, T., Chen, X., Verwaest, T., and Kortenhaus, A. (2016). Wave overtopping of sea dikes with very shallow foreshores. *Coastal Engineering*, 116:236 – 257.

Anderson, M. E., Smith, J. M., and McKay, S. K. (2011). Wave dissipation by vegetation. *Vicksburg, MS: US Army Corps of Engineers Engineer Research and Development Center.*

Baldock, T., Holmes, P., Bunker, S., and Weert], P. V. (1998). Cross-shore hydrodynamics within an unsaturated surf zone. *Coastal Engineering*, 34(3):173 – 196.

Battjes, J. A. (1974). *Computation of set-up, longshore currents, run-up and overtopping due to wind-generated waves.* Delft university of technology.

Bergsma, E. W., Blenkinsopp, C. E., Martins, K., Almar, R., and de Almeida, L. P. M. (2019). Bore collapse and wave run-up on a sandy beach. *Continental Shelf Research*, 174(Water 364 6 2017):132–139.

Boersma, B.-J. (2005). A staggered compact finite difference formulation for the compressible navier–stokes equations. *Journal of Computational Physics*, 208:675–690.

Borsje, B., Van Wesenbeeck, B., Dekker, F., Paalvast, P., Bouma, T., Katwijk, M., and de Vries, M. (2011). How ecological engineering can serve in coastal protection. *Ecological Engineering*, 37:113–122.

Bosboom, J. and Stive, M. J. (2012). *Coastal dynamics I: lectures notes CIE4305.* VSSD.

Boukhemacha, M. A., Bica, I., and Khoudir, M. (2013). New procedures to estimate soil erodibility properties from a hole erosion test record. *Periodica Polytechnica Civil Engineering*, 57:77–82.

Bouma, T., de Vries, M., Low, E., Peralta, G., Tánczos, I., van Koppel, L., and Herman, P. (2005). Trade-offs related to ecosystem engineering: a case study on stiffness of emerging macrophytes. *Ecology*, 86(8):2187–2199.

Bradley, K. and Houser, C. (2009). Relative velocity of seagrass blades: Implications for wave attenuation in low-energy environments. *Journal of Geophysical Research: Earth Surface*, 114(1):1–13.

Cacabelos, E., Martins, G. M., Thompson, R., Prestes, A. C., Azevedo, J. M. N., and Neto, A. I. (2016). Material type and roughness influence structure of inter-tidal communities on coastal defenses. *Marine Ecology*, 37(4):801–812.

Cazzuffi, D., Cardile, G., and Gioffrè, D. (2014). Geosynthetic engineering and vegetation growth in soil reinforcement applications. *Transportation Infrastructure Geotechnology*.

Chen, H., Ni, Y., Li, Y., Liu, F., Ou, S., Su, M., Peng, Y., Hu, Z., Uijttewaal, W., and Suzuki, T. (2018). Deriving vegetation drag coefficients in combined wave-current flows by calibration and direct measurement methods. *Advances in Water Resources*, 122:217–227.

Clevering, O. (1999). Vitaliteit van rietbegroei. *De Levende Natuur*, 100:42 – 45.

Comoss, E. J., Kelly, D. A., and Leslie, H. Z. (2002). Innovative erosion control involving the beneficial use of dredge material, indigenous vegetation and landscaping along the Lake Erie Shoreline. *Ecological Engineering*, 19:203–210.

Coops, H., Geilen, N., Verheij, H. J., Boeters, R., and vand er Velde, G. (1996). Interactions between waves, bank erosion and emergent vegetation: an experimental study in a wave tank. *Aquatic Botany*, 53(3-4):187–198.

Coops, H. and Velde, G. V. D. (1996). Effects of waves on helophyte stands : mechanical characteristics of stems of Phragmites australis and Scirpus lacustris. *Aquatic Botany*, 53:175–185.

Cushman-Roisin, B. (2012). Lake dynamics.

Dalrymple, R., Kirby, J., and Hwang, P. (1984). Wave diffraction due to areas of energy dissipation. *Journal of Waterway Port Coastal and Ocean Engineering-asce - J WATERW PORT COAST OC-ASCE*, 110.

de Baets, S., Poesen, J., Reubens, B., Wemans, K., De Baerdemaeker, J., and Muys, B. (2008). Root tensile strength and root distribution of typical Mediterranean plant species and their contribution to soil shear strength. *Plant and Soil*, 305(1-2):207–226.

de Vree, J. (2020). afkalven.

Dean, R. G. and Bender, C. J. (2005). Static wave setup with emphasis on damping effects by vegetation and bottom friction. *Coastal E*, 53:149–156.

Didier, D., Bernatchez, P., and Marie, G. (2016). Wave runup estimations on platform-beaches for coastal flood hazard assessment. *Nat Hazards*, 83:1443–1467.

Dubi, A. and Torum, A. (1994). Wave damping by kelp vegetation. *Coastal Engineering Proceedings*, 1(24).

Dubi, A. M. (1995). Damping of water waves by submerged vegetation: A case study on laminaria hyperborea. *University of Trondheim, Norway*.

Duró, G., Crosato, A., Kleinhans, M. G., Roelvink, J. A., and Uijttewaal, W. S. J. (2020). Bank erosion processes in regulated navigable rivers. *JGR – Earth Surface*.

Elger, D. F. and Lebret, B. A. (2015). *Coastal dynamics I: lectures notes CIE4305*. Wiley.

Engelstad, A., Ruessink, G., Hoekstra, P., and van der Vegt, M. (2019). Sediment transport processes during barrier island inundation under variations in cross-shore geometry and hydrodynamic forcing. *Journal of Marine Science and Engineering*, 7:210.

Etminan, V., Lowe, R. J., and Ghisalberti, M. (2017). A new model for predicting the drag exerted by vegetation canopies. *Water Resources Research*, 53:3179–3196.

Etminan, V., Lowe, R. J., and Ghisalberti, M. (2019). Canopy resistance on oscillatory flows. *Coastal Engineering*, 152(April):103502.

Holakoo, A., Weeraratne, R., and Kugathasan, K. (2017). Sheet Pile Retaining Walls – Design and Construction in a Brown Fields Environment. *Australian Small Bridges Conference*, 8.

Janssen, T. and Battjes, J. (2007). A note on wave energy dissipation over steep beaches. *Coastal Engineering*, 54:711–716.

Kabir, M. R. and Torfs, H. (1992). Comparison of Different Methods to Calculate Bed Shear Stress. *Water Science and Technology*, 25(8):131–140.

Kimiaghalam, N., Clark, S. P., and Ahmari, H. (2016). An experimental study on the effects of physical, mechanical, and electrochemical properties of natural cohesive soils on critical shear stress and erosion rate. *International Journal of Sediment Research*, 31(1):1 – 15.

Koch, E. W. (2001). Beyond light: Physical, geological, and geochemical parameters as possible submersed aquatic vegetation habitat requirements. *Estuaries*, 24(1):1–17.

Koch, E. W., Ackerman, J. D., Verduin, J., and Keulen, M. v. (2006). *Fluid Dynamics in Seagrass Ecology—from Molecules to Ecosystems*. Springer Netherlands, Dordrecht.

Liao, X. (2015). *Cross-shore Velocity Moments in the Nearshore: Validating SWASH*. PhD thesis, Delft University of Technology.

Lima, S. F., Neves, C. F., and Rosauro, N. M. L. (2006). Damping of gravity waves by fields of flexible vegetation. *Coastal Engineering*, pages 491–503.

Loeb, I. M. R., Lamers, L., Kooijman, A., Cirkel, D., and Jaarsma, N. (2012). Een meer natuurlijk peilbeheer: relaties tussen geohydrologie, ecosysteemdynamiek en natura 2000. Technical report, Bosschap.

Lohrmann, R. (2018). Technisch advies afzanden kralingse plas. Technical report, Witteveen+Bos.

M. Ben Meftah, F. De Serio, M. M. &. A. P. (2012). LONGITUDINAL CHANNEL FLOW THROUGH SQUARE ARRAYS OF VEGETATION. *Nazionale di Idraulica e Costruzioni Idrauliche*.

McCall, R., van Thiel de Vries, J., Plant, N., van Dongeren, A., Roelvink, J., Thompson, D., and Reniers, A. (2010). Two-dimensional time dependent hurricane overwash and erosion modeling at santa rosa island. *Coastal Engineering*, 57(7):668–683.

Melby, J., Nadal-Caraballo, N. C., and Kobayashi, N. (2012). Wave runup prediction for flood mapping. *Coastal Engineering Proceedings*, 1.

Mendez, F. J. and Losada, I. J. (2004). An empirical model to estimate the propagation of random breaking and nonbreaking waves over vegetation fields. *Coastal Engineering*, 51(2):103–118.

Ministerie van Verkeer en Waterstaat (1999a). *Belastin en Sterkte*. Natuur vriendelijke oevers. CUR.

Ministerie van Verkeer en Waterstaat (1999b). *Vegetatie langs grote wateren*. Natuur vriendelijke oevers. CUR.

Moore, G. E., Burdick, D. M., Peter, C. R., and Keirstead, D. R. (2012). Belowground Biomass of Phragmites australis in Coastal Marshes. *Northeastern Naturalist*, 19(4):611 – 626.

Nash, K. T., Hendry, K., and Cragg-Hine, D. (1999). The use of brushwood bundles as fish spawning media. *Fisheries Management and Ecology*, 6(5):349–355.

Nepf, H. M. (1999). Drag, turbulence, and diffusion in flow through emergent vegetation. *Water Resources Research*, 35(2):479–489.

Nepf, H. M. (2011). *Flow Over and Through Biota*, volume 2. Elsevier Inc.

Ostendorp, W., Iseli, C., Krauss, M., Krumscheid-plankert, P., Moret, J.-l., Rollier, M., and Schanz, F. (1995). ENGINEERING Lake shore deterioration , reed management and bank restoration in some Central European lakes. *Ecological Engeneering*, 5:51–75.

Partheniades, E. (1965). Erosion and deposition of cohesive soils. *Journal of the Hydraulics*, 91:105–139.

Pelsma, T., Weenink, E., and Hoogland, G. (2009). Principe ontwerpen natuurvriendelijke oevers. Technical report, Waternet.

Phan, K. L., Stive, M. J., Zijlema, M., Truong, H. S., and Aarninkhof, S. G. (2019). The effects of wave non-linearity on wave attenuation by vegetation. *Coastal Engineering*, 147:63–74.

Pujara, N., Liu , P., and Yeh, H. (2015). The swash of solitary waves on a plane beach: Flow evolution, bed shear stress and run-up. *Journal of Fluid Mechanics*, 779:556–597.

Putrevu, U. and Svendsen, I. A. (1991). Wave induced nearshore currents: a study of the forcing, mixing and stability characteristics. *Center for Applied Coastal Research, Department of Civil Engineering, University of Delaware.*

Rahgozar, M. and Saberian, M. (2016). Geotechnical properties of peat soil stabilised with shredded waste tyre chips. *Mires and Peat*, 18.

Rijksoverheid (2011). stimulering oeverplanten.

RIVM (2019). Indeling in grondsoortregio's.

Roelvink, D., McCall, R., Mehvar, S., Nederhoff, K., and Dastgheib, A. (2018). Improving predictions of swash dynamics in xbeach: The role of groupiness and incident-band runup. *Coastal Engineering*, 134:103 – 123. RISC-KIT: Resilience-increasing Strategies for Coasts – Toolkit.

Roelvink, D., Reniers, A., van Dongeren, A., van Thiel de Vries, J., Lescinski, J., and McCall, R. (2009). Modeling storm impacts on beaches, dunes and barrier islands. *Coastal Engineering*, pages 1684–1696.

Roelvink, D., van Dongeren, A., McCall, R., Hoonhout, B., Rooijen, v. A., Geer, v. P., de Vet, L., and Nederhoff, K. (2015). *XBeach Manual.* Deltares, UNESCO-IHE Institute of Water Education and Delft University of Technology.

Sayah, S. M., Boillat, J. L., and Schleiss, A. (2004). The use of soft shore protection measures in shallow lakes: Research methodology and case study. *Limnologica*, 34(1-2):65–74.

Sayah, S. M. and Schleiss, P. D. A. J. (2005). Efficiency of brushwood fences in shore protection against wind-wave induced erosion. *Environment Naturel Architectural et construit (ENAC).*

Schiereck, G. J. (2001). *Introduction to bed, bank and shore protection.* VSSD.

Sollie, S., Bouwer, E., and de Kwaadsteniet, P. (2011). *Handreiking Natuurvriendelijke Oevers, een standplaatsbenadering.* Stichting Toegepast Onderzoek Waterbeheer.

Sollie, S., Coops, H., and Verhoeven, J. (2006). Oeverzones langs ondiepe meren, peilbeheer en nutriënten. Technical report, Institute of Environmental Biology.

Sonnenwald, F., Stovin, V., and Guymer, I. (2018). Estimating drag coefficient for arrays of rigid cylinders representing emergent vegetation. *Journal of Hydraulic Research*, 57(4):591–597.

Sonnenwald, F., Stovin, V., and Guymer, I. (2019). A stem spacing-based non-dimensional model for predicting longitudinal dispersion in low-density emergent vegetation. *Acta Geophysica*, 67(3):943–949.

Stam, M. (2018). Reliability of willow for wave load reduction on river dikes. *repository Tudelft.*

Sumer, B. M. and Fredsoe, J. (1997). *Hydrodynamics around cylindrical structures*, volume 33. World Scientific.

SWASH team (2011). User manual swash version 1.05.

Thornton, E. B. and Calhoun, R. J. (1972). Spectral resolution of breakwater reflected waves. *Journal of Waterway, Harbour and Coastal Engineering Division.*

Uddin, N. and Robinson, R. (2017). Responses of plant species diversity and soil physical-chemical-microbial properties to phragmites australis invasion along a density gradient. *Scientific Reports*, 7.

van Breukelen, S., Vuister, L., Bongaards, E., Oomen, E., Boudier, H. S., and Rijneker, B. (2003). *Natuurvriendelijke Oevers, Handreiking*. WUR E-depot.

van de Ven, D. (2018.). Ecosystem engineers.

van Dongeren, A., Lowe, R., Pomeroy, A., Trang, D., Roelvink, D. J., Symonds, G., and Ranasinghe, R. (2013). Numerical modeling of low-frequency wave dynamics over a fringing coral reef. *Coastal Engineering*, 73:178–190.

van Rooijen, van Vries, T. D., Dongeren, V., Version, D., Research-oceans, J. O. G., Rooijen, V., and Dongeren, V. (2016). Modeling the effect of wave-vegetation interaction on wave setup. *Journal Of Geophysical Research-Oceans Citation*.

van Vossen, J. and Verhagen, D. . (2009). *Handreiking natuurvriendelijke oevers*. stichting toegepast onderzoek Waterbeheer stoWa, utrecht.

Vretare, V., Weisner, S. E., Strand, J. A., and Granéli, W. (2001). Phenotypic plasticity in phragmites australis as a functional response to water depth. *Aquatic Botany*, 69(2):127 – 145. SPECIAL ISSUE ON PHRAGMITES-DOMINATED WETLANDS,THEIR FUNCTIONS AND SUSTAINABLE USE.

Water Land en Dijken (2018). Resultaten onderzoek natuurvriendelijke oevers. Technical report, Water Land and Dijken, Sterk in plattelandsnatuur.

Wu, W., Ozeren, Y., Wren, D., Chen, Q., Zhang, G., Holland, M., Ding, Y., Kuiry, S., Zhang, M., Jadhave, R., Chatagnier, J., Chen, Y., and Gordji, L. (2011). Phase i report for serri project no. 80037: Investigation of surge and wave reduction by vegetation.

Yan, Z., Yan, C., and Wang, H. (2010). Mechanical interaction between roots and soil mass in slope vegetation. *Science China Technological Sciences*.

Zijlema, M., Stelling, G., and Smit, P. (2011). SWASH: An operational public domain code for simulating wave fields and rapidly varied flows in coastal waters. *Coastal Engineering*, 58(10):992–1012.

Zijlema, M. and Stelling, G. S. (2008). Efficient computation of surf zone waves using the nonlinear shallow water equations with non-hydrostatic pressure. *elsevier*, 55:780–790.